Pancreatic cancer inhibitory potential of hydrazine ligands and their corresponding metal complexes

Yanga Stofile

(2300787)

Submitted to the Faculty of Health Science, University of Witwatersrand in fulfilment of the requirements for the degree of

Master of Science

Supervisor : Prof P Fru

Co-supervisor: Prof V Uahengo

Co-supervisor: Dr Y Yako

DECLARATION

I, Yanga Stofile (2300787), declare this dissertation is my work. It is submitted for the degree of Master of Science in Medicine in the Faculty of Health Science, University of Witwatersrand, Johannesburg. It has not been submitted before for any degree or examination at any other University.

Signature of candidate:  Date: 13 September 2024

DEDICATION

To my late father who has always encouraged education.

MHSRIP 31 January 1955 – April 2010

ACKNOWLEDGEMENT

I would like to first thank GOD almighty for the strength and courage to start and complete my MSc degree. Completing this degree comes with great support from a collective of individuals, my supervisor, and my family. My supervisor Prof Fru gave me an opportunity and supported the vision. I would like to thank Prof Uahengo and the team from the University of Namibia for the synthesis and characterization of the metal complexes. Dr Y Yako for the referral and guidance.

I would like to thank Dr Marietha Nel for guidance with cell culturing. I would also like to thank Ms. Jeanet Mazibuko and Ms Karabo Mosiane for their assistance with several techniques in the lab.

Finally, I would like to thank the Research, Innovation and Development, Finance Division at Walter Sisulu University for financially supporting part of the travel and accommodation logistics for the first year of commencement of the laboratory experiment.

ABSTRACT

Introduction: Pancreatic cancer remains one of the deadliest cancers in the world. According to GLOBOCAN, in 2022, Pancreatic ductal adenocarcinoma cancer (PDAC) was the third leading and soon to become the second leading cause of cancer deaths. Current drugs used to manage PDAC demonstrate adverse side effects. Metal complexes such as Cisplatin (Cis) are more effective when combined with the first-line drug, gemcitabine. Unfortunately, there are limitations with these and existing drugs such as the development of drug resistance. In a quest to find novel therapeutic drugs, a series of hydrazone ligands and metal complexes were synthesized and characterized for screening their antioxidant activity, cytotoxicity and potential modes of cell death in pancreatic cancer cells.

Methodology: The nitrogen-sulfur Schiff base Ligands (L1-L3) were synthesized by the reaction of hexyl dithiocarbamate and 4-methylbenzaldehyde in a 2:1 molar ratio with various divalent metal ions to form the neutral complexes AgL1, RuL1, NiL2, AgL2, CuL2, NiL3, ZnL3, and CuL3. Established physicochemical and spectroscopic techniques were used to characterize each compound, in which geometrical variations that occur in the coordination of the ligand to the single crystal structures were studied. The cytotoxic effect of the compounds was assessed against a pancreatic cancer cell line, MIA PaCa-2, using the (3-(4, 5-dimethylthiazol-2-yl)-2, 5-diphenyl tetrazolium bromide) MTT assay tested across a range of concentrations (0.78 – 100 μM). The antioxidant activity was evaluated using 2, 2-Diphenyl-1-picrylhydrazyl (DPPH). Compounds that showed cytotoxic effects were further analyzed for the mode of cell death using the flow cytometric assays, Annexin V/propidium iodide (PI) for apoptosis and necrosis determination and PI for cell cycle analysis.

Results: The metal complexes AgL1 and RuL1 derived from the free ligand L1, demonstrated potent cytotoxicity against MIA Paca-2 cells, with IC_{50} values of 1.55 ± 0.59 μM and 1.44 ± 0.61 μM respectively. L1 demonstrated the highest cytotoxicity value with IC_{50} of 0.45 ± 0.25 μM. Complex NiL2 exhibited a cytotoxic potency against MIA Paca-2 with an IC_{50} value of 1.25 ± 0.71 μM. The free drug L2 exhibited a cytotoxicity of 21.41 ± 14 μM. In comparison, gemcitabine demonstrated a stronger cytotoxicity on MIA Paca-2 with IC_{50} of 6.57 ± 0.632 μM, while its effect on Vero cells was 11.30 ± 0.04 μM.

An analysis of the antioxidant activity indicated that L1 and its metal complex RuL1 demonstrated antioxidant activity with an IC_{50} of 5.11 ± 0.47 µM, in comparison to L-ascorbic acid (Vitamin C), which showed an IC_{50} of 6.42 ± 0.24 µM. CuL3 exhibited the highest activity with a value of (4.25 ± 0.56 µM) when compared to all other complexes, including the ZnL3 complex (with a concentration of 5.62 ± 0.28 µM). Apoptosis determination was statistically significant ($p < 0.001$) for both the metal complexes of L1 with each exhibiting a percentage of 7.75% for AgL1 and 14.33% for RuL1 in comparison to the L1 (1.3%) when tested at the IC_{50} concentration of 1.48 µM. Cell cycle assessment showed that MIA Paca-2 cells treated with L1 and its complex AgL1 caused the sub-G1 phase arrest at 28 ± 2.97% and 18 ± 1.01%, respectively. The cell population grew by 34.83% in the S phase for L1 and 52% for RuL1. AgL1 was statistically significant ($p < 0.001$) in the G1 phase and $p < 0.01$ in the S phase, while RuL1 was significant ($p < 0.001$) in both phases. NiL2 treatment caused a sub-G1 phase arrest from 6.44 ± 1.45% to 16.9 ± 2.1%. L2 treated cells showed a 36.4 ± 5.6% arrest of the S phase when compared to the complex NiL2 (27.3 ± 10.35%).

Conclusion: This study has established that complexation of nitrogen-sulphur Schiff base hydrazone ligands with metal complexes such as RuL1 results in anticancer properties. The complexation enhances the complexes' ability to induce apoptosis and cell arrest in pancreatic cancer cells. These preliminary findings suggest that more investigations are needed to further understand the anticancer mechanism such as pathway analysis studies.

TABLE OF CONTENTS

LIST OF ABBREVIATIONS

5-FU	5 fluorouracil
AFL	Atypical flat lesion
CAF	Cancer-associated fibroblasts
CT	Computed tomography
DMEM	Dulbecco's Modified Eagle Medium
DMSO	Dimethyl sulfoxide
DPPH	2,2-Diphenyl-1-picrylhydrazyl
ECM	Extracellular matrix
EtOH	Ethanol
EUS	Endoscopic ultrasound
FBS	Foetal bovine serum
FC	Flow cytometer
FOLFIRINOX	FOLinic acid, and 5 Fluorouracil with IRINoctecan and OXaliplatin
HCL	Hydrochloric acid
HIF	Hypoxia inducible factor
IC_{50}	50% inhibitory concentration
IPMN	Papillary mucinous neoplasm
L	Ligand
LPA	Lysophosphatidic acid
MCN	Mucinous cystic neoplasm

MMPs	Metalloproteinases
MRI	Magnetic resonance imaging
MTT	3-(4,5-dimethylthiazol-2-yl)-2,5-diphenyl tetrazolium bromide
MW	Molecular weight
PanINs	Pancreatic Intraepithelial neoplasias
PBS	Phosphate buffered saline
PDAC	Pancreatic ductal adenocarcinoma
PI	Promidium Iodide
PSA	Prostate-specific antigen
PSC	Pancreatic stellate cells
RNase A	Ribonuclease A
ROS	Reactive oxygen species
TGF	Tumour growth factor
TME	Tumour microenvironment
XTT	2,3-bis[2-methoxy-4-nitro-5-sulfophenyl]-2H-tetrazolium-5-carboxanilide

LIST OF FIGURES

CHAPTER 1

CHAPTER 2

CHAPTER 3

`LIST OF TABLES

CHAPTER 1

Introduction and Literature Review

1.1 INTRODUCTION

The pancreas is said to be a retroperitoneal organ because of its anatomical position. It is divided into the head, neck, body, and tail (Figure 1.1). Microscopically, the pancreas appears to be lobulated and contained in a capsule. It has both exocrine and endocrine functions, the endocrine regulates metabolism and glucose homeostasis through the secretion of hormones into the bloodstream (Karpińska and Czauderna, 2022). The pancreas has a main pancreatic duct (Wirsung), which runs the length of the gland from the tail to the head and is closely related to the bile duct. It is said that 90% of pancreatic cancer or tumours arise from the pancreatic duct, which has given rise to it being referred to as pancreatic ductal adenocarcinoma (PDAC) (Atkinson et al., 2020).

A five-year survival rate is indicative of the fact that PDAC continues to be an extremely fatal disease. It is anticipated that by 2030, PDAC will be the second leading cause of cancer-related fatalities, currently ranking third. PDAC often presents at an advanced stage making diagnosis difficult, a contributing factor to its poor prognosis (Mai and Inkielewicz-Stepniak, 2021). Kirsten rat sarcoma oncogene (KRAS) is the most common mutation of pancreatic tumours contributing to approximately 95% of mutations (Fang et al., 2023).

Drugs currently used to manage PDAC are gemcitabine, Folfirinox which is a combination of the drugs 5-fluorouracil (5-FU), leucovorin, irinotecan and oxaliplatin and nab-paclitaxel. These are used as the standard first-line chemotherapy either in combination or individually (Yang et al., 2023). These drugs are moderately effective as they have been unsuccessful in improving patient survival with PDAC indicative to be high drug resistance (Anderson et al., 2021). Surgical resection is the only curative option, but it however has its limitations (Adamska et al., 2017). Due to the ongoing increase in drug resistance, there is a need to develop novel effective therapies that are aimed at advancing the current treatment options. Our study seeks to investigate the potential synthesised ligands and their hydrazone-based metal complexes as anti-pancreatic cancer agents. A wide range of hydrazones have been

investigated for their anticancer properties and have shown potential as novel anticancer agents (Šermukšnytė et al., 2022).

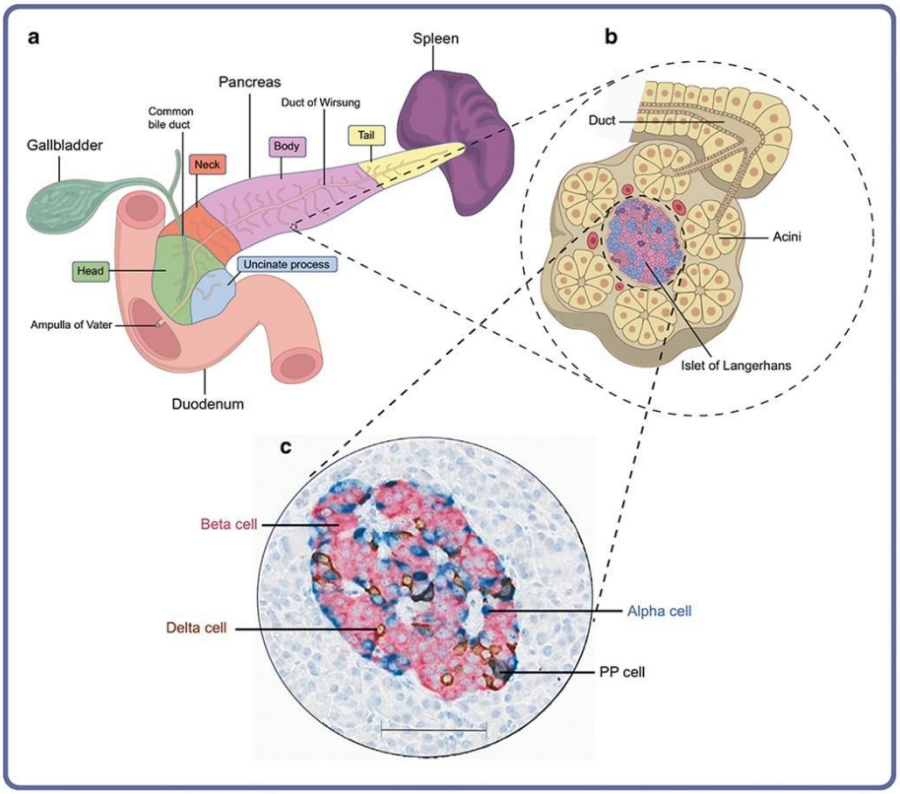

Figure 1.1: Fundamental features of the human pancreas. **(a)** Illustration of the pancreas and its neighbouring organs **(b)** Illustration of the cellular organisation of the functional pancreas, the endocrine and exocrine **(c)** Display of the four endocrine cell types. This open-access article is distributed under the terms of the Creative Commons CC-BY license, which permits unrestricted use, distribution, and reproduction in any medium, provided the original work is properly cited (Atkinson et al., 2020).

The determination of cytotoxicity on anticancer activity is important so that the efficacy of the drug is determined. The most used methods to measure cell viability/compound cytotoxicity are (3-[4,5-dimethylthiazol-2-yl]-2,5 diphenyl tetrazolium bromide (MTT) and 2,3-bis[2-methoxy-4-nitro-5-sulfophenyl]-2H-tetrazolium-5-carboxanilide (XTT) which is what we used in the current study. The absorbance of the formazan product of these tetrazolium salts indicates cytotoxicity (Wang et al., 2011). We further investigated the antioxidant activity of the compounds using 2,2-Diphenyl-1-picrylhydrazyl (DPPH) with Vitamin C as a positive control. Antioxidant enhancements have been employed in some anticancer therapies as a strategy to inhibit or treat cancer cells (Kim et al., 2019). Biological systems inevitably produce free radicals and are known to cause various deteriorating and degenerative disorders, like

mutagenesis, carcinogenesis, cardiovascular disturbances and aging (Kedare and Singh, 2011). Cell damage caused by free radicals intensifies with damaging consequences (Soberanes et al., 2019). Regulation of both the reactive oxygen species (ROS) formation and removal from the biological system is essential for the maintenance of diverse cellular processes (Kim et al., 2019). High levels of free radicals are generated by different types of anticancer drugs such as Doxorubicin which is known and studied to induce severe DNA damage (Vera-Ramirez et al., 2012). Antioxidant enhancements have been employed for some anticancer therapies as a strategy to inhibit or treat cancer cells DPPH can react with various natural and synthetic antioxidants (Tăbăcaru et al., 2020) hence its usefulness in determining antioxidant activity. Researching a drug's effects on the cell cycle would thus provide a simple way to estimate its anti-tumour effect (Lee et al., 2019). Cell death occurs when the cell cycle terminates in the G1 phase because the cells were unable to progress through mitosis, proliferation, and the S and G2 phases. Cell cycle is used to calculate the DNA fragments of apoptotic cells and intracellular DNA fragments are one of the most basic characteristics of cell death. The fragments of the apoptotic cells can be seen by the appearance of the peak in the histogram's sub-G1 region. Cells grow during the G1 phase, preparing the cells to synthesise the enzymes for DNA replication in the S phase, this is continuous to the G2 phase where cells now synthesize protein then cells divide into two identical daughter cells during the M phase, lastly the cells continue to be metabolically active in the G0 phase (Polychronis et al., 2019). The cell cycle was also investigated using Propidium Iodide.

1.2 LITERATURE REVIEW

A breakthrough in cancer treatment was accidentally discovered in the late 1960s by Barnett Rosenberg (Makovec, 2019), a platinum-based anticancer drug, Cisplatin and ever since newer metal-based anticancer drugs have been developed to improve therapeutic effects (Zhang et al., 2022). Since the approval of Cisplatin in 1974 by the Food and Drug Administration (FDA), there has been growth in the field to explore other platinum-based drugs and as such, Carboplatin and Oxaliplatin also formed part of the first line of therapeutic anticancer drugs (Jeon et al., 2021). Although these platinum-based anticancer agents are effective, their long-term usage have adverse reactions (Lin et al., 2022). The study involved an exploration of various metal-based complexes and their mechanisms of action in pancreatic cancer cell lines.

1.3 EPIDEMIOLOGY OF PDAC

According to Global Cancer Observatory (GLOBOCAN, 2022), PDAC is ranked 12th globally with a worldwide record of new cases of approximately 510 992 in 2022, and 467 409 deaths with Eastern Asia leading on new cases with 232 537 followed by Europe with 146 477. The African continent has 18993 cases with Northern Africa leading with new cases of 6264, Southern Africa having 2078 new cases. In Southern Africa, 4.9% of people per 100,000 people are diagnosed with pancreatic cancer, with a mortality rate of 4.3%. Of the new incidences between male and female cases, there was no significant difference, however, the mortality of males was more than that of females. This is a result of late-stage diagnosis. It is unfortunate that 85% of patients present at an incurable stage (Pereira et al., 2020). There are no biomarkers for early detection of pancreatic cancer (Yang et al., 2021). South Africa's statistics remain unclear although the National Cancer Registry for the year 2020 reports 254 males and 248 females of all population groups diagnosed with cancer of the pancreas. Of these, there were 80 black males 71 black females, 129 white males and 128 white females, suggesting a higher prevalence in the white population, although this could be due to them having access to clinical facilities due to their improved socioeconomic status.

1.3.1 Diagnosis

Patients with PDAC often present with advanced metastatic disease, and this accounts for 80-90% of the total case, and only a few patients (10-20%) present with treatable options (Timmer et al., 2021). PDAC lacks biomarkers hence patients present with late-stage diagnosis (Singhi et al., 2019). There are generalised symptoms of PDAC such as weight loss, abdominal pain and jaundice with no specificity making it difficult to diagnose (Sarantis et al., 2020). PDAC, unlike other types of cancers such as breast, colon, and prostate, does not have screening tests. Prostate cancer, for example, uses prostate-specific antigen (PSA) for screening. Several techniques are used for PDAC diagnosis such as computed tomography (CT), magnetic resonance imaging (MRI) and Endoscopic ultrasound (EUS). However, these also have restrictions such as the replacement of functional with excess fibrous connective tissue when

the tumour is treated with neoadjuvant treatment (NAT). Additionally, NAT causes necrosis, oedema, and inflammation, which hinders the radiologic assessment of tumour regression (Yoo et al., 2023).

1.3.2 Pathogenesis of PDAC

Pancreatic cancer forms from the ductal epithelial cells of the exocrine part of the pancreas (Grant et al., 2016). The pathophysiology of PDAC is personified by intricate multiple genetic steps (Park et al., 2021). The growth of the non-invasive precancerous lesions precedes by years before the presence of the tumour despite the aggressiveness of the tumour (Kung and Yu, 2023). Through the development of the percussor lesions, the Pancreatic Intraepithelial neoplasias (PanINs) and the intraductal papillary mucinous neoplasm (IPMN), mucinous cystic neoplasm (MCN) and a rare atypical flat lesion (AFL), they tend to grow into the invasive adenocarcinoma (Ho et al., 2020, Grant et al., 2016). Of these, the PanIN is the most popular precursor of these lesions (Opitz et al., 2021). The progression of PanIN into PDAC is shown in Figure 1.2, as classified according to early stage (PanIN-1) where there is *K-Ras* mutation, Telomere shortening and P16 ^{INK4a} loss, followed by intermediate stage (PanIN-2) where there is inactivating of mutation or epigenetic silencing of *(CDKN2A)*, and late stage (PanIN-3) where there is loss of P53, SMAD4 which are categorized as major molecular changes that accumulate during pancreatic carcinogenesis depending on the histopathology of the tissue (Guo et al., 2016).

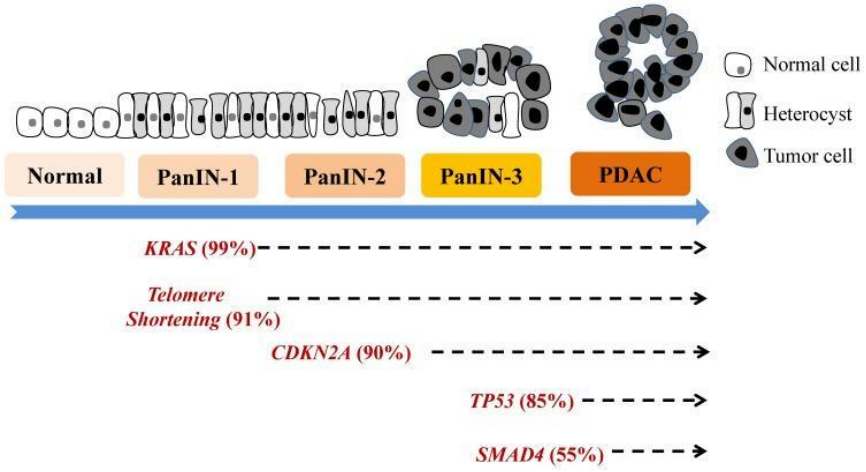

Figure 1.2: Progressive cell stages of normal cells into PDAC mutation. Pancreatic carcinogenesis involves early (telomere shortening and activating KRAS mutations), intermediate (inactivating mutations or epigenetic silencing of CDKN2A), and late (TP53 and SMAD4 inactivating mutations) genetic events. New molecular markers are appearing. (Digitized articles that are in the public domain carry a statement indicating that they are free from known copyright as described by the Creative Commons Public Domain Mark 1.0. These articles are also included in the PMC Open Access Subset) (Guo et al., 2016).

1.3.3 Pancreatic cancer microenvironment

The tumour microenvironment (TME) is said to play a role in the progression of cancer and how the treatment responds. Generally, the TME is characterised by molecular and cellular features that play significant roles in biological activity. The pancreatic ductal adenocarcinoma (PDAC) is vigorous and has dense tumour stroma which includes but is not limited to cancer-associated fibroblasts (CAF), and immunosuppressive cell populations such as T-cells make it a complex tumour hence difficulties in providing effective therapy (Mijit et al., 2023). The PDAC microenvironment is composed of stromal cells, dense extracellular matrix (ECM) and immune cells. Myofibroblasts are metabolically active stromal cells derived from pancreatic stellate cells (PSC) and produce the dense ECM which forms a barricade for the tumour as seen in Figure 1.3. CAF are believed to take part in the procurement of the malignant properties while the normal fibroblasts suppress the effect of cancer cell function. A study by (Takai et al., 2023) investigated the involvement of lysophosphatidic acid (LPA) in regulating cellular function by TME of pancreatic cancer cells (PANC-1 cells). Their results showed that the involvement of LPA signalling via LPA_2 and LPA_3 promotes malignant properties. The dense desmoplastic stroma in PDAC constitutes 80% of the tumour volume, and signalling pathways within the stroma include but are not limited to tumour growth factor (TGF), a cytokine leading to cell cycle arrest, integrin, nuclear factor kappa beta (NF-κB), a protein transcription factor and regulator of innate immunity responsible for pathogenic signalling, metalloproteinase (MMPs) and β-catenin, (Sagini et al., 2018). Another crucial piece related to desmoplasia in the TME of PDAC is hypoxia as it results in immunosuppression and aggravates cellular autophagy (Orth et al., 2019). Various molecules and signalling pathways are stimulated promoted under hypoxia and the discovery of Hypoxia-inducible factor (HIF)- 1α is involved in cell functions such as cell proliferation, apoptosis and angiogenesis (Yamasaki et al., 2020).

Signalling pathways need to be studied to improve PDAC treatment (Abou Khouzam et al., 2023).

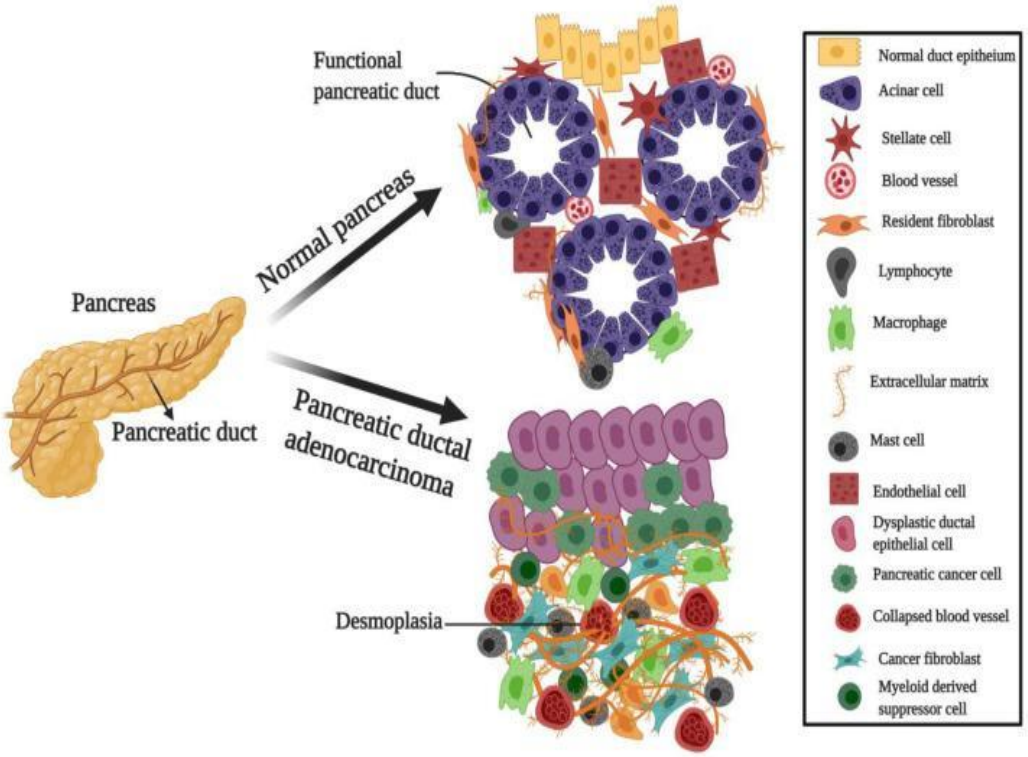

Figure 1.3: The Metabolically active stromal cells derived from pancreatic stellate cells (PSC) produce the dense ECM which forms a barricade for the tumour. Environmental factors influencing pancreatic ductal adenocarcinoma. Pancreatic ducts and acinar cells are lined with epithelial cells in a healthy exocrine pancreas; interlobular septa and pancreatic ducts contain the majority of the extracellular matrix; and the peri-acinar space is surrounded by resident fibroblasts and pancreatic stellate cells. PDAC cells breach the basal membrane of malignant pancreatic ducts to gain access to and infiltrate normal tissue. (Iqbal et al., 2023).

1.3.4 Signalling pathway for PDAC

Cancers are described as cells that are uncontrolled because of their symbolic evasion of apoptosis, overstimulation of cell proliferation and upregulation of NF-κB. It is well reported that NF-κB signalling is critical for the regulation of cell growth, apoptosis, inflammation, stress response and other cellular processes (Li et al., 2015). Pancreatic tumour angiogenesis

and metastasis have been reported to be induced by the activation of the NF-κB signalling pathway. However, inhibition of the NF-κB signalling pathway increases the number of apoptotic activities by expressing phosphorylation defective IκB∝ and significantly suppresses pancreatic cancer cell tumourigenesis. Identifying novel treatments that could modulate the NF-κB signalling pathway could be an important treatment strategy for pancreatic cancer (Wang et al., 2017). Therefore, deciding which part of the NF-κB cascade to target becomes as important as the specificity of the molecules with which to intervene to achieve selective anti-cancer activity.

1.4 PDAC TREATMENTS

1.4.1 Current treatments of PDAC

Advancing knowledge in understanding cancer, its impact and improving the livelihood of patients with more therapeutic interventions has since grown (Sen et al., 2022). Cancer is generally treated by surgical resection if diagnosed early. Late-stage diagnosis involves a combination of radiotherapy, chemotherapy and palliation (Revia et al., 2019). PDAC is no different concerning treatment, however, its prognosis and survival rates are of concern. Since their discovery, the Platinum (Pt) -based anticancer drugs have gained enormous interest however they too are having adverse side effects which hinder their therapeutic efficiency (Vaidya et al., 2022).

Current treatments for pancreatic cancer include chemotherapy, radiation, and first-line drugs such as fluorouracil, erlotinib, gemcitabine, mitomycin C and cisplatin drugs (Wang and Hamann, 2019). At times a combination of FOLinic acid, and 5 Fluorouracil with IRINoctecan and Oxaliplatin (FOLFIRINOX) has shown efficacy compared to monotherapy. At various stages these are administered to patients depending on their response to the drug thus modifications can be made (Singh and O'Reilly, 2020). These tend to be inadequate, abrupt, and resistant with unbearable side effects. The only potentially curative treatment for pancreatic cancer is surgical resection, however, the survival of patients remains poor, while the results of adjuvant chemotherapy and radiotherapy are unsatisfactory (Matsuoka and Yashiro, 2016). From various disciplines, the search for nonconventional chemotherapeutic agents has greatly sparked the attention of scientists who continue to seek novel therapeutics (Taha et al., 2016).

The purpose of this research is to investigate the potential synthesised ligands and their hydrazone-based metal complexes as potential medicines for the treatment of pancreatic cancer. The anticancer properties of a wide variety of hydrazones have been investigated, and it has been demonstrated that hydrazones also have the potential to be used as novel anticancer agents.

1.4.2 Advancing research on PDAC treatment – Metal complexes and Hydrazones

An increasing number of metal-based compounds, including those derived from Ruthenium (Ru), are being investigated as possible substitutes for the existing platinum (Pt) metal complexes. A group of scientists (Wernitznig et al., 2019) discovered a Ruthenium III complex, imidazolium Ru^{III}-based ionic compounds KP418 and KP1019/NKP-1339 to have anticancer activity against colorectal cancer in mice and is currently in clinical trials Phase IIA. Other metal complexes such as Copper (Cu), Nickel (Ni), Selenium (Se), Iron (Fe), Silver (Ag), and Zinc (Zn) have also gained popularity and have been studied for their anticancer activity against various cancers (Elsayed et al., 2019). However, these studies have not targeted pancreatic-related cancers, and form part of our investigation in this study.

1.5 ANTICANCER ACTIVITY OF METAL COMPLEXES

1.5.1 Metallodrugs

Metal-based drugs exhibit unique chemistry and flexibility in their electronic and structural properties (Ferraro et al., 2022). These properties include, but are not limited to, oxidation states, coordination geometries, ligand substitutions, types of ligands, and the number of ligands attached to the metal. Due to their ability to transform into active species through ligand exchange, these drugs are referred to as prodrugs and are designed to target specific sites. (Anthony et al., 2020).

Silver (Ag) is well documented for its medical uses against Gram-negative and Gram-positive bacteria and fungi and as such has become an antimicrobial agent (Roy et al., 2019). Some researchers have investigated Silver complexes for their anticancer activity e.g. Liang and colleagues wrote a review on the cytotoxic activity of Ag(1) complexes

[$Ag(PPh_3)(L^{OMe})]NO_3$ (**3**), [$Ag(PPh_3)(L^{2OMe})]NO_3$ (**4**) and Ag(I) complex [$Ag(PTA)(L^{2OMe})]NO_3$ (**5**) and ve463their ligands [$HC(pz)_2COOCH_3$] (L^{OMe}, **1**) and [$HC(pz^{Me2})_2COOCH_3$] (L^{2OMe}, **2**) against several solid tumours specifically the human colon (HCT-15), pancreatic (PSN-1), cervical (A431), breast (MDA-MB-231) and ovarian carcinoma as well as of lung SCLC (U1285), Ag (1) **3- 5** complexes expressed the most effective when compared with Cisplatin especially on the U1285 in reducing the viability of the cancer cell averaging IC_{50} of 7.5, 4.0 and 3.0 µM respectively (Liang et al., 2018). A popular well known antifungal drug Miconazole (MCZ) was synthesized with Ag (1) salts and complexes [$Ag(MCZ)_2NO_3$] ***(1)*** and [$Ag(MCZ)_2ClO_4$] (***2)*** were obtained and evaluated for their anticancer activity against the human liver cancer cell line, HepG2 and murine fibroblast Balb/c3T3 cell line. In comparison with the Cisplatin, the IC_{50} in the HepG2 cells was lower than those of fibroblast in the LDH assay. These triazoles and miconazole have shown to express anti-proliferative effects and anticancer agents (Stryjska et al., 2020). Varna and colleagues have tested several Ag (1) complexes for their bioactivity potentials, in this particular article they report the potential growth inhibition of four Ag (1) complexes bearing the CH3- substituted thiadiazole-based thioamide 1,3,4-thiadiazole-2(3H)-thione (mtdztH) and phosphines against Ovarian (SKOV-3), Pancreatic Hup-T3, Lung DMS114, and prostate (PC3), as well as normal lung cell line MRC5. All compounds exhibited a potent cytotoxic effect on all cell lines, however compound 4 ($[Ag (mtdztH)(dppe)(NO_3)]_n$) displayed the most of its efficacy, especially against the Ovarian SKOV-3 (Varna et al., 2023).

The discovery of Cisplatin by Rosenberg in the 1960s recuperated work done by Dwyer and co-workers where they investigated its anticancer activity together with that of Ru complexes in the 1950s (Levina et al., 2009). There is a distinctive property on the platinum group elements Ruthenium, Rhodium, palladium, Osmium, and Iridium as anticancer agents (Ferraro et al., 2022), however, Ruthenium (Ru) complexes are an emerging anticancer therapeutic agent as many of its complexes have gone through to the stage of human clinical trial (Lee et al., 2020). The two prospective Ru complexes under clinical trial are [imiH][*trans*-[Ru(*N*-imi)(*S*-dmso-S)Cl_4] (imi = imidazole, DMSO = dimethyl sulfoxide), also known as NAMI-A, and [indH][*trans*-[Ru(*N*-ind)$_2Cl_4$] (ind = indazole), also known as KP1019. Extensive work is being done on studying the mechanisms of action, and their bioactivity which includes and is not limited to apoptosis, autophagy, cell cycle arrest, necrosis, and anti-metastasis, (Gałczyńska et al., 2020a). Nano-ruthenium complexes were synthesized and tested for their bioactivity by Petruk and colleagues (Petruk et al., 2019) where they encapsulated Apoferritin nanocages of

dinuclear trithiolato-bridged arene ruthenium complex diruthenium-1, on several cell lines and showed high cytotoxicity but with moderate selectivity. Some of the issues related to degradation can be overcome by bionanomaterial which promotes permeability and selectivity and carries large amounts of the drug (Sonkar et al., 2022).

Zinc (Zn) is a profuse element after iron in the body. It is crucial for human physiological processes where it plays a role as a cofactor of several enzymes that are involved in DNA and protein synthesis and regulates intracellular signalling pathways of the immune system. supports immunity such that a deficiency leads to numerous body malfunctions (Skalny et al., 2021). It has been reported that Zn deficiency could lead to loss of function of zinc-dependent proteins involved in maintaining DNA integrity, thus contributing to the development of cancer. It has been suggested that the presence of sufficient quantities of Zn in cancer patient may reduce the burden of tumour (Skrajnowska and Bobrowska-Korczak, 2019). Notably, zinc complexes have exhibited strong bioactivity (Raducka et al., 2022).

1.5.2 Hydrazones as anticancer agents

The variety of structures of hydrazones an their biological application as anticancer, antibacterial, antioxidant, antifungal (Kazeminejad et al., 2022), anti-inflammatory, and their cytotoxic activities have attracted considerable attention in the field of cancer research (Fekri et al., 2018). A study by Sahin and colleagues showed high anti-tumour effects of the synthesized coumarin-thiazole Schiff (metal) base and its platinum II and palladium II complexes on human cancer lines and found that palladium complexes had better activity with lower inhibitory concentration (IC_{50}) than the platinum complexes (Sahin et al., 2018). Rahman and colleagues showed considerable anticancer activity for a series of homoleptic and heteroleptic Pt (II) hydrazine complexes (Rahman et al., 2018). Damghani and team synthesized and evaluated a series of twelve imidazo [1,2-α] pyridine derivatives bearing 1,2,3-triazole moiety for the potential to inhibit mesenchymal-epithelial transition factor (c-MET) a signalling path that plays a role in the development and progression of cancer and tested their anticancer activity on lung (EBC-1) and pancreatic cancer cells (AsPc-1, Suit-2 and Mia-PaCa-2). Of the twelve derivatives, three [R=4-Methyl-benzene, (6d), R=4 t Buthyl-benzene (6e), and R=3,4-Dichloro-benzene] showed considerable potential anticancer activity against lung (EBC-1) and pancreatic cancer cells (AsPc-1, Suit-2 and Mia-PaCa-2) (Damghani et al., 2021).

A group of scientists Nasr synthesized a series of coumarin hydrazide-hydrazone derivatives and evaluated their anticancer activity against a PDAC cell PANC-1. The complexes; 7-Hydroxy-2-oxo-N'-((pyridin-3-yl)methylene)-2H-chromene-3-carbohydra-zide (10d), N'-((2-chloro-6-ethoxyquinolin-3-yl)methylene)-7-hydroxy-2-oxo-2H-chromene-3-carbohydrazide (12d), 6-bromo-N'-((2-chloroquinolin-3-yl)methylene)-2-oxo-2H-chromene-3-carbohydra-zide (11b) showed what the authors described as an excellent anticancer activity with IC_{50s} (μM) of 0.129 ± 0.019, 2.525 ± 0.782 and 5.449 ± 1.380 respectively compared to Doxorubicin (Dox) as a reference standard with an IC_{50} of 6.9 ± 0.32 with compound 11b exceeding its expectation as a chemical carrier presented to be a promising radiopharmaceutical imaging drug for cancer (Nasr et al., 2018). A study of *in vitro* proliferation potential of new isatin-based hydrazonoindolin-2-ones against colon (HT-29), breast (ZR-75), and lung (A549) human cancer cell lines have shown to be the most active congeners with average IC_{50} values lower than that of reference drug sunitinib (Attia et al., 2017). The synthesis of hydrazones has grown over the years due to their wide range of bioactivity. In this study, we screen a series of metal-based hydrazone complexes for anti-cancer activity against PDAC. The metal complexes of interest were copper, silver, ruthenium, nickel, Iron, and zinc. These have been reported by Elsayed and colleagues to have activity against various cancers (Elsayed et al., 2019).

1.6 STUDY RATIONALE

PDAC remains the most aggressive cancer of the pancreas due to its characteristic asymptomatic nature in its early developmental stages and rapid progression to affect neighbouring organs. There is a lack of specific clinical symptoms and reliable biomarkers for early diagnosis and the associated antagonistic metastatic nature hence there is poor response to treatments (Chari et al., 2015). To date, available therapeutic possibilities include surgery, radiation, chemotherapy, immunotherapy, and the use of delivery systems through targeting (Adamska et al., 2017). However, despite attempts to improve on more effective therapeutic strategies for PDAC, the efficacy of newly developed drugs remains low coupled with adverse side effects (Kenner et al., 2017). Some of the general side effects that have been observed for

all therapeutic regimens include complications associated with a reduction in blood cell counts, vomiting and nausea, diarrhoea, constipation, mouth ulcers, poor appetite, hair loss, nervous system changes, and infertility. It is speculated that some of these adverse effects may be the result of ineffectiveness due to early termination of treatment. Currently, surgical resection of the affected part of the pancreas remains the only curative possibility for PDAC patients in the earlier stages of the disease (Gharibi et al., 2016). Only a small percentage (less than 20%) of PDAC patients benefit from this curative option as the remaining patients usually present with tumours that are already affecting major vessels, nerve fibres, and/or organs limiting surgical removal. The lack of effective therapeutic strategies necessitates the development of novel, more effective strategies for PDAC. The synthesis of hydrazones has grown over the years due to their wide range of bioactivities such as antimicrobial, anticonvulsant, analgesic, anti-inflammatory, anti-platelet, anti-tubercular, and anti-tumoural activities (Popiolek, 2017). In addition, Bonnett and colleagues have reported less toxicity of hydrazones in mice when the compounds were tested for inhibitory activity against strains of *Mycobacterium tuberculosis* (Bonnett et al., 2018). Biological systems inevitably produce free radicals and are known to cause various deteriorating and degenerative disorders, like mutagenesis, carcinogenesis, cardiovascular disturbances and aging (Kedare and Singh, 2011). Cell damage caused by free radicals intensifies with damaging consequences (Soberanes et al., 2019). Regulation of both the reactive oxygen species (ROS) formation and removal from the biological system is essential for the maintenance of diverse cellular processes (Kim et al., 2019). High levels of free radicals are generated by different types of anticancer drugs such as Doxorubicin which is known and studied to induce severe DNA damage (Vera-Ramirez et al., 2012). Antioxidant enhancements have been employed for some anticancer therapies as a strategy to inhibit or treat cancer cells (Kim et al., 2019).

A number of in vitro tests are used to evaluate the anticancer activity of new compounds. The tetrazolium salt (3-(4,5-dimethylthiazol-2-yl)-2,5-diphenyl tetrazolium bromide) MTT and 2,3-Bis-(2-Methoxy-4-Nitro-5-sulfophenyl)-2H-Tetrazolium-5-carboxanilide salt (XTT) assays are the most commonly used essays to assess the efficacy and interactions of anticancer agents (van Meerloo et al., 2011). The MTT assay is based on the conversion of MTT to formazan crystals by living cells which determines mitochondrial activity (Buranaamnuay, 2021). Viable cells with active metabolism convert MTT into a purple-coloured formazan product with an absorbance maximum near 570 nm. When cells die, they lose their ability to

convert into formazan, thus colour formation serves as a useful tool and convenient marker for only the viable cells (Riss et al., 2004)

The importance of hydrazone compounds warrants their investigation as anti-tumour agents for PDC as there are currently no studies of this nature, to our knowledge.

1.7 STUDY AIM AND OBJECTIVES

1.7.1 Aim

This study aimed to determine the effectiveness of hydrazone derivatives against pancreatic cancer.

1.7.2 Objectives

- To determine the cytotoxic effect and 50% inhibitory concentration (IC_{50}) of metal-based compounds of hydrazone on the pancreatic cancer cell line, MIA PaCa-2 and Vero (normal) cell line using 3-(4,5-dimethylthiazol-2-yl)-2,5-diphenyl tetrazolium bromide (MTT) and 2,3-Bis-(2-methoxy-4-nitro5-sulfophenyl)-2H-tetrazolium-5-carboxanilide salt (XTT).
- To determine the antioxidant activity of the metal-based compounds using 2,2-Diphenyl-1-picrylhydrazyl (DPPH)
- To determine the ability of the metal-based compounds to induce cell death and cell cycle arrest using flow cytometry assays.

1.8 STATISTICAL ANALYSIS

Each assay was performed at least three times unless stated otherwise. The data is presented as mean ± standard error of the mean (SEM) and was analyzed using Microsoft Office Excel. The IC_{50} values from the cytotoxicity studies were calculated for both the pancreatic cancer cell line MIA PaCa-2 and normal cell lines (Vero cells) using GraphPad Prism. The selectivity which provides the relative cytotoxicity of the compounds was calculated by dividing the IC_{50} of the compound from normal cells by that of the cancerous cells. Antioxidant activity was calculated using Microsoft Excel and IC_{50} values were determined using GraphPad prism. Flow cytometer

data from the analysis of apoptosis and cell cycle was analyzed using FlowJo v10.07 (LLC) software and fold changes were determined. The p-value was calculated using the student's t-test and $p < 0.05$ was considered statistically significant.

CHAPTER 2:

Materials and methods

2.1 Ethical consideration

Ethical clearance waiver for this study was obtained from the University of Witwatersrand Human Ethics Committee (Medical) (Clearance certificate W-CBP-200302-01) (Appendix A)

2.2 Methodology

A flow diagram representing the steps undertaken in this study is shown in Figure 2.1.

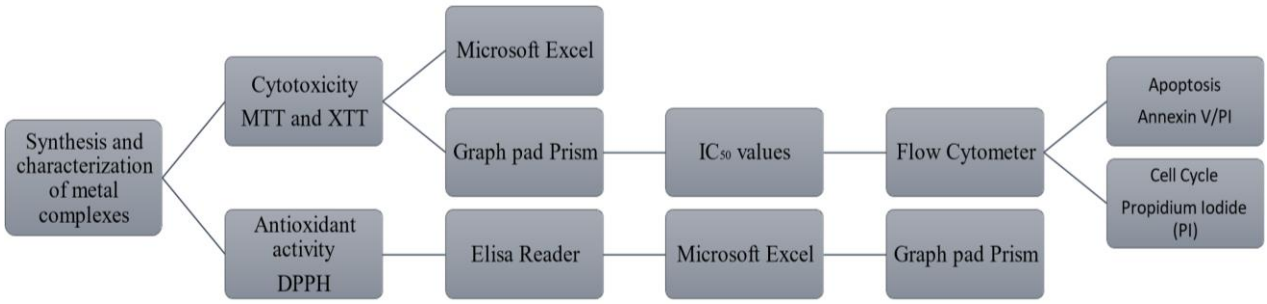

Figure 2.1: Flow diagram illustrating overall methodology.

2.2.1 COMPOUND SYNTHESIS AND CHARACTERIZATION

The synthesis of the ligands and complexes was done by collaborators at the Department of Chemistry, University of Namibia. Selected ligands were characterized by infrared spectroscopy while others were characterized using ^{1}H NMR spectroscopy, see Appendix B for images.

2.2.2 Synthesis of Ligands

The Ligands were synthesized based on Schiff‘s base reaction procedures with slight modifications according to the literature (Endjala et al., 2021) as follows. The ethanolic solution (15 ml) of 1 (Salicylaldehyde), (0.5g, 1 mmol) was mixed with a solution (15 ml) of 2 (Amino-2,1,3-benzothiadiazole) (0.6g, 1 mmol) in ethanol, while magnetically stirring, and catalyzed with a few drops of acetic acid. The solution was refluxed for four hours, before a yellowish precipitate appeared in the solution, upon room temperature cooling. The precipitate was filtered off and washed with ethanol several times. The product was dried in a vacuum at room temperature and recrystallized in ethanol.

L1 (1 is Salicylaldehyde, 2 is Amino-2,1,3-benzothiadiazole): Yield 80%; ^{1}H NMR (500 MHz, DMSO) δ 9.78, (s, H_{OH}), 8.56 (s, 1H_{CH}), 8.09 (s, H_{ben}), 7.97 (s, H_{ben}), 7.84 (s, H_{ben}), 7.56 (s, H_{ben}), 7.50 (s, H_{ben}), 7.44 (s, H_{ben}), 7.38, 7.11 (s, H_{ben}) (Figure S2).

L2 (1 is 4-phenylthiosemicarbazide, 2 is 1,8-naphthalic acid anhydride): Yield 74%; ^{1}H NMR (500 MHz, DMSO) δ 9.78, (s, H_{OH}), 8.56 (s, 1H_{CH}), 8.09 (s, H_{ben}), 7.97 (s, H_{ben}), 7.84 (s, H_{ben}), 7.56 (s, H_{ben}), 7.50 (s, H_{ben}), 7.44 (s, H_{ben}), 7.38, 7.11 (s, H_{ben}), (Figure S3).

L3 (1 is methyl hydrazinecarbodithioate, 2 is 1,8-naphthalic acid anhydride): Yield 88%; ^{1}H NMR (500 MHz, DMSO) δ 12.43 (d, H_{NH}), 8.60 (s, H_{ben}), 7.96 (s, H_{ben}), 7.95 (s, H_{ben}), 7.93 (s, H_{ben}), 7.91(s, H_{ben}), 3.35, 2.68 (s, H_{CH}) (Figure S4).

2.2.3 Synthesis of the metal complexes (RuL1, AgL1, NiL3, AgL2, CuL2, FeL3, ZnL3, CuL3)

Metal complexes listed on (Table 2.1) were synthesized based on a known method by (Begum et al., 2023). A solution of $Ni(OAc)_2.4H_2O$ (0.125 mmol) in methanol (7 ml) was added to a solution of L_2 (0.25 mmol) in methanol (15 ml). The resulting mixture was stirred at room

temperature for 4 h. The dark reddish-brown precipitate that formed was filtered off, washed with methanol, and dried in vacuo over anhydrous $CaCl_2$. Dark reddish-brown NiL2 was obtained by slow evaporation from a mixture of chloroform and toluene (2:1). The corresponding copper(II), zinc(II), silver(I), and iron(II) complexes were prepared following the same procedure as described for NiL2, using $Cu(OAc)_2H_2O$, $Zn(OAc)_22H_2O$, $Fe(OAc)_23H_2O$ and $AgNO_3$ respectively. The products were recrystallized from a methanol solution, and characterization was carried out by FTIR and ^{1}H NMR (see Appendix B)

NiL3: Yield 62%; ^{1}H NMR (500 MHz, DMSO) δ 12.43 (d, H_{NH}), 8.60 (s, H_{ben}), 7.96 (s, H_{ben}), 7.95 (s, H_{ben}), 7.93 (s, H_{ben}), 7.91(s, H_{ben}), 2.68 (s, H_{CH}). (Figure S4)

RuL1: Yield 67%; ^{1}H NMR (500 MHz, DMSO) δ 12.04, (s, H_{OH}), 10.82 (s, 1H_{CH}), 8.09 (s, H_{ben}), 7.97 (s, H_{ben}), 7.84 (s, H_{ben}), 7.56 (s, H_{ben}), 7.50 (s, H_{ben}), 7.44 (s, H_{ben}), 7.38, 7.11 (s, H_{ben}). (Figure S5)

ZnL3: Yield 73%; ^{1}H NMR (500 MHz, DMSO) δ 12.43 (d, H_{NH}), 8.56 (s, H_{ben}), 8.54 (s, H_{ben}), 7.93 (s, H_{ben}), 7.90 (s, H_{ben}), 7.78(s, H_{ben}), 2.68 (s, H_{CH}). (Figure S6).

2.2.4 Cytotoxicity assays

We first determined the cytotoxicity of the compounds in high throughput screening assays using tetrazolium salts. From this, the inhibitory concentration values (IC_{50}) were determined from the concentrations range (0.78-100) µM. An ideal anticancer drug would be able to target cancer cell lines more effectively than healthy cells, and the ability of these agents to be highly selective toward cancer cells is therefore a quality that is advantageous for them to possess (Canga et al., 2022). Complexes containing essential elements may demonstrate more favourable outcomes compared to metal compound cancer treatments used in the past. This is because metal ions are more consistently homeostatic with human physiological conditions (Abdolmaleki et al., 2023). IC_{50} values that were obtained from these assays (please see Chapter 3: Results) were used for further apoptosis and cell cycle analysis.

2.2.5 Antioxidant assays using DPPH

The DPPH antioxidant assay was used to investigate the antioxidant activity of the synthetic drugs to induce oxidative stress which is a trademark for aging and contributes significantly to the advancement of cancers. It is well documented that antioxidants have medicinal significance, therefore drugs with strong antioxidant properties are said to treat some diseases (Raffenne et al., 2021).

2.2.6 Flow cytometry-based assays

Two different flow cytometry-based assays were used to further determine the mechanism of cell death for selected metal complexes where cytotoxicity from the tetrazolium salts had been observed. Cell number is regulated by a fine balancing act between cell death and proliferation. Cancer and viral infections are caused by cell accumulation through suppression of death, while degenerative diseases and developmental delays are caused by excessive death (Fotedar et al., 1996).

Table 2.1: Chemical structures of the ligands and metal complexes tested in this study.

Hydrazone Ligands	**Metal Complexes**	**Metal Complexes**	**Metal Complexes**	**Metal Complexes**
L1 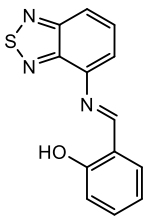	**RuL1** 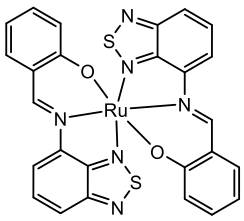	**AgL1** 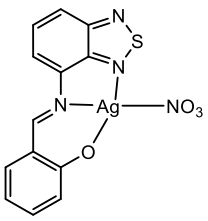		
L2 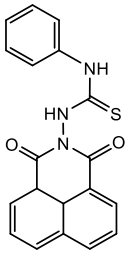	**NiL2** 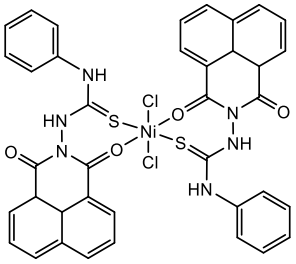	**AgL2**	**CuL2** 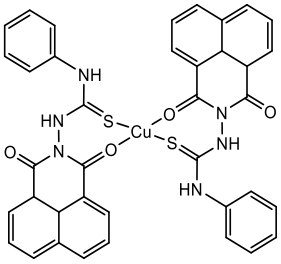	**ZnL2** 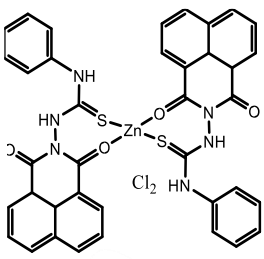

		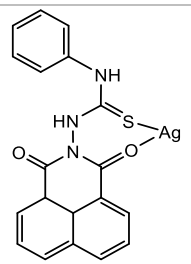		
L3	**NiL3**	**ZnL3**	**CuL3**	
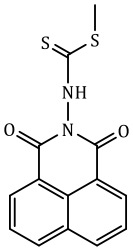	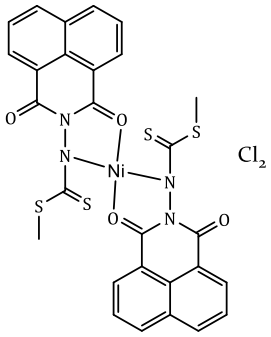	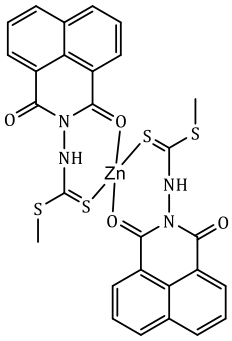	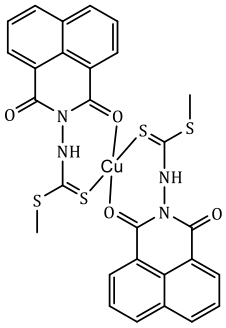	

2.3 COMPOUND PREPARATION

The working concentration of compounds was prepared using their Molecular weight (MW). The compounds were dissolved in tissue culture grade dimethyl sulfoxide (DMSO) (Sigma-Aldrich, St. Louis, MO, USA) and were stored at -20°C in single-use 10 µl aliquots at a stock concentration of 20 mg/ml. DMSO is known for its ability to dissolve both polar and non-polar molecules hence it was chosen as a solvent of choice (Karim et al., 2023).

Complete Dulbecco's Modified Eagle Medium (DMEM) (Sigma-Aldrich, St. Louis, MO, USA) supplemented with 10% heat-inactivated foetal bovine serum (FBS) (56°C, 30 minutes) was used to make up the compounds to 1 mg/ml concentration for the experimental treatments and further diluted to concentrations between 0.78 – 100 µM for the bioassays.

2.4 CELLS CULTURE

The pancreatic cell line, the MIA PaCa-2 cell, and the Vero cells were used to test the effect of the compounds. Both the MIA PaCa-2 cells and Vero cells are adherent. The MIA Paca-2 are human epithelial cells of the pancreas that were established in 1975 by Yunis and colleagues (Yunis et al., 1977) while the Vero cell lines are cells from an African green monkey kidney (Ammerman et al., 2008). The MIA PaCa-2 cells were obtained from the Japanese Collection of Research Bioresources (JCRB) Cell Bank (JCRB Cell Bank; Ibaraki, Japan). The MIA PaCa-2 cells were cultured in complete Dulbecco's Modified Eagle Medium (DMEM, Sigma-Aldrich, Missouri USA) supplemented with 3.7g/L of Sodium bicarbonate ($NaHCO_3$) (S5761, South Africa), 1% antibiotic antimycotic solution (10,000 units/mL of penicillin, 10,000 µg/mL streptomycin and 25 µg/mL amphotericin B). Complete DMEM was also used for the Vero cell line with slight modification and was further supplemented with 1.1 mM sodium pyruvate, 25 mM Hepes buffer, 250 µg/ml gentamicin, and 0.5% antibiotic antimycotic solution containing 10 000 units/mL of Penicillin, 10 000 µg/mL streptomycin and 25 µg/mL amphotericin B (Sigma-Aldrich, St Louis, MO, USA). Both media were supplemented with 10% inactivated foetal bovine serum (FBS, Celtic Molecular Diagnostics (Pty)Ltd, Cape Town, South Africa) for sub-culturing. Cell culture conditions were 37°C temperature, 5% carbon dioxide (CO_2), and 95% humidity.

Cells were propagated every 2-4 days depending on their confluence. Cells were harvested by rinsing the 75 cm^2 vented flasks (Thermo Fisher Scientific, Waltham, MA, USA) with phosphate-buffered saline (PBS). The PBS was discarded, the cells trypsinized, and trypsin-EDTA (Sigma-Aldrich, St. Louis, MO, USA) added to detach the cells after incubating for 2-3 minutes. The cells were centrifuged at 277 *xg* for 5 minutes at room temperature (23°C). The supernatant was discarded, and the pellet was resuspended in a complete growth medium. Cells were diluted 2x, and a haemocytometer was used for cell counting. The following equation (1) was used to calculate the concentration of cells that were harvested:

$$concentration\ of\ cells\ for\ cell\ treatment\ (cells/ml) = \frac{(number\ of\ cells\ counted)\ x\ (dilution\ factor)}{number\ of\ squares\ counted} \text{x } 1000 \quad (1)$$

2.5 CYTOTOXICITY ACTIVITY USING MTT AND XTT ASSAY

Cells were seeded in a 96 well plate (Thermo Fisher Scientific, Waltham, MA, USA) at a concentration of $1x10^5$ unless otherwise stated, to a volume of 100 µl in each well and incubated for 24 hours to allow the cells to adhere to the surface of the plate. The cells were treated with different concentrations of test compounds, the positive control, gemcitabine and vehicle control containing DMSO (1%). The compound (20 mg/ml) stock in DMSO was further diluted to a concentration of 1 mg/ml using complete DMEM. Following further dilutions, the compound was tested at a final concentration of 0.78 – 100 µl of the test compounds. Each compound was tested in triplicate and a serial dilution was done from high to low concentrations (100 – 0.78 µM). Cells were further incubated for 72 hours after treatment at 37°C, 5% (CO_2), and 95% humidity.

The plates were centrifuged at 277 *xg* for 5 minutes at 25°C using a universal 320R benchtop plate centrifuge. The supernatant was carefully removed making sure cells were not disturbed. A master mix with concentration of 5 µg/mL (100 µl of the medium and 10 µl of the MTT solution) was added and placed in the dark. The plates were wrapped with foil and allowed to incubate for 4 hours. A deep purple formazan colour change was observed consisting of crystals. The formazan crystals were dissolved by the process of solubilization by substituting the media that contained MTT with 100 µL of a hydrochloric acid-isopropanol (1:9) solubilizing reagent. This was then followed by additional incubation at 37 degrees Celsius with a humidity of 95% and a carbon dioxide concentration of 5% for a minimum of 15 minutes. This was followed by the measurement of absorbance at 570 nm and the background was read at 650 nm using the Multiscan Sky 384 microplate reader (Thermo Fisher Scientific, Waltham, MA, USA). The IC_{50} values were determined by first calculating the corrected absorbance by subtracting the background from the absorbance. A mean blank was determined from the cells only and medium only wells. The mean was subtracted from the corrected absorbance. Averages were calculated for each compound and viability determined (equation 2) and then cytotoxicity (equation 3) and standard deviations were calculated. GraphPad prism was used to calculate the IC_{50} from the standard deviations.

$$Viability = \frac{mean\ absorbance\ of\ sample}{mean\ absorbance\ of\ control} \text{ x } 100 \quad (2)$$

$$Cytotoxicity = 100 - Viability \quad (3)$$

In the case of XTT, the spent medium was discarded after centrifugation (200 *xg*, 5 min). The XTT master mix containing 100 µl medium and 25 µl XTT solution was added to each well to a total of 125 µl each and incubated for 4 hours at 37°C. Since metabolically active cells convert the water soluble XTT to orange coloured formazan, this experiment did not require a solubilisation step. The absorbance of the developed formazan was measured using a Multiscan Sky spectrophotometer (Thermo Fisher Scientific, Waltham, MA, USA) at a wavelength of 450 nm and a reference wavelength of 690 nm.

2.6 ANTIOXIDANT ACTIVITY USING DPPH ASSAY

The DPPH radical scavenging activity was carried out using a method that was slightly modified from the one described by Mbaebie et al. (2012).

L Ascorbic acid (Vitamin C) was used as positive control. The ligands and their metal complexes were tested at a range of concentrations between 0.78 – 100 µM. The compounds were dissolved in DMSO, and aliquots of stock concentrations stored as previously described. DPPH was prepared in the dark to avoid degradation at a concentration of 133.33 µM and stored in the dark. A solution of *L*-ascorbic acid was prepared at a concentration of 1100 µM. Briefly, 200 µl of dddH_2O was added to the first 9 wells of the first row of the plate and 110 µl was added to the last 3 wells on the first row and the rest of the plate. This was followed by the addition of 20 µl of the ligands and their metal complexes, Ascorbic acid and DMSO in the appropriate wells. A 110 µl serial dilution was performed, and 90 µl of DDPH was added in the dark to all wells except the wells of the blank (negative control). The plates were then covered with aluminium foil and placed in a dark cupboard at room temperature for 30 minutes. Absorbance was measured at 512 nm using the Multiscan^{TM} Sky 384 microplate reader

(Thermo Fisher Scientific, Waltham, MA, USA). Antioxidant activity was measured using the following formula:

$$\%\ Antioxidant\ activity = \left(\frac{Absorbance_{(control)} - Absorbance\ _{(sample)}}{Absorbance_{(control)}}\right) * 100 \quad (4)$$

Microsoft Excel was used to determine the % Antioxidant activity, the compound's ability to inhibit at least 50% of DPPH was assessed using a non-linear regression analysis in GraphPad Prism to produce dose-dependent curves.

2.7 APOPTOSIS DETECTION USING FITC ANNEXIN V DETECTION KIT

The mode of cell death induced by the ligands and their metal complexes on the MIA Paca-2 cells was determined using the BD FITC Annexin V apoptosis detection kit I (BD Bioscience, California, USA).

Apoptosis is expulsion of genetically altered cells through the programmed cell death mechanism with morphological classification that include loss of plasma membrane integrity. This happens in the early stage of apoptosis and leads to the externalization of phosphatidylserine (PS) (Cui et al., 2023). Ca^{2+} is dependent on phospholipid-binding protein, which has a strong affinity for PS, Annexin V employs the idea of exposing PS to the external cellular environment. FITC also aids in the labelling of apoptotic cells. While PI is used to identify dead cells from viable cells, it also labels dead cell DNA to help distinguish false positives from false negatives.

The assay was performed according to the manufacturer's protocol with slight adjustments (BD Biosciences, California, USA). Cultured cells were trypsinized and 1ml was seeded at $1x10^5$ cells/ml on a 24 well-plate and incubated for 24 hours. The cells were then treated with different concentrations of the ligands and metal complexes, vehicle control, positive control and incubated for 72 hours. The compound stock dissolved in DMSO (20 mg/mL) was further

diluted to the appropriate concentration. The concentrations of the compounds were those that showed IC_{50} results that were promising when compared to the positive control of the MTT assay. After 72 hours, the cells were harvested, and the supernatant was removed from the wells and added into a 5 ml Corning falcon tube. Each well was rinsed with 500 µl of 1xPBS and transferred to the respective labelled tubes. A 100 µl of accutase was added and incubated for 5 minutes to detach the cell and 1 ml of complete DMEM was added to inactivate the Accutase. The detached cells were transferred to the labelled tubes containing the rinsed supernatant. The cells were centrifuged at 277 *xg* for 8 minutes. The supernatant was discarded, and the pellet of cells was re-suspended in 2 ml of complete DMEM. The cells were allowed to recover from the trypsinization and were incubated for 45 minutes. After incubation cells were centrifuged for 8 minutes at 277 *xg* and supernatant discarded. The pellet of cells was washed with 2 ml PBS (8 minutes at 277 *xg*) before staining with 2 µl FITC Annexin V and PI respectively.

2.7.1 Staining of cells with FITC Annexin V/PI for flow cytometry

Various controls are used in flow cytometry. One of them is the compensation control which corrects for spillover between channels. After washing the cells with PBS, the compensation controls were prepared by fixing the cells using the BD Cytofix fixation/permeabilization solution. The cells were washed with a fix/perm buffer before they were single stained using Annexin V and PI. Fixed and unfixed untreated control cells were not stained as part of compensation control.

Experimental control treated cells were stained with both Annexin V and PI except the untreated unstained controls.

The treatment cells were washed with PBS, centrifuge for 8 minutes at 277 *xg* and the cells were resuspended in 100µl of the binding buffer (BD biosciences Annexin V-FITC apoptosis kit). Cells were then stained with 2µl of the Annexin V and ice incubated for 15 minutes, the tubes were removed from the ice and centrifuged for 8 minutes, and the supernatant was discarded. The cells were resuspended in 100µl of the binding buffer, and 2µl of PI was added,

then incubated for 15 minutes on ice in an enclosed Styrofoam box. The reaction was stopped by adding 250 µl.

2.8 CELL CYCLE DETERMINATION USING PROPIDIUM IODIDE DYE

Following the 72 hours of treatment of cells, the Propidium iodide (PI) staining technique was used to determine the cell cycle of the cells. The cells were seeded at 2 x 10^6 cells/ml, then harvested, added to the labelled tubes through trypsinization and washed at 277 *xg*. The pellet was resuspended with 2 ml ice-cold 1xPBS, the supernatant was discarded and re-suspended in 1 ml 1xPBS, and 1 ml of 70% ice-cold ethanol (EtOH) was added in a dropwise manner while vortexing to avoid clumping. The cells were fixed at -20°C for at least 24 hours before staining with PI.

2.8.1 Staining with PI for Cell Cycle Analysis

PI was prepared at a concentration of 50 µg/ml and Ribonuclease A (RNase A) at a concentration of 100 µg/ml in 1xPBS. The fixed cells were removed from the -20°C freezer and placed at room temperature for at least 30 minutes. The cells were then centrifuged to obtain a pellet at high speed of 400 *xg*, for 10 minutes to enable improved pellet formation since the ethanol fixed cells are more buoyant. The cells were washed with 5 mL ice-cold 1xPBS, re-suspended in 1 mL 1xPBS and discarded. The pellet was re-suspended in 50 µl of RNase to cleave the RNA from the DNA. This was followed by the addition of 200 µl of PI stain to a final concentration of 0.1 µg/ml. The cells were allowed to stand in the dark for 30 minutes.

DNA quantification of cells was analyzed for the cell cycle by acquiring 30,000 events using a BD LSRFortessa Analyser and FACSDiva software (BD Biosciences, California, USA) with the fluorescent signal detected on a 530/30 filter and PI on a 610/20 bandpass filter.

2.9 Flow Cytometer Data Acquisition

Cells must pass through the uniformly bright centres of focussed laser beams for a flow cytometer to measure the optical characteristics of the cells with any degree of accuracy. To capture dispersed light and fluorescence from cells, light collection optics are directed toward the location where the laser beams intersect the cells. The sensing zone is situated inside a cuvette in some cytometers, and approximately 0.3 mm beneath the nozzle tip in stream-in-air cell sorters (Cossarizza et al., 2019). FITC excites at 488 nm and emits at 519 nm, whereas PI excites at 488 nm and emits at 620 nm. The Corning® round-bottom polypropylene tubes (The Scientific Group, Johannesburg, South Africa) containing the suspension of cells were analyzed for apoptosis and necrosis by acquiring 30 000 events using a BD LSRFortessa Analyser (BD Biosciences, California, USA) with FITC detected on a 530/30 filter and PI on a 610/20 bandpass filter. Data obtained from the FACSDiva Software (BD Biosciences, Franklin Lakes, NJ, USA) on the flow cytometer was exported as flow cytometry standard (FCS) files and analyzed on the FlowJo version 10.1.1 (FlowJo, LLC, Ashland, KY, USA).

CHAPTER 3

Results

3.1 CYTOTOXICITY DETERMINATION USING MTT ASSAY

3.1.1 Cytotoxic effect of gemcitabine on Vero and MIA Paca-2 cell lines.

The cytotoxicity effect of gemcitabine was assessed on both the Vero (non-malignant) cell line and the pancreatic cell line. As previously mentioned, gemcitabine is a drug used alone or in combination with chemotherapy in the treatment of pancreatic cancer. Treatment of MIA Paca-2 cells with gemcitabine produced a potent cytotoxic effect of 6.57 ± 0.63 µM than with the Vero cells 11.30 ± 0.04 µM (Figure 3.1).

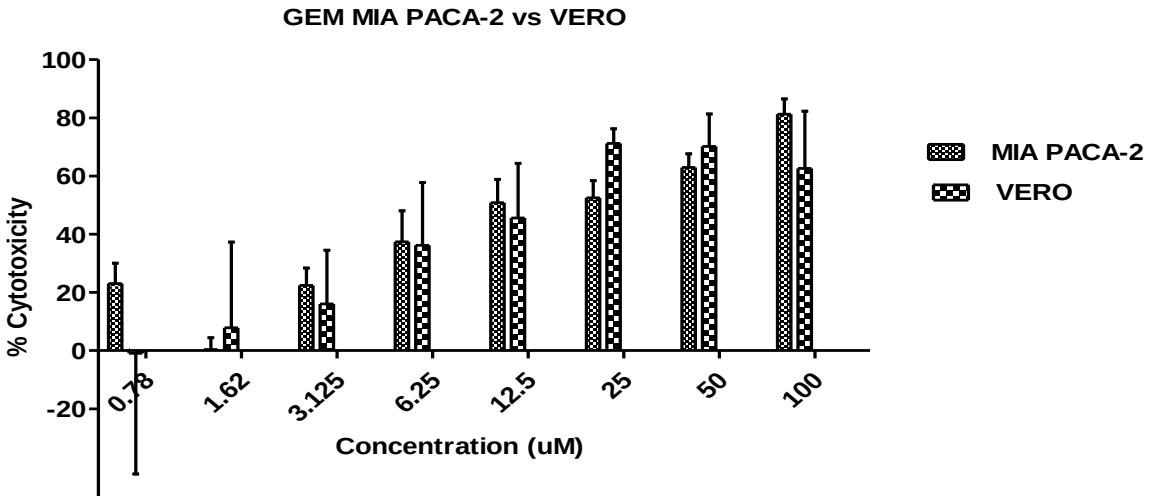

Figure 3.1: The cytotoxic effect of gemcitabine on MIA Paca-2 and Vero cells was evaluated after 72 hours using the MTT assay. Exposure to different concentrations (ranging from 0.78 to 100 µM) of gemcitabine led to a cytotoxic effect that was dependent on the dose, but only on the MIA Paca-2 cells. The results are presented as the mean± standard error of the mean (SEM), n= 4 independent repeats.

3.1.2 Cytotoxic effect of L1 and its metal complexes (AgL1 and RuL1) on MIA PaCa-2 and Vero cell viability

The effect of ligand 1 when compared to its corresponding complexes, ruthenium conjugate (RuL1) and silver conjugate (AgL1) on the MIA Paca-2 cells was measured. In this group of compounds, both AgL1 and RuL1 exhibited potent cytotoxicity to MIA Paca-2 cells with IC_{50} values of 1.55 ± 0.59 μM and 1.44 ± 0.61 μM respectively with the ligand having a value of 0.45 ± 0.25 μM.

The effect of compounds on the MIA Paca-2 was compared to that of the positive control, gemcitabine, on different test concentrations. It was noted that at concentrations of 12.5 μM and 100 μM gemcitabine and AgL1 showed statistically significant effects ($p < 0.05$). Additionally, RuL1 exhibited notable statistical significance effect ($p < 0.05$ at 50 μM and $p < 0.01$ at 100μM). The cytotoxic effect of AgL1 on the Vero cells was 2.32 ± 0.57 μM

During the testing of the non-malignant cell line (control cell lines), both the ligand and metal complexes showed a strong cytotoxic effect (Appendix E). The ligand had a potency of 7.85 ± 3.5 μM, while the metal complex RuL1 had a lower cytotoxic effect on normal cells, with an IC_{50} of 36.12 ± 12.78 μM, compared to gemcitabine IC_{50} of 7.24 ± 0.66 μM as seen on table 3.1

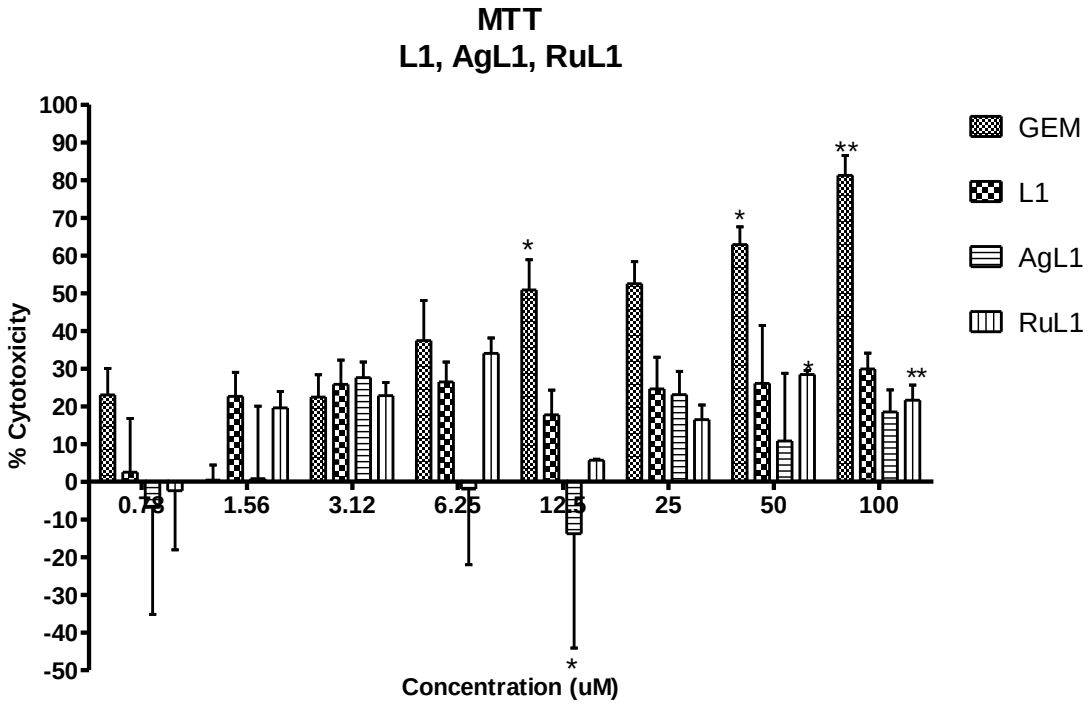

Figure 3.2: The cytotoxic effect of L1 and its metal complexes (AgL1 and RuL1) on MIA Paca-2 cells was assessed using the MTT assay. MIA PaCa-2 cells were treated with L2 and its metal complexes at concentrations ranging from 0.78 to 100 µM for 72 hours at 37°C (95% humidity, 5% CO_2). AgL1 and RuL1 showed significant cytotoxicity against MIA Paca-2 cells, with IC_{50} values of 1.55 ± 0.59 µM and 1.44 ± 0.61 µM, respectively, and a ligand of 0.45 ± 0.25 µM. AgL1 demonstrated a significant difference at 12.5 µM and 100 µM ($p < 0.05$). RuL1 was statistically significant ($p < 0.05$ at 50 µM and $p < 0.01$ at 100 µM). The results are presented as the mean± standard error of the mean (SEM), n= 4 independent repeats, $p < 0.05$.

3.1.3 Cytotoxic effect of L2 and its metal complexes (AgL2, NiL2, ZnL2, CuL2)

Among all the four complexes of L2 tested (AgL2, NiL2, ZnL2, CuL2), NiL2 showed a noticeable effect with a cytotoxic potency (IC_{50} of 1.25 ± 0.71 µM) on MIA Paca-2 cells. The ligand showed an IC_{50} of 21.41 ± 14 µM. At a concentration of 12.5 µM, NiL2 and CuL2 showed statistical differences with p-value < 0.05 and < 0.01, respectively, when compared to gemcitabine. The cytotoxic effect of the complexes of L2 on the normal cell line varied, with the ligand exhibiting an IC_{50} value of 7,50 ± 3,1 µM and complexes AgL2, NiL2, ZnL2, CuL2 33,90 ± 14,8 µM; 1,65 ± 0,72 µM ; 3,34 ± 0,20 µM; 2,33 ± 0,57 µM respectively as tabulated on table 3.1. AgL2 was least cytotoxic toward the Vero cells.

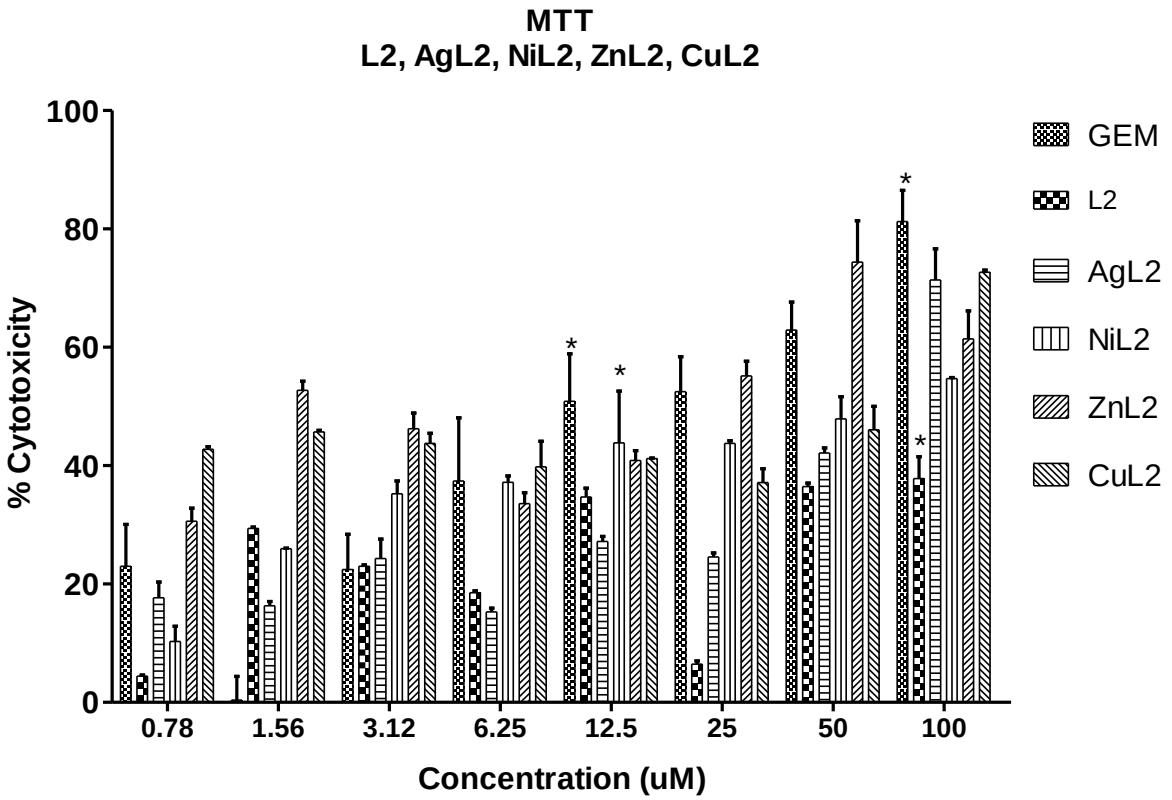

Figure 3.3: Cytotoxic effect of L2 and its metal complexes (AgL2, NiL2, ZnL2, CuL2) on MIA Paca-2 cells was assessed using the MTT assay tested at concentrations ranging from 0.78 to 100 µM. NiL2 was the most potent against MIA Paca-2 with an IC_{50} of 1.25 ± 0.71 µM. The results are presented as the mean± standard error of the mean (SEM), n= 4 independent repeats, $p < 0.05$.

3.1.4 Cytotoxic effect of L3 and its metal complexes (CuL3, NiL3, ZnL3)

The three tested metal complexes of ligand 3 exhibited low cytotoxicity (below 40%). Table 3.1 shows the IC_{50} values of all the tested compounds. Highlighted are the compounds which had an anticancer potential when compared to gemcitabine. We compared across all tested concentrations and a Bonferroni post-test was used to compare the cytotoxicity between treatment of all drugs, and at 12,5 µM gemcitabine and CuL3 **($p < 0.001$) and L3, CuL3 and NiL3 *($p < 0.05$) as per Figure 3.4.

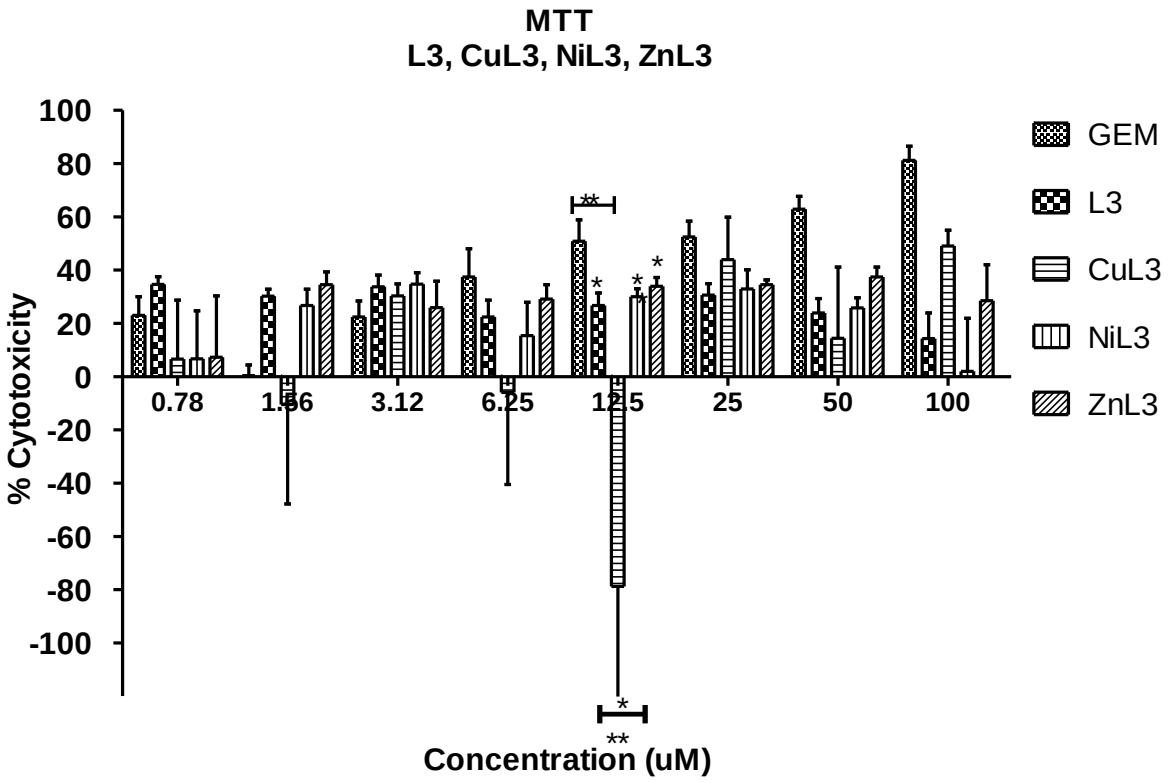

Figure 3.4: Cytotoxic effect of L3 and its metal complexes (CuL3, NiL3, ZnL3) on MIA Paca-2 cells was assessed using the MTT assay. MIA PaCa-2 cells were treated with L3 and its metal complexes at concentrations ranging from 0.78 to 100 µM for 72 hours at 37℃ (95% humidity, 5% CO_2). Compared to the positive control gemcitabine, their potency observed for L3 was minimal. The results are presented as the mean± standard error of the mean (SEM), n= 3 independent repeats.

3.1.5 Comparison of metal complexes with the same metal but coupled to different ligands.

Out of the 12 synthesized metal complexes, 8 had the same metal element coupled to different ligands. The below listed metal complexes' cytotoxicity were compared against each other.

AgL1	**AgL2**
NiL2	**NiL3**
CuL2	**CuL3**
ZnL2	**ZnL3**

None of these compounds showed any statistical significance with the exception of NiL2 and NiL3 which showed a statistical significance on the tested concentration of 100 µM $p < 0.05$ (see Appendix C)

Table 3.1: The Comparison of IC_{50} values when cells were treated with the Ligands and their metal complexes using MTT and XTT assays.

Tested compounds	**MIA Paca-2 MTT**	**MIA Paca-2 XTT**	**Vero Cells MTT**
	IC_{50} (µM)	IC_{50} (µM)	IC_{50} (µM)
Gemcitabine	6.57	8.80	7,14
L1	0,44	8,41	7,80
AgL1	**1,55**	13,63	2,31
RuL1	**1,47**	30,60	27,87
L2	21,41	12,99	7,50
AgL2	51,54	115,65	33,90
NiL2	**1,24**	16,27	1,65
ZnL2	91,40	1,70	3,34
CuL2	3,39	265,98	2,33
L3	0,02	0,90	
CuL3	147	14,51	15,56
NiL3	1146,23	21,66	13,56
ZnL3	50,72	16,16	7,14

*__Bold__ is showing compounds that had potent cytotoxicity using MTT

3.1.6 Cytotoxicity effect of the Compounds using XTT assay

The compounds that exhibited cytotoxic effects when the MTT assay was used did not exhibit cytotoxicity in XTT see Table 3.1. The XTT assay failed to detect the effect of cytotoxicity with the exception of the ZnL2 complex which had a cytotoxicity of 1.70 ± 0.82 µM. Some compounds from the XTT assay results showed an improved cytotoxicity especially for L3 (appendix F and G). The IC_{50} values for the complexes CuL3 improved greatly with XTT when compared to MTT by (14.51 ± 8.4 µM vs 147 ± 13,2 µM); NiL3 (21.66 ± 14.34 vs 1146,23 ± 660 µM); ZnL3 (16,16 ± 10,31 µM vs 49,46 ± 11,99 µM).

3.2 POTENTIAL ANTIOXIDANT ACTIVITY USING DPPH ASSAY

DPPH Assay and *L* Ascorbic acid (Vitamin C) standards were used to test for the antioxidant potential of the ligands and their metal complexes. Ascorbic acid was used as a positive control. All the compounds were tested at a concentration ranging from (0.78 – 100) µM. The amount of antioxidant needed to reduce 50% of DPPH is represented by an IC_{50} value. The IC_{50} value of vitamin C was 6.42 µM suggesting that IC_{50} 's lower than that of the positive control suggests good antioxidant activity.

3.2.1 Antioxidant activity of Ligand 1 and its metal complexes (AgL1 and RuL1)

When comparing L1 and its metal complexes, RuL1 showed better antioxidant activity in the DPPH assay with an antioxidant activity of 5.11 ± 0,47 µM even better than vitamin C, with an IC_{50} of 6.42 ± 0.09 µM. Overall, there were dose dependent increases in antioxidant activity for both the ligands as shown on (Figure 3.5). The complexes and Vitamin C with L1 vs AgL1 showing a significant effect at 100 µM with $p < 0.05$, whereas L1 vs RuL1 exhibited a significant effect at the concentrations of 12.5 ± 1.99 µM, $p < 0.05$ and at 25 ± 2.98 µM, $p < 0.01$. The antioxidant activity of RuL1 against vitamin C was greatest at the concentrations of 0.78 µM ($p < 0.01$), 1.56 µM ($p < 0.001$), 3.12 µM ($p < 0.01$), 6.25 µM ($p < 0.001$), and 12.5 µM ($p < 0.001$). The AgL1 was significantly effective at a concentration of 25 µM ($p < 0.01$) and 50 µM ($p < 0.05$).

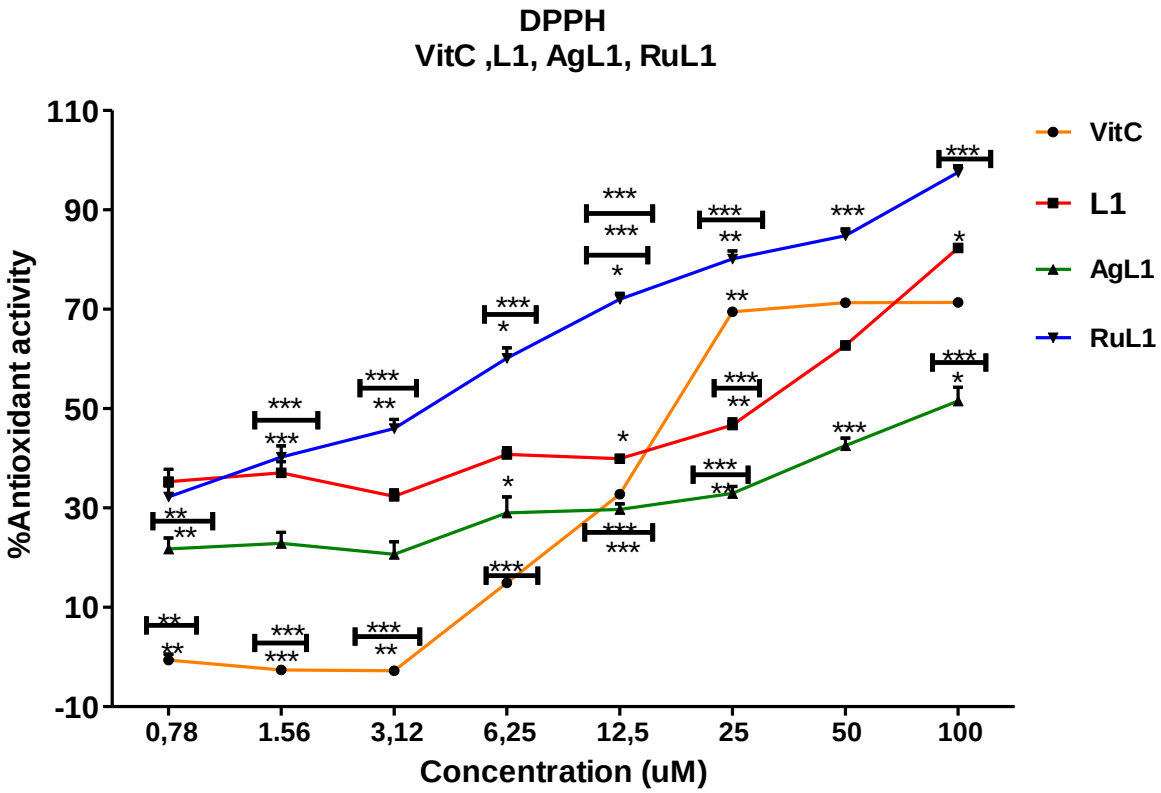

Figure 3.5: The Antioxidant activity of the ligands 1 and its metal complexes evaluated using DPPH. L1 and its metal complexes were tested at concentrations ranging from 0.78 to 100 µM. All the compounds resulted in a dose dependent manner of antioxidant activity with RuL1 being the most potent (5.11 ± 0.47 µM) compared to L1 and AgL1 and even Vitamin C, the positive control. P < 0.05), n=4, Data is presented as mean ±SEM.

3.2.1 Antioxidant activity of Ligand 2 and its metal complexes (AgL2, NiL2, ZnL2, CuL2)

When comparing ligand 2 and its metal complexes NiL2 and CuL2, administration with DPPH had no effect on antioxidant inhibition however AgL2 and ZnL2 exhibited a greater antioxidant activity of 4.90 ± 0.51 µM and 4.31 ± 0.51 µM respectively. Figure 3.6 shows dose dependent increases of antioxidant activity of all complexes. Comparing the tested concentrations, the ligand and AgL2 only showed a significant effect at 100 µM with $p < 0.05$. AgL2 and ZnL2 showed a significant antioxidant activity when compared to L2 at both concentrations of 50 µM and 100 µM (AgL2: 50 ± 7.82 µM, $p < 0.01$; 100 ± 11.33 µM $p < 0.001$); (ZnL2: 50 ± 6.97

µM; 100 ± 9.86 µM $p < 0.001$). Compared to VitC, L2 showed significant antioxidant activity at the concentrations 3.12 µM with $p < 0.05$; 25 µM with $p < 0.001$; 50 µM with $p < 0.01$. AgL2 exhibited a significant antioxidant effect on concentrations 25 µM with $p < 0.001$, 50 µM with $p < 0.001$ and 100 µM with $p < 0.001$ when compared to VitC. NiL2 showed the significant antioxidant effect on concentrations 1.56 µM with $p < 0.05$; 25 µM with $p < 0.001$, 50 µM with $p < 0.01$ when compared to VitC. ZnL2 showed significant antioxidant effects on concentrations 3.12 µM with $p < 0.05$; 25 µM with $p < 0.001$, 50 µM with $p < 0.001$, 100 µM with $p < 0.001$. CuL2 showed significant effect on concentrations 25 µM with $p < 0.001$; 50 µM with $p < 0.05$ and 100 µM with $p < 0.05$ when compared with VitC.

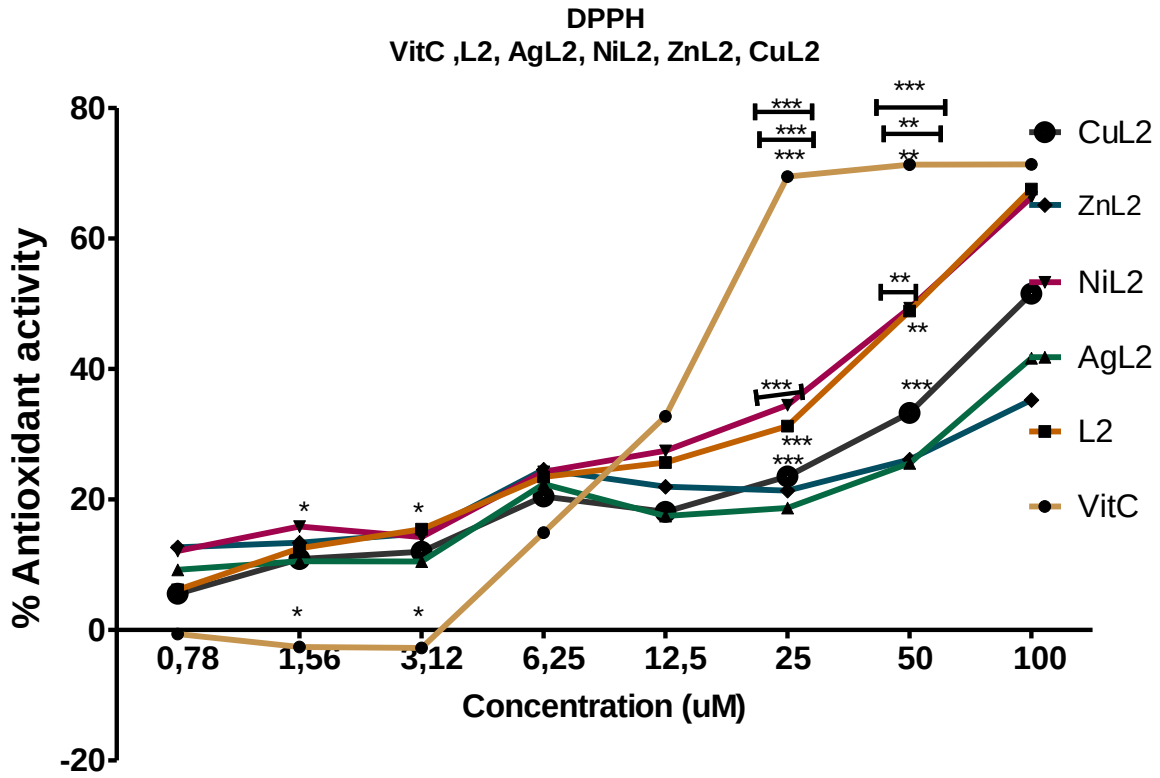

Figure 3.6: The antioxidant activity of the ligands 2 and its metal complexes evaluated using DPPH. Test concentrations for L2 and its metal complexes ranged from 0.78 to 100 µM. 50% inhibition was observed for AgL2 at 4.90 ± 0.51 µM and ZnL2 at 4.31 ± 0.51 µM, respectively. The ligand versus AgL2 only had a significant effect at 100 µM ($p < 0.05$). Each of the compounds exhibited dose-dependent antioxidant activity. Comparing L2 complexes to VitC at 25 µM revealed a significant effect ($p < 0.001$). In comparison to one another at 50 and 100 Test concentrations for L1 and its metal complexes ranged from 0.78 to 100 µM. At $p < 0.01$ and $p < 0.001$, every metal complex was statistically significant.

3.2.2 Antioxidant activity of Ligand 3 and its metal complexes (CuL3, NiL3, ZnL3)

When comparing L3 and its metal complexes, CuL3 and ZnL3 showed better antioxidant activity with IC_{50} of 4.25 ± 0.56 µM and 5.62 ± 0.28 µM in the DPPH assay when compared, with CuL3even better than VitC which had an IC_{50} of 6.42 ± 0.09 µM. Of the tested concentrations range of 0.78 – 100 µM the compounds were compared with VitC across the concentration range. The antioxidant activity of L3, CuL3, NiL3 and ZnL3 and VitC was greatest between (25 - 100) with $p < 0.01$, $p < 0.001$ as seen on Figure 3.7.

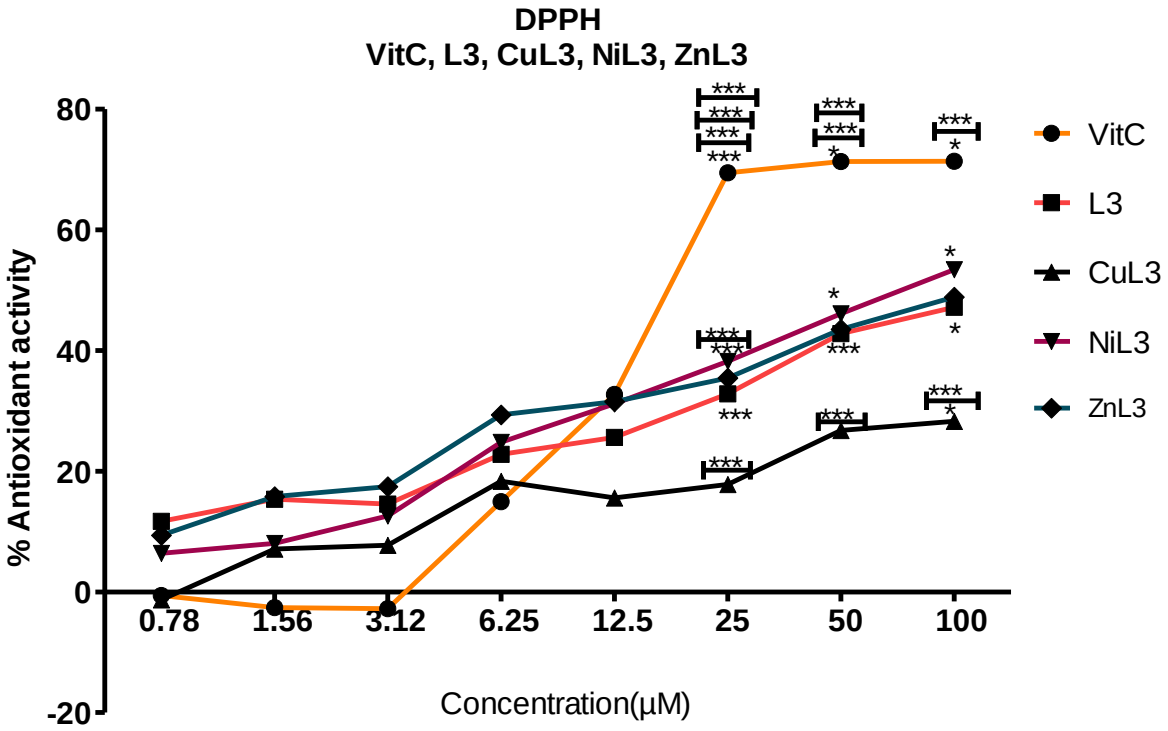

Figure 3.7: The antioxidant activity of the ligands 3 and its metal complexes evaluated using DPPH. CuL3, NiL3, ZnL3. CuL3 and ZnL3 showed higher 50% inhibition (4.25 ± 0.56 µM and 5.62 ± 0.28 µM). VitC vs L3 significantly impacted concentrations of 25 µM ($p < 0.001$), 50 µM ($p < 0.01$), and 100 µM ($p < 0.05$ Vitamin C and CuL3 significantly impacted concentrations of 25 µM, 50 µM, and 100 µM ($p < 0.001$). Compared to VitC, NiL3 showed significant effects at 25 µM ($p < 0.001$) and 50 µM ($p < 0.05$). VitC vs ZnL3 significantly impacted concentrations of 25 µM ($p < 0.001$), 50 µM ($p < 0.01$), and 100 µM.

3.2.3 Comparison of the antioxidant activity of the same metal complexes with different Ligands.

The below listed metal complexes were compared against each other based on the same metal coupled to different ligands.

AgL1	**AgL2**
NiL2	**NiL3**
CuL2	**CuL3**
ZnL2	**ZnL3**

When comparing CuL2 and CuL3, they only exhibit significant difference on the tested concentration at (100 µM, $p < 0.05$), see Appendix D, the rest of the compounds did not show any statistically significant differences in the antioxidant assays.

3.3 DETERMINING OF APOPTOSIS USING ANNEXIN V /PI ASSAY

3.3.1 Gating strategy used between cell populations.

The degree of apoptosis was evaluated using the double staining of Annexin V and PI. The amount of apoptosis has been deemed a good predictor of any prodrug or therapeutic compounds' anticancer potential (Fru et al., 2021). After 72 hours of incubation, MIA PaCa-2 treated cells were analyzed for the apoptotic activity. Using the BD LSRFortessa Analyzer (BD Biosciences, Franklin Lakes, NJ, USA) and the FACSDiva Software, at least 30,000 events were collected and recorded for every sample. Enough flow rate—less than 400 events per second—to allow for accurate cell classification (Mosiane et al., 2023). FCS files were exported and analyzed in FlowJo 10.9.0 to gate the appropriate cell populations. For apoptosis analysis, dot plots for annexin V and PI are defined by four quadrants, Q1 region, necrotic cells

(Annexin V−/PI+); Q2, late apoptotic cells (Annexin V+/PI+); Q3, early apoptotic cells (Annexin V+/PI−) and Q4, viable cells (Annexin V−/PI−) (Chen et al., 2020). These quadrants are used to describe populations of cells as per Figure 3.9.

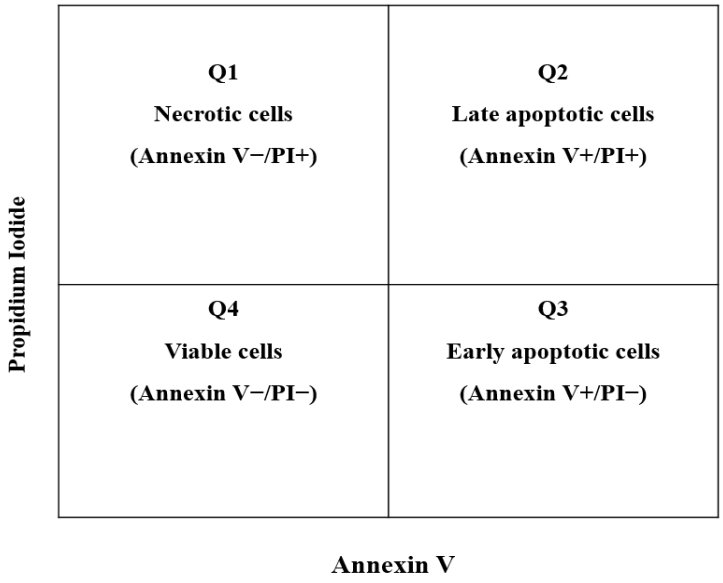

Figure 3.9: A quadrant plot of AnnexinV/PI double staining. This figure depicts the four quadrants used to distinguish between cell populations. Annexin V-/PI+ showing necrosis (Q1). The AnnexinV+/PI+ cells represent cells that had undergone late apoptosis (Q2). Annexin V+/P- denotes cells that have undergone early apoptosis (Q3) and Annexin V-/PI- are viable cells (Q4).

Each sample was analyzed with 30 000 counts recorded, debris was excluded by the gating forward scatter (FSC –A) and side scatter (SSC-A) dot plots (A), following this, the FSC-A vs. FSC-H (B) gate was used to separate single cells (also known as the parent 1 or P1 population) and omit doublets. To distinguish between cells progressing through the various stages of cell death (apoptosis and necrosis), the last gate was a quadrant gate. Curly quadrant plots (C), which are exponentially based quadrilateral gates that can divide the cells according to their fluorescence signals, were used to achieve this as shown in Figure 3.10.

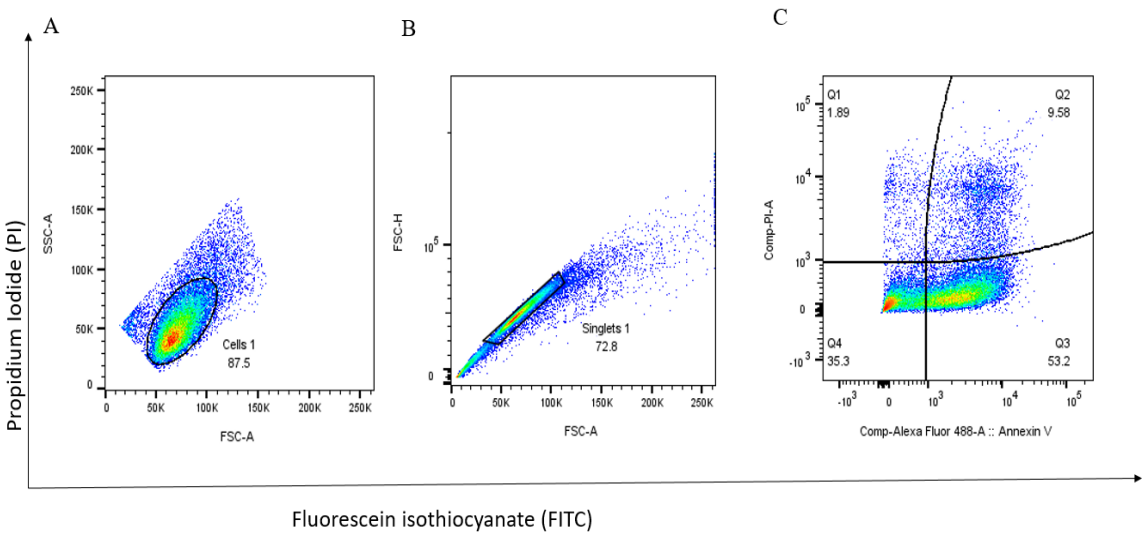

Figure 3.10: Gating strategy to identify the mode of cell death. FlowJo was used to gate cell populations. First debris was excluded using a threshold of 5000 on SSC to identify the cell population using FSC-A and SSC-A (A). This was followed by singlet discrimination plots (B). To differentiate cell death the fluorescent signals from the FITC and PI dyes (C) were used, Q1 (necrosis), Q2 (late apoptosis), Q3 (early apoptosis), and Q4 (viable cells).

3.3.2 Induction of cell death following treatment with L1 and metal complexes AgL1 and RuL1 on MIA PaCa-2 cells

Administration of AgL1 and RuL1 to the MIA Paca-2 cells induced early apoptosis (Q3) of 7.75% and 14.33% in comparison to the L1 (1.3%) at 1.48 μM for AgL1 and 1.55 μM for RuL1. Coupling the ligand with a metal certainly improved the induction of apoptosis. Regarding viability (Q4), cells treated with AgL1 remained 76.12 ± 2.05 % live and 68.6 ± 3.8 % for RuL1 remained viable.

When comparing the L1 and corresponding metal complexes to gemcitabine which induced early apoptosis of 47.2%, late apoptosis of 9.0% and 2% necrosis there were statistically significant differences for early apoptosis with a p-value of $p < 0.001$. Figure 3.12 displays the average quantities of cells at the different cell death phases i.e. apoptosis versus necrosis based on their annexin V-positive or PI-positive staining status. Necrosis on the untreated MIA Paca-

2 cells stained with AnnexinV/FITC was observed (2.31 ± 0.3%), which we believed could have been caused by trypsinization and injury that occurred during pipetting.

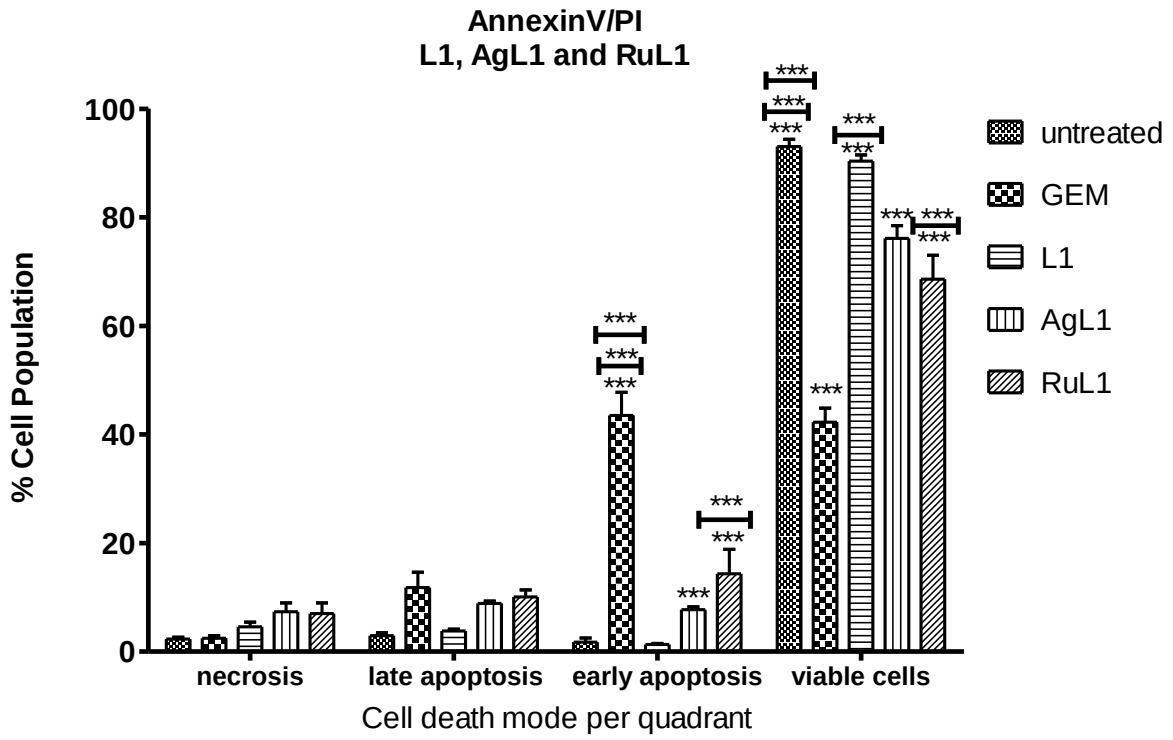

Figure 3.11: Cell death was induced in MIA PaCa-2 cells following a 72-hour treatment with L1, AgL1, RuL1 using the Annexin V/PI assay. Majority of cells treated with L1, AgL1 and RuL1 maintained their viability. A very small proportion of the cells experienced necrosis. The majority of the cells treated with gemcitabine exhibited early apoptosis. The bar graph depicts the four cell statuses with the mean values and standard error of the mean (SEM) indicated. The number of experimental repeats for each treatment was n=4, with $p < 0.05$.

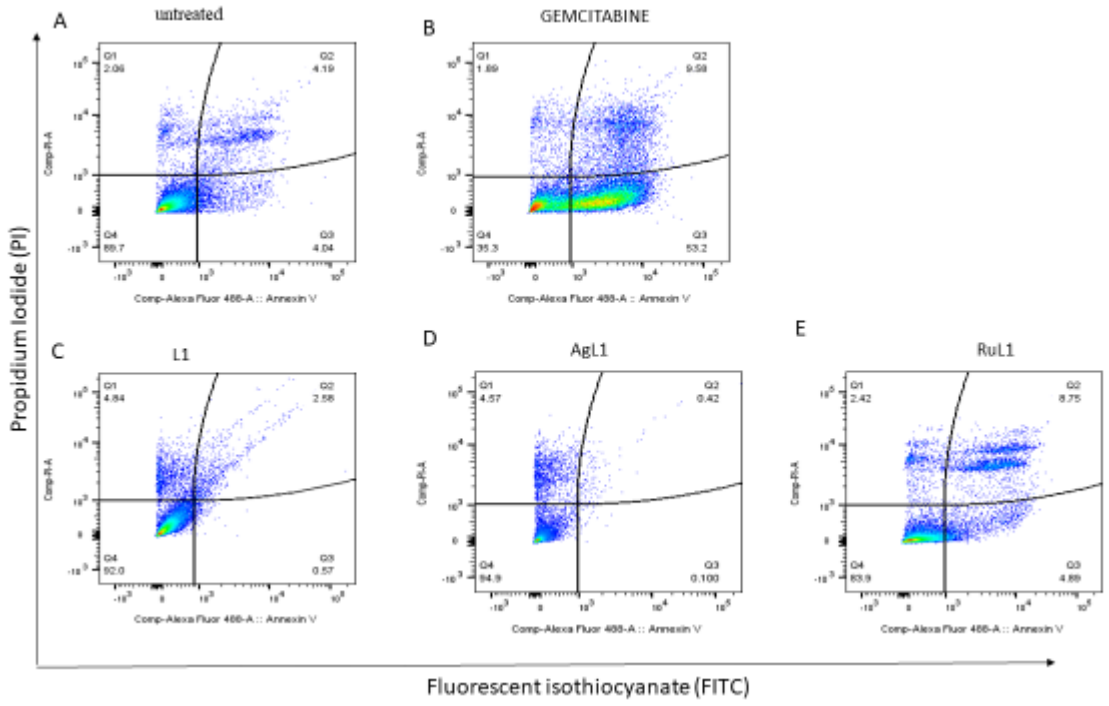

Figure 3.12: Cell death was induced in MIA Paca-2 cells following a 72-hour treatment with L1, AgL1 and RuL1 using the Annexin V/PI assay. Representative dot plots illustrating the presence of (Q1) necrotic cells, (Q2) late apoptotic cells, (Q3) early apoptotic cells, and (Q4) live cells. A very small proportion of the cells on RuL1 experienced necrosis however AgL1 experienced necrosis of almost 5%. The majority of the cells treated with gemcitabine exhibited early apoptosis while some of the cells remained viable.

3.3.3 Induction of cell death following treatment with L2 and metal complexes NiL2

After MIA Paca-2 cells were subjected to treatment with IC_{50} of 1.25 µM of the ligand and NiL2, the ligand induced apoptosis at 7.99 % and the complex 11.90 %.

In comparison to L2 the administration of NiL2 to MIA Paca-2 cells resulted in the metal complex inducing apoptosis. A majority of the cells remained viable despite treatment with the compounds. When compared to the untreated cells, L2 and NiL2 had a percentage viability of 78.48% and 78.03% respectively. A comparison of the untreated cells across all quadrants whether they induced late apoptosis and/or necrosis was performed. It was notable that L2 showed late apoptosis for the range between (6-8) % and necrosis (4-6) % as seen in Figure 3.13.

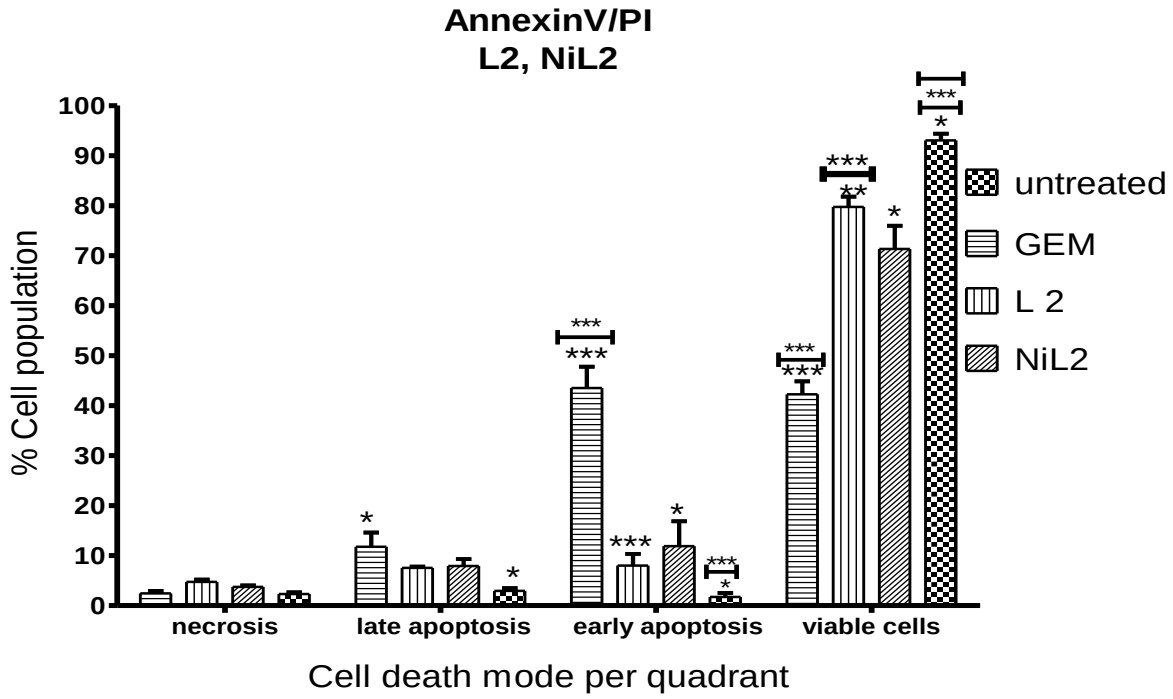

Figure 3.13: Cell death was induced in MIA Paca-2 cells following a 72-hour treatment with L1 and AgL1 using the Annexin V/PI assay. The majority of cells treated with L1 and RuL1 maintained their viability. A very small proportion of the cells experienced necrosis. The majority of the cells treated with gemcitabine exhibited early apoptosis while some of the cells remained viable. The graph depicts the four cell statuses following treatment, with the mean values and standard error of the mean (SEM) indicated, n=3

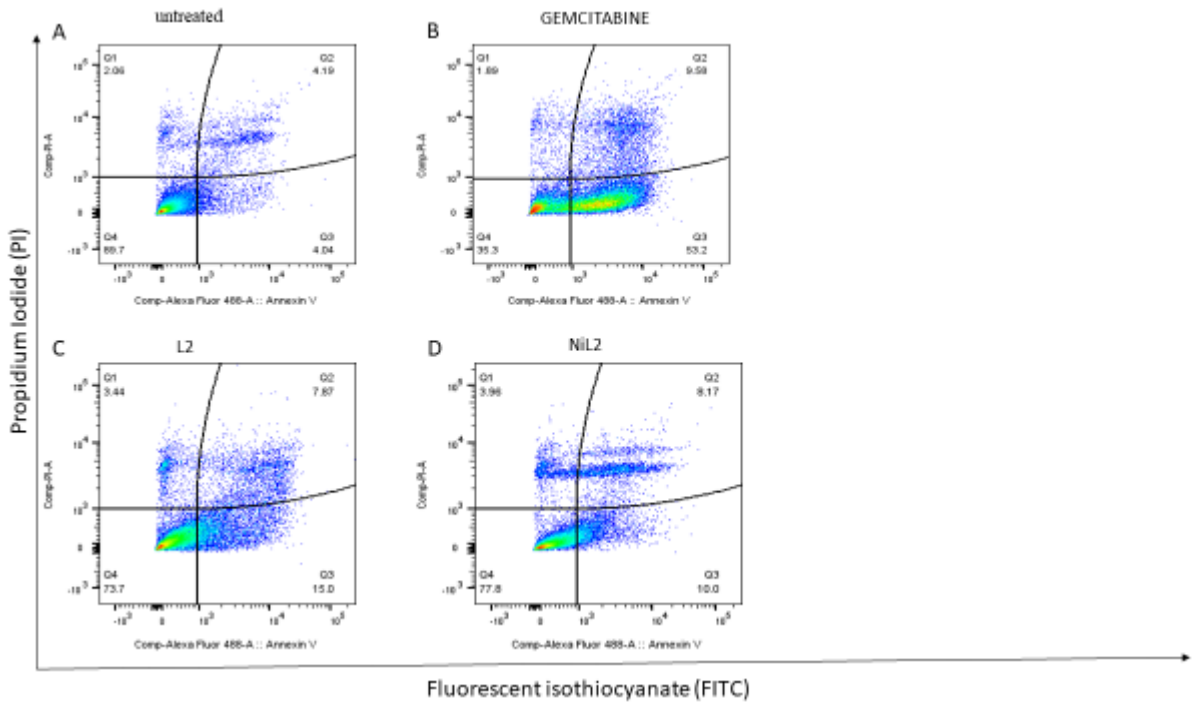

Figure 3.14: Cell death was induced in MIA Paca-2 cells following a 72-hour treatment with L2 and NiL2 using the Annexin V/PI assay. Coupling of L2 with metal Ni did not improve the apoptotic effect of NiL2. Representative dot plots illustrating the presence of (Q1) necrotic cells, (Q2) late apoptotic cells, (Q3) early apoptotic cells, and (Q4) live cells.

3.4 CELL CYCLE DETERMINATION USING PROPIDIUM IODIDE

Flow cytometer was used to identify and quantify MIA Paca-2 cells in different phases of the cell cycle to determine the possible cell cycle arrest before and after treatment with AgL1 (1.48 µM), 1.55 µM of RuL1 and 1.25 µM of NiL2.

Membrane integrity is one of the best indicators of cell proliferation (Santa-González et al., 2020). Figure 3.15 illustrates the gating strategy used to determine the induction of cell proliferation in the cell cycle phases of the MIA-Paca-2 cells.

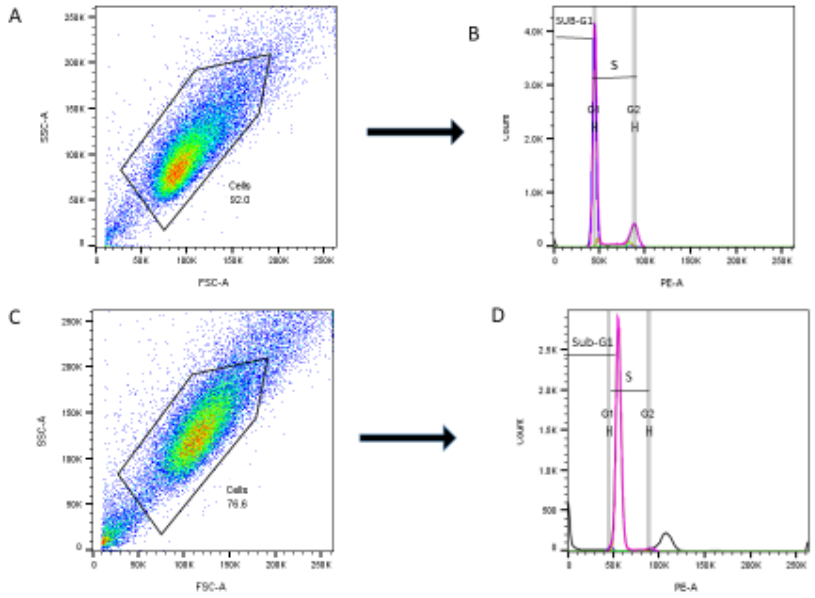

Figure 3.15: Gating strategy used for cell cycle analysis. The FCS files acquired from the flow cytometer using the FACSDiva software were gated using the FlowJo software. Gating was used to select cells of interest based on SSC-A vs FSC-A values (A&C), and then their cell cycle status was analyzed. The histograms display the quantification of DNA content using PI. A&B are the untreated control and C&D is positive control gemcitabine.

3.4.1 Effect of L1, AgL1 and RuL1 treatment on the MIA PaCa-2 cell cycle.

The DNA histograms and cell percentages for each phase are presented on Figure 3.17 shows untreated control cells, positive control cells treated with gemcitabine and cells treated with metal compounds whose concentration was determined from the IC_{50} values in the cytotoxicity studies. According to research, the presence of cells in the sub-G_1 phase implies the activation of apoptosis since this phase represents hypodiploid cells with less DNA than the G_1 phase (Mosiane et al., 2023). Both the Ligand 1 and its complex AgL1 induced the sub-G_1 phase by 28 ± 2.97% and 18 ± 1.01%, respectively, even better than the positive control gemcitabine whose cell population on the sub-G_1 phase is 8.23 ± 0.57%. There was an increased cell population of 34.83% on the S phase for the L1 and 52 % for RuL1. In comparison with the untreated cells, AgL1 and RuL1 were statistically significant with a $p < 0.001$ value in the G1 phase and $p < 0.01$ in the S phase.

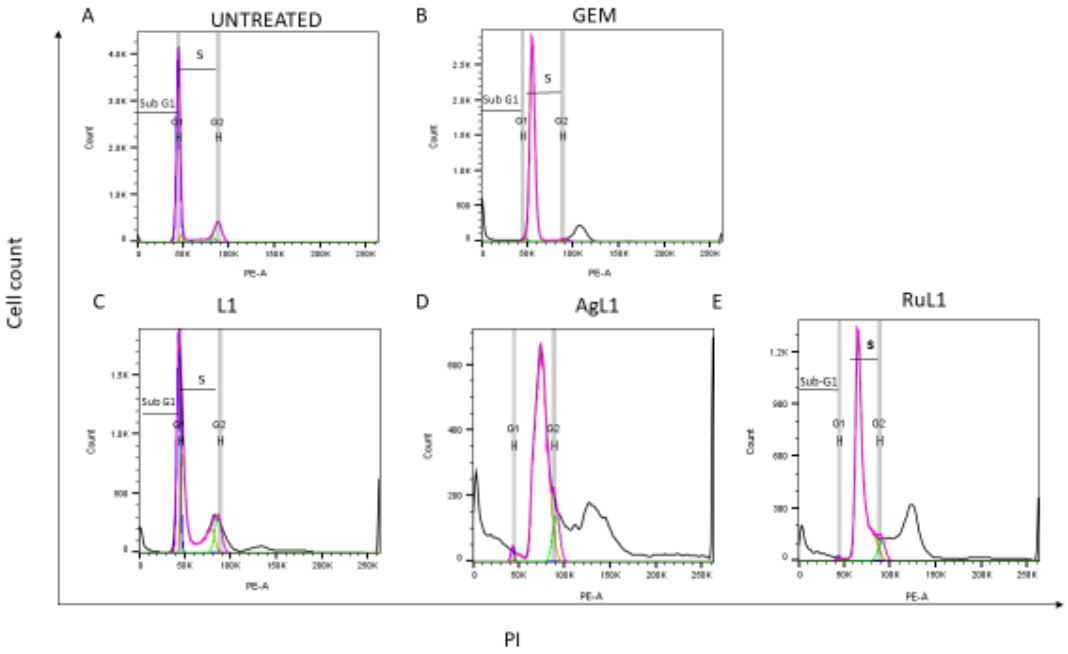

F

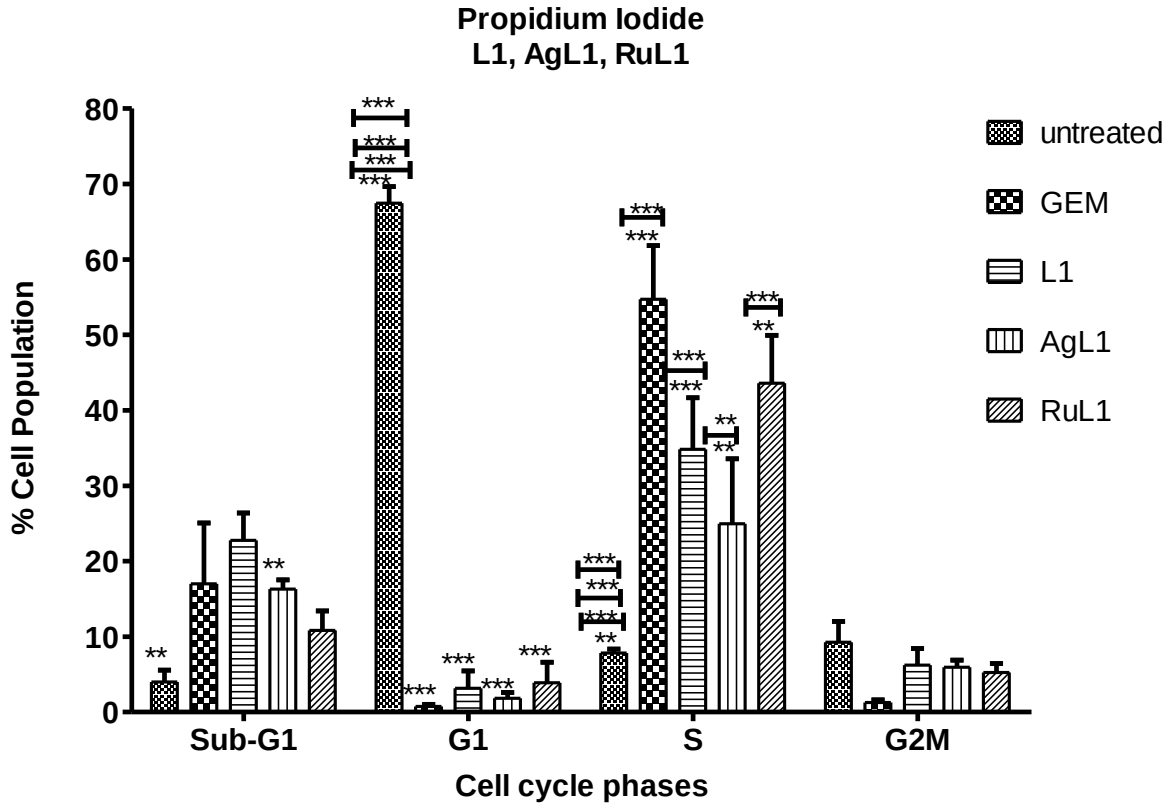

Figure 3.17: The Cell cycling status of MIA PaCa-2 cells post-treatment with L1, AgL1 and RuL1. (A) The histograms show untreated cells with distinct phases of the cell cycle indicated by the white (sub-G1), purple (G1/G0), yellow (S) and green (G2/M) peaks. Interval arrow lines were inserted to highlight the sub-G1 and S phases. (B) is the positive control gemcitabine.

D&E, both AgL1 and RuL1 caused a shift in arrest in the G1/G0 and an increment in apoptotic cells (sub-G1). The conjugates arrested cells in the S-phase. Quantitative bar graphs (F) indicating the overall cycling status of the pancreatic cancer cells (mean ± SEM), n=3, $p < 0.05$.

3.4.2 Effect of L2, and NiL2 treatment on the cell cycle

The effect on MIA Paca-2 cell cycle was analyzed after treatment with L2 and NiL2 for 72 hours. The NiL2 treated cells showed an increase in the sub G1 phase from 6.44 ± 1.45% to 16.9 ± 2.1% even better than the positive control gemcitabine whose cell population on the sub-G_1 phase is 8.23 ± 0.57%. However, for the L2 treated cells, increases were noted for the S phase by 36.4 ± 5.6% compared to the corresponding NiL2 metal complex (27.3 ± 10.35%, with the positive control gemcitabine cell population on the S phase being 39.85 ± 3.89%.

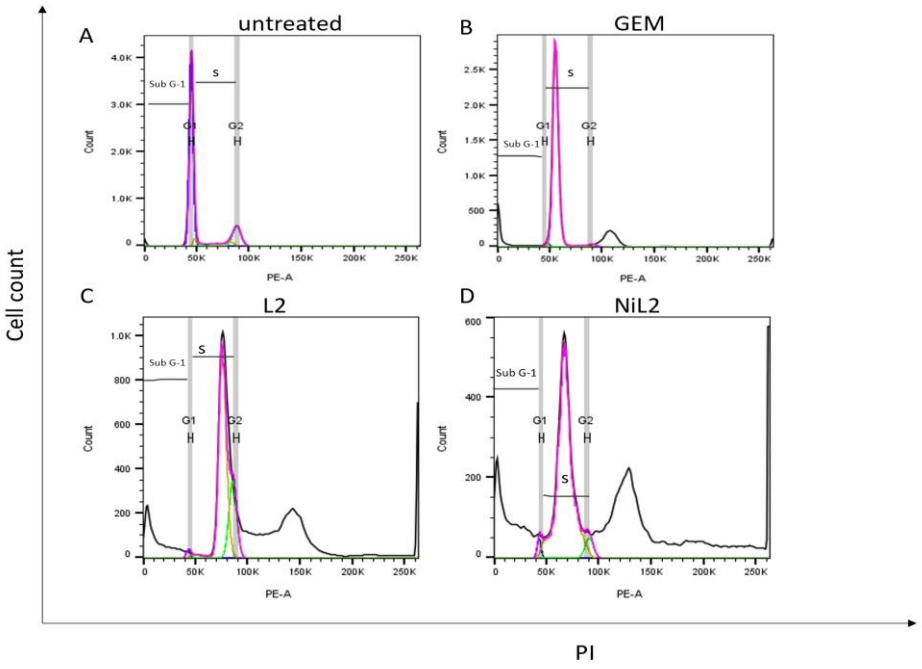

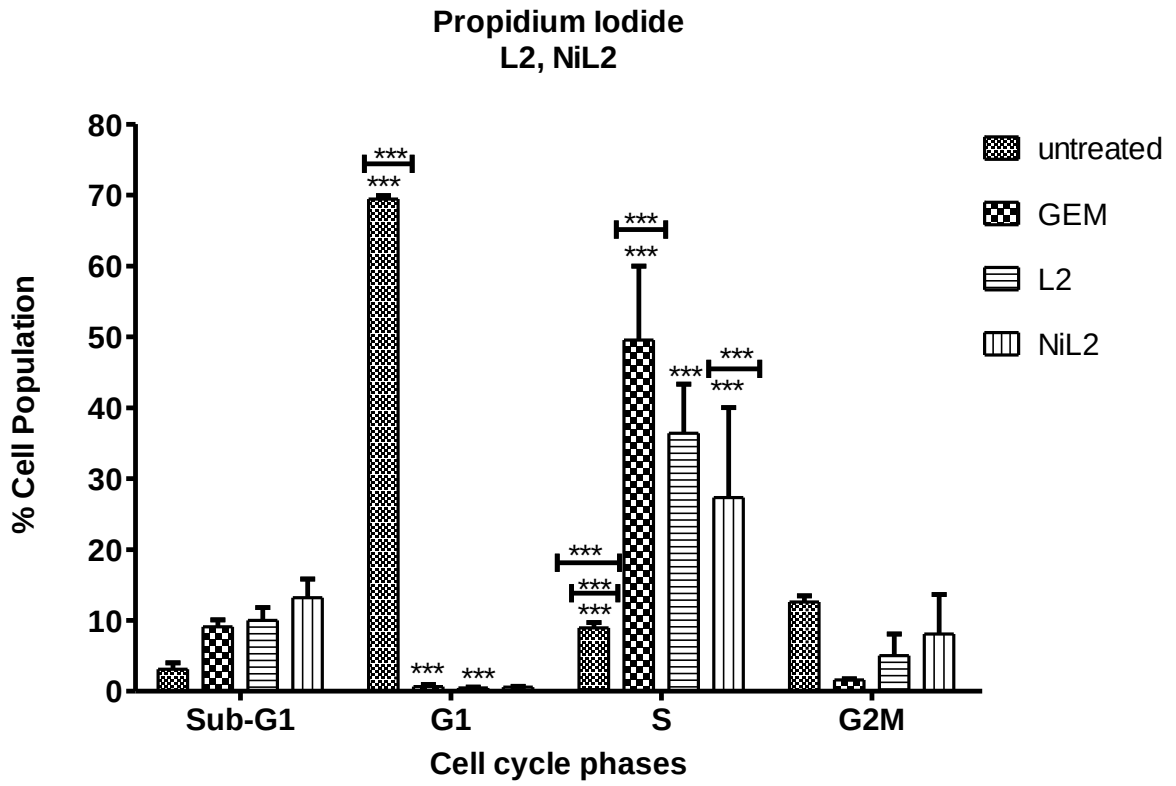

Figure 3. 18: Cell cycling status of MIA PaCa-2 cells post-treatment with L2 and NiL2. The histograms show the distinct phases of the cell cycle indicated by the white (sub-G1), purple (G1/G0), yellow (S) and green (G2/M) peaks. Interval arrow lines were inserted to highlight the sub-G1 and S phases. Both the L2 and NiL2 caused a shift in arrest and an increase in apoptotic cells (sub-G1). In addition, the ligand arrested cells in the S-phase. (F) Quantitative bar graphs indicating the overall cycling status of the pancreatic cancer cells (mean ± SEM), n=3, $p < 0.05$.

CHAPTER 4

Discussion

This study was aimed at investigating the potential anticancer activity of the free ligands L1, L2, L3 and corresponding conjugated metal complexes of AgL1 and RuL1; NiL2, AgL2, CuL2 and ZnL2; and NiL3, ZnL3 and CuL3 respectively. We assessed their cytotoxicity, antioxidant, mode of cell death at selected concentrations deduced from the high throughput tetrazolium dye based cytotoxicity assays (MTT and XTT) and their effect on the cell cycle. The findings were compared to the well-known and clinically used first line drug, gemcitabine.

Available chemotherapy for cancers including cisplatin, a metal-based drug, has brought about a significant transformation in the medical approach to cancer treatment in the last half of the 20th century (Cocetta et al., 2020). Unfortunately, these drugs continue to have uncomfortable side effects with the development of drug resistance. This continues to necessitate investigation for the identification and development of new drugs for the treatment of cancers including pancreatic cancer. It has been reported that the complexation of ligands to metal increases the anti-cancer activity.

4.1 CYTOTOXICITY ACTIVITY

In vitro cytotoxic studies serve as a basic test for efficacy of the chemotherapeutic drugs. Its evaluation is dependent on the calculation of viability of the monolayer of the cancer cell lines, in validating a predictive dose-dependent curve and the pronounced cytotoxicity is reflected by an IC_{50} value (Anthony et al., 2020). Herewith, the ligand and their metal complexes were evaluated for their cytotoxicity on the MIA Paca-2 and Vero cells using MTT and XTT assays. A dose-dependent cytotoxic effect was expected.

The metal complex NiL2 exhibited the greatest cytotoxicity with IC_{50} of 1.25 ± 0.71 µM, AgL1 and RuL1 induced cytotoxicity at IC_{50} of 1.47 µM and 1.55 µM, respectively. It has been shown that complexes of Cu(II), Co(II), Ni(II), and Zn(II) exhibit higher cytotoxic potency effects

when compared with their ligands and Cisplatin (Betanzos-Lara et al., 2012). It is the biologically active ligand clotrimazole (clotri) that has a synergistic effect on human cancer cell growth suppression by binding to these metal ions. In another study, findings showed that InsP6 and the InsP6-Ni(II) complex have cytotoxic and anti-proliferation effects on human acute leukaemia Jurkat T cells, suggesting that InsP6-Ni(II) could be developed as an anticancer drug (de Lima et al., 2015). A ligand H_2L and its complexes Zn(L)(EtOH)(H2O), Cu(L)$(H_2O)_2$] and [Ni(HL)(OAc)$H_2O)_3$ showed cytotoxic activity against HepG2 cell lines (El-Asmy et al., 2015). Zangrando and colleagues (2017) tested the same compounds we explored in this study for their antibacterial activity against the prevalent pathogens *Escherichia coli, Salmonella typhi* and *Shigella flexneri*, only ligand 1 showed antibacterial efficacy against all three tested pathogens with an inhibitory zone of 6-7 mm. Their results suggest that CuL2 has an antibacterial effect demonstrating distinct inhibitory zones against E. coli. There is consistency with ligand 1 as it is cytotoxic against the MIA Paca-2 cells with an IC_{50} of 0.45 ± 0.25 µM surpassing even its metal complex AgL1 and RuL1 with IC_{50} values of 1.55 ± 0.59 µM and 1.47 ± 0.61 µM, respectively.

4.1.1 Assessing the outcomes from both the MTT and XTT colourimetric assays

Assessment of cell proliferation and cytotoxicity has improved over the years since their introduction in the early 80's (Mosmann, 1983). Roehm and colleagues (1991) indicated that when dehydrogenase enzymes in metabolically active cells cleave XTT, they produce a water-soluble, brightly coloured formazan product. In a study that quantified bovine neutrophil bactericidal activity using both the XTT and MTT colourimetric assays, the authors noted limitation on the use of both these assays however XTT was regarded to be faster as it does not require a solubilising agent to be added (Stevens and Olsen, 1993).

In this study, there was disparity in sensitivity across the metabolic tests using MTT and XTT which could perhaps be attributed to their distinct reduction mechanisms. XTT is reduced extracellularly at the plasma membrane surface by trans-plasma membrane electron transport, whereas MTT reduction occurs intracellularly in the association with mitochondria, the cytoplasm, and other membranous compartments (Schröterová et al., 2009). The annexin V/PI

assays which also measure toxicity are more specific and were therefore used not only to determine the mode of cell death but to further confirm the cytotoxic effect of the promising compounds.

4.1.2 Comparison of the effect of Cytotoxicity of the ligands

The ligands were compared against each other across all tested concentrations. There was no significant difference in the effect of cytotoxicity of the ligands (appendix C).

4.2 ANTIOXIDANT ACTIVITY

RuL1 of ligand 1 and CuL3 of ligand 3 inhibited DPPH activity with IC_{50}'s of 5.11 ± 0.47 µM and 4.25 ± 0.56 µM, respectively. It is well documented in literature that transition metal hydrazone complexes exhibit strong antioxidant activity (Mohanraj et al., 2016). Biological role in repairing or inhibiting oxidative damage have been found to be clinically significant in promoting cell proliferation, survival, and metabolic adaptation at higher concentration doses, (Xu et al., 2019). In a study by Rohini and colleagues, the authors established that Ru(II) arene complexes were potential anticancer metallodrugs other than the platinum because of the intrinsic features such as redox accessible oxidation states imitating Iron (Fe) (Rohini et al., 2018). RuL1 possessed the greatest antioxidant activity, indicating that the compound not only targets pancreatic cancer cells selectively, but also has antioxidant properties. This makes it an excellent candidate as an anticancer agent, as some anticancer compounds, like curcumin, exert their anticancer effects by acting as antioxidants.

4.3 APOPTOSIS - CELL DEATH

Flow cytometry-based assay Annexin V/PI was utilized to further determine the mechanism of cell death for specific metal complexes that had been observed to exhibit cytotoxicity due to

the presence of tetrazolium salts. Metal complexes AgL1, RuL1 and NiL2 showed cytotoxic effects that necessitated them to be tested for their mode of cell death. Ruthenium (III/II) (Ru–acac compounds) such as [Ru(dpqy)(acac)(py)](PF_6) studied by Gupta and colleagues, were found to induce apoptosis in MDA-MB-231 cells (Gupta et al., 2021) (Kalaivani et al., 2014). To discover the nickel complexes as potential anticancer drugs, it is highly recommended that additional research be conducted on animal models to shed light on the precise mechanism of action of the complex.

4.4 CELL CYCLE

Cell cycle is a sequential process in which cellular components undergo duplication and subsequent precise distribution into daughter cells (Han et al., 2023). The cell cycle consists of four consecutive phases: G1 (Gap 1), S (synthesis), G2 (Gap 2), and M (mitosis). The sub-G1 cell death detection method uses fragmented low-molecular-weight DNA released from cells during prolonged fixation after DNA endonucleolytic cleavage. Since G1 is the longest phase of the cell cycle, most cells are in G1. This will reduce the number of cells that bind PI, a quantitative DNA stain. Consequently, a population of cells will emerge to the left of the G1 peak. The regulation of the mammalian cell cycle involves a complex system of controlled mechanisms that are activated by external signals, causing the cell to transition from its inactive state known as G0 (Barnum and O'Connell, 2014). The metal complexes showed a high cell population on the S-phase except for RuL1 which has exhibited an equal cell population of 52% for both the sub-G1 and S phase. Ruthenium based metal complexes have emerged as potential compounds for the development of drugs against tumour growth because of their redox nature, which enables ruthenium to exist in oxidation states +II and +III under physiological conditions. Due to its lower reactivity compared to Ru (II), Ru (III) allows for the development of prodrug strategies that can be activated through the reduction in the reductive environment of solid tumours (Fuereder and Berger, 2017). Ruthenium complexes are currently undergoing phase 1 human trials, specifically sodium trans-(tetrachlorobis(1H-indazole). In this clinical trial, Ruthenate(III), previously referred to as NKP-1339, was assessed to determine its safety, tolerability, maximum-tolerated dose (MTD), pharmacokinetics, and pharmacodynamics in patients with advanced solid tumors. The study

revealed that it effectively inhibited the stress-induced expression of GRP78 in cancer cells (Burris et al., 2016). This suggests that combining the metal complexes with gemcitabine improves their anticancer activity. GRP78 plays a crucial role in controlling the processing of misfolded proteins, and when its levels increase in tumours, it is linked to both inherent and drug-induced resistance.

The coupling of the NiL2 complex improved the mode of cell death from 6.44 ± 1.45% to 16.9 ± 2.1% in our study. In previous research, it was established that Ni and its compounds are capable of inducing cell death and DNA damage (Guo et al., 2021). Qin and colleagues (2017) synthesized and characterized oxoaporphine complexes with Co(II), Ni(II), and Zn(II) (1-3) and tested in vitro and animal models and the Oxoaporphine complexes with Co(II), Ni(II), and Zn(II) were more toxic to five different types of human tumour cells than the free ligand, except for HepG2, T-24, and SK-OV-3 cells. The complexes 1-3, even at low concentrations, they caused HepG2 cells to enter S-phase. This was evident on the NiL2 complex we studied which caused an S-phase cell arrest in vitro.

The chemical activities and medical applications of metal complexes are significantly influenced by the type of ligand, in addition to the metal itself. Therefore, altering the ligand can result in modifications of photophysical, electrochemical, spectroscopic, and biological properties of the complexes. Drugs such as gemcitabine induces arrest of the cell cycle on the S-phase and controls the expression of proteins related to the cell cycle in PK-1 cells which is PDAC cell line (Namima et al., 2020). Drugs that inhibit the S phase are said to be inhibitors of DNA synthesis. This suggests that the metal complex RuL1 which also inhibit the S phase, mimic gemcitabine, an inhibitor of DNA synthesis.

The silver complex $[[Ag(\mu\text{-PTA})(Df)(H_2O)]_n \cdot 3nH_2O]$ (1) has demonstrated considerably greater cytotoxicity compared to the ligand precursors on the AsPc-1 compared to the other cancer cell lines that were tested. An analysis of the cell lines revealed that the addition of AgNPs stimulated an increase in apoptosis of the pancreatic cancer cells. This effect was associated with an increase in the amount of Bax protein, which promotes apoptosis, and a decrease in the level of Bcl 2 protein, which inhibits apoptosis. Additionally, AgNPs significantly increased the levels of the tumour suppressor protein p53. Furthermore, the researchers found that the pancreatic cell line became more susceptible to the toxic effects of the silver nanoparticles and can induce different forms of programmed cell death in PANC-1

cells, potentially contributing to the fight against chemo resistance (Nedelcu et al., 2021). This is evident on the AgL1 complex which has shown to arrest the sub G1 and S-phase.

CHAPTER 5

Conclusion and recommendations

5.1 CONCLUSION

The results presented have evidence that complexes such as Ruthenium showed anticancer potential. Metal complexes AgL1, RuL1 and Nil2 showed good antioxidant activity, induced cell death in pancreatic cancer cells and enhanced the S phase of cell cycle arrest.

5.2 RECOMMENDATIONS

RuL1 which has shown cytotoxic effect of 1.44 ± 0.61 when compared to the control gemcitabine's cytotoxicity of 7.24 ± 0.66 µM, antioxidant activity of 5.11 ± 0,47 when compared to the control VitC 6.42 ± 0.09 µM and anticancer effect S phase 52 % for RuL1 61 when compared to the control gemcitabine's S phase of 39%. It has been consistent and needs further investigation. Assessing the mechanism of action using NF-κB assay will give insight of the complexes target sites on the malignant cells. Since many ruthenium metallodrugs are prodrugs, a key question is how their molecular reactivity affects their selectivity and target interaction. Many clinically used agents can damage DNA but are also cytotoxic. DNA damage detection and repair involve different mechanisms. Modulation of these pathways affects clinical outcome and often causes therapeutic resistance. Thus, pharmacological inhibition of DNA damage repair pathways has to be investigated to prove drug efficacy.

To address the resistance of PDAC to gemcitabine, a combination of nabpaclitaxel, folic acid, fluorouracil, irinotecan, and oxaliplatin (FOLFIRINOX) has been used alongside gemcitabine. This combined treatment has demonstrated enhanced effectiveness and increased survival time when compared to using gemcitabine alone. To also navigate through the efficacy of the complexes, I suggest combining the metal complexes with gemcitabine to improve their anticancer activity.

The ruthenium (III) complex labelled KP1019, which was synthesized in Keppler laboratories, interacts with DNA and induces varying degrees and types of damage, distinct from the effects of cisplatin (Depenbrock et al., 1997). However, the precise mechanism by which this occurs has not been fully understood yet. In vitro studies have demonstrated that the ruthenium complex NAMI-A interacts with DNA. However, its anti-metastatic activity does not depend on this interaction (Gałczyńska et al., 2020b). A mechanism for the RuL1 complex we studied needs to be investigated.

A look at the morphological changes of the MIA Paca-2 when treated with the metal complexes to assess at which concentration the metal complexes possess change in morphology of the cells and after how long of time 24, 48 or 72 hours.

References

ABDOLMALEKI, S., KHAKSAR, S., ALIABADI, A., PANJEHPOUR, A., MOTIEIYAN, E., MARABELLO, D., FARAJI, M. H. & BEIHAGHI, M. 2023. Cytotoxicity and mechanism of action of metal complexes: An overview. *Toxicology,* 492**,** 153516.

ABOU KHOUZAM, R., LEHN, J. M., MAYR, H., CLAVIEN, P. A., WALLACE, M. B., DUCREUX, M., LIMANI, P. & CHOUAIB, S. 2023. Hypoxia, a Targetable Culprit to Counter Pancreatic Cancer Resistance to Therapy. *Cancers (Basel),* 15.

ADAMSKA, A., DOMENICHINI, A. & FALASCA, M. 2017. Pancreatic Ductal Adenocarcinoma: Current and Evolving Therapies. *Int J Mol Sci,* 18.

AMMERMAN, N. C., BEIER-SEXTON, M. & AZAD, A. F. 2008. Growth and maintenance of Vero cell lines. *Curr Protoc Microbiol,* Appendix 4**,** Appendix 4E.

ANDERSON, E. M., THOMASSIAN, S., GONG, J., HENDIFAR, A. & OSIPOV, A. 2021. Advances in Pancreatic Ductal Adenocarcinoma Treatment. *Cancers (Basel),* 13.

ANTHONY, E. J., BOLITHO, E. M., BRIDGEWATER, H. E., CARTER, O. W. L., DONNELLY, J. M., IMBERTI, C., LANT, E. C., LERMYTE, F., NEEDHAM, R. J., PALAU, M., SADLER, P. J., SHI, H., WANG, F. X., ZHANG, W. Y. & ZHANG, Z. 2020. Metallodrugs are unique: opportunities and challenges of discovery and development. *Chem Sci,* 11**,** 12888-12917.

ATKINSON, M. A., CAMPBELL-THOMPSON, M., KUSMARTSEVA, I. & KAESTNER, K. H. 2020. Organisation of the human pancreas in health and in diabetes. *Diabetologia,* 63**,** 1966-1973.

ATTIA, M. I., ELDEHNA, W. M., AFIFI, S. A., KEETON, A. B., PIAZZA, G. A. & ABDEL-AZIZ, H. A. 2017. New hydrazonoindolin-2-ones: Synthesis, exploration of the possible anti-proliferative mechanism of action and encapsulation into PLGA microspheres. *PLoS One,* 12**,** e0181241.

BALACHANDRAN, C., HARIBABU, J., JEYALAKSHMI, K., BHUVANESH, N. S. P., KARVEMBU, R., EMI, N. & AWALE, S. 2018. Nickel(II) bis(isatin thiosemicarbazone) complexes induced apoptosis through mitochondrial signaling pathway and G0/G1 cell cycle arrest in IM-9 cells. *Journal of Inorganic Biochemistry,* 182**,** 208-221.

BARNUM, K. J. & O'CONNELL, M. J. 2014. Cell cycle regulation by checkpoints. *Methods Mol Biol,* 1170**,** 29-40.

BEGUM, M. S., DAS, D., ZANGRANDO, E., RAHMAN, S., ALODHAYB, A., BEGUM, M. K., SHEIKH, C. M., MIYATAKE, R., HOWLADER, M. B. H., KARIM, M. R. & CHOWDHURY, M. B. 2023. A dithiocarbazate N,S Schiff base ligand with a long alkyl chain: Synthesis, characterization, DFT study and antimicrobial activity of its Ni(II) complex. *Journal of Molecular Structure,* 1277**,** 134808.

BETANZOS-LARA, S., GÓMEZ-RUIZ, C., BARRÓN-SOSA, L. R., GRACIA-MORA, I., FLORES-ÁLAMO, M. & BARBA-BEHRENS, N. 2012. Cytotoxic copper(II), cobalt(II), zinc(II), and nickel(II) coordination compounds of clotrimazole. *Journal of Inorganic Biochemistry,* 114**,** 82-93.

BONNETT, S. A., DENNISON, D., FILES, M., BAJPAI, A. & PARISH, T. 2018. A class of hydrazones are active against non-replicating Mycobacterium tuberculosis. *PLoS One,* 13**,** e0198059.

BURANAAMNUAY, K. 2021. The MTT assay application to measure the viability of spermatozoa: A variety of the assay protocols. *Open Vet J,* 11**,** 251-269.

BURRIS, H. A., BAKEWELL, S., BENDELL, J. C., INFANTE, J., JONES, S. F., SPIGEL, D. R., WEISS, G. J., RAMANATHAN, R. K., OGDEN, A. & VON HOFF, D. 2016. Safety and activity of IT-139, a ruthenium-based compound, in patients with advanced solid tumours: a first-in-human, open-label, dose-escalation phase I study with expansion cohort. *ESMO Open,* 1**,** e000154.

CANGA, I., VITA, P., OLIVEIRA, A. I., CASTRO, M. & PINHO, C. 2022. In Vitro Cytotoxic Activity of African Plants: A Review. *Molecules,* 27.

CHARI, S. T., KELLY, K., HOLLINGSWORTH, M. A., THAYER, S. P., AHLQUIST, D. A., ANDERSEN, D. K., BATRA, S. K., BRENTNALL, T. A., CANTO, M., CLEETER, D. F., FIRPO, M. A., GAMBHIR, S. S., GO, V. L. W., HINES, O. J., KENNER, B. J., KLIMSTRA, D. S., LERCH, M. M., LEVY, M. J., MAITRA, A., MULVIHILL, S. J., PETERSEN, G. M., RHIM, A. D., SIMEONE, D. M., SRIVASTAVA, S., TANAKA, M., VINIK, A. I. & WONG, D. 2015. Early Detection of Sporadic Pancreatic Cancer: Summative Review. *(Cossarizza et al., 2019)*44**,** 693-712.

CHEN, J., TAO, Q., WU, J., WANG, M., SU, Z., QIAN, Y., YU, T., WANG, Y., XUE, X. & LIU, H.-K. 2020. A lysosome-targeted ruthenium(II) polypyridyl complex as photodynamic anticancer agent. *Journal of Inorganic Biochemistry,* 210**,** 111132.

COCETTA, V., RAGAZZI, E. & MONTOPOLI, M. 2020. Chapter Three - Links between cancer metabolism and cisplatin resistance. *In:* GALLUZZI, L. (ed.) *International Review of Cell and Molecular Biology*. Academic Press.

COSSARIZZA, A., CHANG, H. D., RADBRUCH, A., ACS, A., ADAM, D., ADAM-KLAGES, S., AGACE, W. W., AGHAEEPOUR, N., AKDIS, M., ALLEZ, M., ALMEIDA, L. N., ALVISI, G., ANDERSON, G., ANDRÄ, I., ANNUNZIATO, F., ANSELMO, A., BACHER, P., BALDARI, C. T., BARI, S., BARNABA, V., BARROS-MARTINS, J., BATTISTINI, L., BAUER, W., BAUMGART, S., BAUMGARTH, N., BAUMJOHANN, D., BAYING, B., BEBAWY, M., BECHER, B., BEISKER, W., BENES, V., BEYAERT, R., BLANCO, A., BOARDMAN, D. A., BOGDAN, C., BORGER, J. G., BORSELLINO, G., BOULAIS, P. E., BRADFORD, J. A., BRENNER, D., BRINKMAN, R. R., BROOKS, A. E. S., BUSCH, D. H., BÜSCHER, M., BUSHNELL, T. P., CALZETTI, F., CAMERON, G., CAMMARATA, I., CAO, X., CARDELL, S. L., CASOLA, S., CASSATELLA, M. A., CAVANI, A., CELADA, A., CHATENOUD, L., CHATTOPADHYAY, P. K., CHOW, S., CHRISTAKOU, E., ČIČIN-ŠAIN, L., CLERICI, M., COLOMBO, F. S., COOK, L., COOKE, A., COOPER, A. M., CORBETT, A. J., COSMA, A., COSMI, L., COULIE, P. G., CUMANO, A., CVETKOVIC, L., DANG, V. D., DANG-HEINE, C., DAVEY, M. S., DAVIES, D., DE BIASI, S., DEL ZOTTO, G., DELA CRUZ, G. V., DELACHER, M., DELLA BELLA, S., DELLABONA, P., DENIZ, G., DESSING, M., DI SANTO, J. P., DIEFENBACH, A., DIELI, F., DOLF, A., DÖRNER, T., DRESS, R. J., DUDZIAK, D., DUSTIN, M., DUTERTRE, C. A., EBNER, F., ECKLE, S. B. G., EDINGER, M., EEDE, P., EHRHARDT, G. R. A., EICH, M., ENGEL, P., ENGELHARDT, B., ERDEI, A. 2019. Guidelines for the use of flow cytometry and cell sorting in immunological studies (second edition). *Eur J Immunol*, 49**,** 1457-1973.

CUI, T., LIU, P., CHEN, X., LIU, Z., WANG, B., GAO, C., WANG, Z., LI, C. & YANG, N. 2023. Identification and functional characterization of caspases in turbot (Scophthalmus maximus) in response to bacterial infection. *Fish Shellfish Immunol*, 137**,** 108757.

DAMGHANI, T., MOOSAVI, F., KHOSHNEVISZADEH, M., MORTAZAVI, M., PIRHADI, S., KAYANI, Z., SASO, L., EDRAKI, N. & FIRUZI, O. 2021. Imidazopyridine hydrazone derivatives exert antiproliferative effect on lung and

pancreatic cancer cells and potentially inhibit receptor tyrosine kinases including c-Met. *Sci Rep,* 11**,** 3644.

DE LIMA, E. M., KANUNFRE, C. C., DE ANDRADE, L. F., GRANATO, D. & ROSSO, N. D. 2015. Cytotoxic effect of inositol hexaphosphate and its Ni(II) complex on human acute leukemia Jurkat T cells. *Toxicology in Vitro,* 29**,** 2081-2088.

EL-ASMY, A. A., RAKHA, T. H., ABDEL-RHMAN, M. H., HASSANIEN, M. M. & AL-MOLA, A. S. 2015. Synthesis, spectral, thermal and biological studies on N−(2,4-dinitro-phenyl)-2-mercaptoacetohydrazide and its metal complexes. *Spectrochimica Acta Part A: Molecular and Biomolecular Spectroscopy,* 136**,** 1718-1727.

ELSAYED, S. A., SAAD, E. A. & MOSTAFA, S. I. 2019. Development of New Potential Anticancer Metal Complexes Derived from 2-Hydrazinobenzothiazole. *Mini Rev Med Chem,* 19**,** 913-922.

ENDJALA, P. T., NAIMHWAKA, J. & UAHENGO, V. 2021. Investigation of fluorenyl-thioic-based ditopic as a functional colorimetric probe for heavy metal cations and anions with higher selectivity towards Cu2+ followed by Zn2+, displaying logic functions: Experimental and computational studies. *Chemical Papers,* 75**,** 5471-5488.

FEKRI, R., SALEHI, M., ASADI, A. & KUBICKI, M. 2018. Spectroscopic studies, structural characterization and electrochemical studies of two cobalt (III) complexes with tridentate hydrazone Schiff base ligands: Evaluation of antibacterial activities, DNA-binding, BSA interaction and molecular docking. *Applied Organomettalic chemistry,* 32**,** e4019.

FERRARO, M. G., PICCOLO, M., MISSO, G., SANTAMARIA, R. & IRACE, C. 2022. Bioactivity and Development of Small Non-Platinum Metal-Based Chemotherapeutics. *Pharmaceutics,* 14.

FOTEDAR, R., DIEDERICH, L. & FOTEDAR, A. 1996. Apoptosis and the cell cycle. *Prog Cell Cycle Res,* 2**,** 147-63.

FRU, P. N., NWEKE, E. E., MTHIMKHULU, N., MVANGO, S., NEL, M., PILCHER, L. A. & BALOGUN, M. 2021. Anti-Cancer and Immunomodulatory Activity of a Polyethylene Glycol-Betulinic Acid Conjugate on Pancreatic Cancer Cells. *Life (Basel),* 11.

FUEREDER, T. & BERGER, W. 2017. Metal drugs become targeted. *ESMO Open,* 2**,** e000239.

GAŁCZYŃSKA, K., DRULIS-KAWA, Z. & ARABSKI, M. 2020a. Antitumour Activity of Pt(II), Ru(III) and Cu(II) Complexes. *Molecules,* 25; 3492.

GHARIBI, A., ADAMIAN, Y. & KELBER, J. A. 2016. Cellular and molecular aspects of pancreatic cancer. *Acta Histochem,* 118**,** 305-16.

GRANT, T. J., HUA, K. & SINGH, A. 2016. Molecular Pathogenesis of Pancreatic Cancer. *Prog Mol Biol Transl Sci,* 144**,** 241-275.

GUO, H., DENG, H., LIU, H., JIAN, Z., CUI, H., FANG, J., ZUO, Z., DENG, J., LI, Y., WANG, X. & ZHAO, L. 2021. Nickel carcinogenesis mechanism: cell cycle dysregulation. *Environmental Science and Pollution Research,* 28**,** 4893-4901.

GUO, J., XIE, K. & ZHENG, S. 2016. Molecular Biomarkers of Pancreatic Intraepithelial Neoplasia and Their Implications in Early Diagnosis and Therapeutic Intervention of Pancreatic Cancer. *Int J Biol Sci,* 12**,** 292-301.

GUPTA, S., VANDEVORD, J. M., LOFTUS, L. M., TOUPIN, N., AL-AFYOUNI, M. H., ROHRABAUGH, T. N., JR., TURRO, C. & KODANKO, J. J. 2021. Ru(II)-Based Acetylacetonate Complexes Induce Apoptosis Selectively in Cancer Cells. *Inorg Chem,* 60**,** 18964-18974.

HAN, B., CHEN, Y., SONG, C., CHEN, Y., CHEN, Y., FERGUSON, D., YANG, Y. & HE, A. 2023. Autophagy modulates the stability of Wee1 and cell cycle G2/M transition. *Biochem Biophys Res Commun,* 677**,** 63-69.

HO, W. J., JAFFEE, E. M. & ZHENG, L. 2020. The tumour microenvironment in pancreatic cancer - clinical challenges and opportunities. *Nat Rev Clin Oncol,* 17**,** 527-540.

IQBAL, M., KHAWAJA, U. A., SOOMRO, U., RIZVI, S. A. A. & RIZVI, Z. H. 2023. Pancreatic adenocarcinoma in the elderly – recurrence and survival: A physician's challenge. *Advances in Cancer Biology - Metastasis,* 7**,** 100092.

JEON, J., LEE, S., KIM, H., KANG, H., YOUN, H., JO, S., YOUN, B. & KIM, H. Y. 2021. Revisiting Platinum-Based Anticancer Drugs to Overcome Gliomas. *Int J Mol Sci,* 22.

KARIM, M., BOIKESS, R. S., SCHWARTZ, R. A. & COHEN, P. J. 2023. Dimethyl sulfoxide (DMSO): a solvent that may solve selected cutaneous clinical challenges. *Arch Dermatol Res,* 315**,** 1465-1472.

KARPIŃSKA, M. & CZAUDERNA, M. 2022. Pancreas-Its Functions, Disorders, and Physiological Impact on the Mammals' Organism. *Front Physiol,* 13**,** 807632.

KALAIVANI, P., SARANYA, S., POORNIMA, P., PRABHAKARAN, R., DALLEMER, F., VIJAYA PADMA, V. & NATARAJAN, K. 2014. Biological evaluation of new

nickel(II) metallates: Synthesis, DNA/protein binding and mitochondrial mediated apoptosis in human lung cancer cells (A549) via ROS hypergeneration and depletion of cellular antioxidant pool. *European Journal of Medicinal Chemistry,* 82**,** 584-599.

KEDARE, S. B. & SINGH, R. P. 2011. Genesis and development of DPPH method of antioxidant assay. *Journal of food science and technology,* 48**,** 412-422.

KENNER, B. J., GO, V. L. W., CHARI, S. T., GOLDBERG, A. E. & ROTHSCHILD, L. J. 2017. Early Detection of Pancreatic Cancer: The Role of Industry in the Development of Biomarkers. *Pancreas,* 46**,** 1238-1241.

KIM, S. J., KIM, H. S. & SEO, Y. R. 2019. Understanding of ROS-Inducing Strategy in Anticancer Therapy. *Oxidative medicine and cellular longevity,* 2019**,** 5381692-5381692.

KUNG, H. C. & YU, J. 2023. Targeted therapy for pancreatic ductal adenocarcinoma: Mechanisms and clinical study. *MedComm (2020),* 4**,** e216.

LEE, S. Y., KIM, C. Y. & NAM, T. G. 2020. Ruthenium Complexes as Anticancer Agents: A Brief History and Perspectives. *Drug Des Devel Ther,* 14**,** 5375-5392.

LEVINA, A., MITRA, A. & LAY, P. A. 2009. Recent developments in ruthenium anticancer drugs. *Metallomics,* 1**,** 458-470.

LI, Y., GO, V. L. & SARKAR, F. H. 2015. The Role of Nutraceuticals in Pancreatic Cancer Prevention and Therapy: Targeting Cellular Signaling, MicroRNAs, and Epigenome. *Pancreas,* 44**,** 1-10.

LIANG, X., LUAN, S., YIN, Z., HE, M., HE, C., YIN, L., ZOU, Y., YUAN, Z., LI, L., SONG, X., LV, C. & ZHANG, W. 2018. Recent advances in the medical use of silver complex. *Eur J Med Chem,* 157**,** 62-80.

LIN, C., CUI, J., PENG, Z., QIAN, K., WU, R., CHENG, Y. & YIN, W. 2022. Efficacy of platinum-based and non-platinum-based drugs on triple-negative breast cancer: meta-analysis. *Eur J Med Res,* 27**,** 201.

MAI, S. & INKIELEWICZ-STEPNIAK, I. 2021. Pancreatic Cancer and Platelets Crosstalk: A Potential Biomarker and Target. *Front Cell Dev Biol,* 9**,** 749689.

MAKOVEC, T. 2019. Cisplatin and beyond: molecular mechanisms of action and drug resistance development in cancer chemotherapy. *Radiol Oncol,* 53**,** 148-158.

MATSUOKA, T. & YASHIRO, M. 2016. Molecular targets for the treatment of pancreatic cancer: Clinical and experimental studies. *World J Gastroenterol,* 22**,** 776-89.

MIJIT, M., BONER, M., CORDOVA, R. A., GAMPALA, S., KPENU, E., KLUNK, A. J., ZHANG, C., KELLEY, M. R., STASCHKE, K. A. & FISHEL, M. L. 2023. Activation of the integrated stress response (ISR) pathways in response to Ref-1 inhibition in human pancreatic cancer and its tumour microenvironment. *Front Med (Lausanne),* 10**,** 1146115.

MOHANRAJ, M., AYYANNAN, G., RAJA, G. & JAYABALAKRISHNAN, C. 2016. Synthesis, spectral characterization, DNA interaction, radical scavenging and cytotoxicity studies of ruthenium(II) hydrazone complexes. *Journal of Photochemistry and Photobiology B: Biology,* 158**,** 164-173.

MORIWAKI, K. & CHAN, F. K. 2014. Necrosis-dependent and independent signaling of the RIP kinases in inflammation. *Cytokine Growth Factor Rev,* 25**,** 167-74.

MOSIANE, K. S., NWEKE, E. E., BALOGUN, M. & FRU, P. N. 2023. Polyethyleneglycol-Betulinic Acid (PEG-BA) Polymer-Drug Conjugate Induces Apoptosis and Antioxidation in a Biological Model of Pancreatic Cancer. *Polymers (Basel),* 15.

MOSMANN, T. 1983. Rapid colorimetric assay for cellular growth and survival: Application to proliferation and cytotoxicity assays. *Journal of Immunological Methods,* 65**,** 55-63.

NAMIMA, D., FUJIHARA, S., IWAMA, H., FUJITA, K., MATSUI, T., NAKAHARA, M., OKAMURA, M., HIRATA, M., KONO, T., FUJITA, N., YAMANA, H., KATO, K., KAMADA, H., MORISHITA, A., KOBARA, H., TSUTSUI, K. & MASAKI, T. 2020. The Effect of gemcitabine on Cell Cycle Arrest and microRNA Signatures in Pancreatic Cancer Cells. *In Vivo,* 34**,** 3195-3203.

NASR, T., BONDOCK, S., RASHED, H. M., FAYAD, W., YOUNS, M. & SAKR, T. M. 2018. Novel hydrazide-hydrazone and amide substituted coumarin derivatives: Synthesis, cytotoxicity screening, microarray, radiolabeling and in vivo pharmacokinetic studies. *Eur J Med Chem,* 151**,** 723-739.

NEDELCU, A., MOCAN, T., GRAPA, C. & MOCAN, L. 2021. Recent Advances in Nanoparticle-Mediated Diagnosis and the Treatment of Pancreatic Cancer. *International Journal of molecular science,*22**,** 8060.

OPITZ, F. V., HAEBERLE, L., DAUM, A. & ESPOSITO, I. 2021. Tumour Microenvironment in Pancreatic Intraepithelial Neoplasia. *Cancers (Basel),* 13.

ORTH, M., METZGER, P., GERUM, S., MAYERLE, J., SCHNEIDER, G., BELKA, C., SCHNURR, M. & LAUBER, K. 2019. Pancreatic ductal adenocarcinoma: biological hallmarks, current status, and future perspectives of combined modality treatment approaches. *Radiation Oncology,* 14**,** 141.

PARK, W., CHAWLA, A. & O'REILLY, E. M. 2021. Pancreatic Cancer: A Review. *Jama,* 326**,** 851-862.

PEREIRA, S. P., OLDFIELD, L., NEY, A., HART, P. A., KEANE, M. G., PANDOL, S. J., LI, D., GREENHALF, W., JEON, C. Y., KOAY, E. J., ALMARIO, C. V., HALLORAN, C., LENNON, A. M. & COSTELLO, E. 2020. Early detection of pancreatic cancer. *Lancet Gastroenterol Hepatol,* 5**,** 698-710.

PETRUK, G., MONTI, D. M., FERRARO, G., PICA, A., D'ELIA, L., PANE, F., AMORESANO, A., FURRER, J., KOWALSKI, K. & MERLINO, A. 2019. Encapsulation of the Dinuclear Trithiolato-Bridged Arene Ruthenium Complex Diruthenium-1 in an Apoferritin Nanocage: Structure and Cytotoxicity. *ChemMedChem,* 14**,** 594-602.

POPIOLEK, L. 2017. Hydrazide-hydrazones as potential antimicrobial agents: overview of the literature since 2010. *Med Chem Res,* 26**,** 287-301.

QIN, J.-L., SHEN, W.-Y., CHEN, Z.-F., ZHAO, L.-F., QIN, Q.-P., YU, Y.-C. & LIANG, H. 2017. Oxoaporphine Metal Complexes (CoII, NiII, ZnII) with High Antitumour Activity by Inducing Mitochondria-Mediated Apoptosis and S-phase Arrest in HepG2. *Scientific Reports,* 7**,** 46056.

RADUCKA, A., ŚWIĄTKOWSKI, M., KORONA-GŁOWNIAK, I., KAPROŃ, B., PLECH, T., SZCZESIO, M., GOBIS, K., SZYNKOWSKA-JÓŹWIK, M. I. & CZYLKOWSKA, A. 2022. Zinc Coordination Compounds with Benzimidazole Derivatives: Synthesis, Structure, Antimicrobial Activity and Potential Anticancer Application. *Int J Mol Sci,* 23.

RAFFENNE, J., MARTIN, F. A., NICOLLE, R., KONTA, M., BLUM, Y., TORRISANI, J., PULEO, F., BACHET, J. B., SVRCEK, M., BARDIER-DUPAS, A., EMILE, J. F., DEMETTER, P., RADMAN, M., VAN LAETHEM, J. L., HAMMEL, P., REBOURS, V., PARADIS, V., COUVELARD, A. & CROS, J. 2021. Pancreatic Ductal Adenocarcinoma Arising in Young and Old Patients Displays Similar Molecular Features. *Cancers (Basel),* 13.

RAHMAN, F. U., BHATTI, M. Z., ALI, A., DUONG, H. Q., ZHANG, Y., YANG, B., KOPPIREDDI, S., LIN, Y., WANG, H., LI, Z. T. & ZHANG, D. W. 2018. Homo- and heteroleptic Pt(II) complexes of ONN donor hydrazone and 4-picoline: A synthetic, structural and detailed mechanistic anticancer investigation. *Eur J Med Chem,* 143**,** 1039-1052.

REVIA, R. A., STEPHEN, Z. R. & ZHANG, M. 2019. Theranostic Nanoparticles for RNA-Based Cancer Treatment. *Acc Chem Res,* 52**,** 1496-1506.

RISS, T. L., MORAVEC, R. A., NILES, A. L., DUELLMAN, S., BENINK, H. A., WORZELLA, T. J. & MINOR, L. 2004. Cell Viability Assays. *In:* MARKOSSIAN, S., GROSSMAN, A., BRIMACOMBE, K., ARKIN, M., AULD, D., AUSTIN, C., BAELL, J., CHUNG, T. D. Y., COUSSENS, N. P., DAHLIN, J. L., DEVANARAYAN, V., FOLEY, T. L., GLICKSMAN, M., GORSHKOV, K., HAAS, J. V., HALL, M. D., HOARE, S., INGLESE, J., IVERSEN, P. W., KALES, S. C., LAL-NAG, M., LI, Z., MCGEE, J., MCMANUS, O., RISS, T., SARADJIAN, P., SITTAMPALAM, G. S., TARSELLI, M., TRASK, O. J., JR., WANG, Y., WEIDNER, J. R., WILDEY, M. J., WILSON, K., XIA, M. & XU, X. (eds.) *Assay Guidance Manual*. Bethesda (MD): Eli Lilly & Company and the National Center for Advancing Translational Sciences.

ROEHM, N. W., RODGERS, G. H., HATFIELD, S. M. & GLASEBROOK, A. L. 1991. An improved colorimetric assay for cell proliferation and viability utilizing the tetrazolium salt XTT. *Journal of Immunological Methods,* 142**,** 257-265.

ROHINI, G., HARIBABU, J., ANEESRAHMAN, K. N., BHUVANESH, N. S. P., RAMAIAH, K., KARVEMBU, R. & SREEKANTH, A. 2018. Half-sandwich Ru(II)(η6-p-cymene) complexes bearing N-dibenzosuberenyl appended thiourea for catalytic transfer hydrogenation and in vitro anticancer activity. *Polyhedron,* 152**,** 147-154.

ROY, H., DEOLALKAR, M. & DESAI, A. S. 2019. Synthesis of Calix-Salen Silver Corates for Evaluation of Their Antimicrobial and Anticancer Activities. *ACS Omega,* 4**,** 21346-21352.

SAGINI, M. N., ZEPP, M., BERGMANN, F., BOZZA, M., HARBOTTLE, R. & BERGER, M. R. 2018. The expression of genes contributing to pancreatic adenocarcinoma progression is influenced by the respective environment. *Genes Cancer,* 9**,** 114-129.

SAHIN, O., OZDEMIR, U. O., SEFEROGLU, N., GENC, Z. K., KAYA, K., AYDINER, B., TEKIN, S. & SEFEROGLU, Z. 2018. New platinum (II) and palladium (II) complexes of coumarin-thiazole Schiff base with a fluorescent chemosensor properties: Synthesis, spectroscopic characterization, X-ray structure determination, in vitro anticancer activity on various human carcinoma cell lines and computational studies. *J Photochem Photobiol B,* 178**,** 428-439.

SANTA-GONZÁLEZ, G. A., PATIÑO-GONZÁLEZ, E. & MANRIQUE-MORENO, M. 2020. Cell cycle progression data on human skin cancer cells with anticancer synthetic peptide LTX-315 treatment. *Data Brief,* 30**,** 105443.

SARANTIS, P., KOUSTAS, E., PAPADIMITROPOULOU, A., PAPAVASSILIOU, A. G. & KARAMOUZIS, M. V. 2020. Pancreatic ductal adenocarcinoma: Treatment hurdles, tumour microenvironment and immunotherapy. *World J Gastrointest Oncol,* 12**,** 173-181.

SCHRÖTEROVÁ, L., KRÁLOVÁ, V., VORÁČOVÁ, A., HAŠKOVÁ, P., RUDOLF, E. & ČERVINKA, M. 2009. Antiproliferative effects of selenium compounds in colon cancer cells: Comparison of different cytotoxicity assays. *Toxicology in Vitro,* 23**,** 1406-1411.

SEN, S., WON, M., LEVINE, M. S., NOH, Y., SEDGWICK, A. C., KIM, J. S., SESSLER, J. L. & ARAMBULA, J. F. 2022. Metal-based anticancer agents as immunogenic cell death inducers: the past, present, and future. *Chem Soc Rev,* 51**,** 1212-1233.

ŠERMUKŠNYTĖ, A., KANTMINIENĖ, K., JONUŠKIENĖ, I., TUMOSIENĖ, I. & PETRIKAITĖ, V. 2022. The Effect of 1,2,4-Triazole-3-thiol Derivatives Bearing Hydrazone Moiety on Cancer Cell Migration and Growth of Melanoma, Breast, and Pancreatic Cancer Spheroids. *Pharmaceuticals (Basel),* 15.

SINGH, R. R. & O'REILLY, E. M. 2020. New Treatment Strategies for Metastatic Pancreatic Ductal Adenocarcinoma. *Drugs,* 80**,** 647-669.

SINGHI, A. D., KOAY, E. J., CHARI, S. T. & MAITRA, A. 2019. Early Detection of Pancreatic Cancer: Opportunities and Challenges. *Gastroenterology,* 156**,** 2024-2040.

SKALNY, A. V., ASCHNER, M. & TINKOV, A. A. 2021. Zinc. *Adv Food Nutr Res,* 96**,** 251-310.

SKRAJNOWSKA, D. & BOBROWSKA-KORCZAK, B. 2019. Role of Zinc in Immune System and Anti-Cancer Defense Mechanisms. *Nutrients,* 11.

SOBERANES, Y., NAVARRO, R. E., INOUE, M., VELÁZQUEZ-CONTRERAS, E. F., BELTRAN TORRES, M., LUGO, G., SOTELO-MUNDO, R. R. & SALAZAR-MEDINA, A. J. 2019. Syntheses, Characterization, and Antioxidant Evaluation of Cu(2+), Mn(2+), and Fe(3+) Complexes with a 14 Membered EDTA-Derived Macrocycle. *Molecules (Basel, Switzerland),* 24**,** 3556.

SONKAR, C., SARKAR, S. & MUKHOPADHYAY, S. 2022. Ruthenium(ii)-arene complexes as anti-metastatic agents, and related techniques. *RSC Med Chem,* 13**,** 22-38.

STEVENS, M. G. & OLSEN, S. C. 1993. Comparative analysis of using MTT and XTT in colorimetric assays for quantitating bovine neutrophil bactericidal activity. *Journal of Immunological Methods,* 157**,** 225-231.

STRYJSKA, K., RADKO, L., CHĘCIŃSKA, L., KUSZ, J., POSYNIAK, A. & OCHOCKI, J. 2020. Synthesis, Spectroscopy, Light Stability, Single-Crystal Analysis, and In Vitro Cytotoxic Activity on HepG2 Liver Cancer of Two Novel Silver(I) Complexes of Miconazole. *Int J Mol Sci,* 21.

TĂBĂCARU, A., KHAN, R. A., LUPIDI, G. & PETTINARI, C. 2020. Synthesis, Characterization and Assessment of the Antioxidant Activity of Cu(II), Zn(II) and Cd(II) Complexes Derived from Scorpionate Ligands. *Molecules (Basel, Switzerland),* 25**,** 5298.

TAHA, M., SHAH, S. A., MOHD FARIDZ, M. A., ZULKEFLEE, M., SULTAN, S., WADOOD, A., RAHIM, F. & ISMAIL, N. 2016. Morpholine hydrazone scaffold: Synthesis, anticancer activity and docking studies. *Chinese Chemical Letters*.

TAKAI, M., OKUDA, A., AMANO, Y., YASHIRO, N., HARA, K., YAMAMOTO, M. & TSUJIUCHI, T. 2023. Effects of LPA receptor-mediated signaling on the modulation of cellular functions of pancreatic cancer cells cultured in fibroblast supernatants under hypoxic conditions. *J Bioenerg Biomembr*.

TIMMER, F. E. F., GEBOERS, B., NIEUWENHUIZEN, S., DIJKSTRA, M., SCHOUTEN, E. A. C., PUIJK, R. S., DE VRIES, J. J. J., VAN DEN TOL, M. P., BRUYNZEEL, A. M. E., STREPPEL, M. M., WILMINK, J. W., VAN DER VLIET, H. J., MEIJERINK, M. R., SCHEFFER, H. J. & DE GRUIJL, T. D. 2021. Pancreatic Cancer and Immunotherapy: A Clinical Overview. *Cancers (Basel),* 13.

UPTON, J. W., KAISER, W. J. & MOCARSKI, E. S. 2010. Virus inhibition of RIP3-dependent necrosis. *Cell Host Microbe,* 7**,** 302-313.

VAIDYA, S. P., GADRE, S., KAMISETTI, R. T. & PATRA, M. 2022. Challenges and opportunities in the development of metal-based anticancer theranostic agents. *Biosci Rep,* 42.

VAN MEERLOO, J., KASPERS, G. J. & CLOOS, J. 2011. Cell sensitivity assays: the MTT assay. *Methods Mol Biol,* 731**,** 237-45.

VARNA, D., GEROMICHALOU, E., KARLIOTI, G., PAPI, R., DALEZIS, P., HATZIDIMITRIOU, A. G., PSOMAS, G., CHOLI-PAPADOPOULOU, T., TRAFALIS, D. T. & ANGARIDIS, P. A. 2023. Inhibition of Cancer Cell Proliferation

and Bacterial Growth by Silver(I) Complexes Bearing a CH(3)-Substituted Thiadiazole-Based Thioamide. *Molecules,* 28.

VERA-RAMIREZ, L., RAMIREZ-TORTOSA, M., PEREZ-LOPEZ, P., GRANADOS-PRINCIPAL, S., BATTINO, M. & QUILES, J. L. 2012. Long-term effects of systemic cancer treatment on DNA oxidative damage: The potential for targeted therapies. *Cancer Letters,* 327**,** 134-141.

WANG, L., ZHOU, W., ZHONG, Y., HUO, Y., FAN, P., ZHAN, S., XIAO, J., JIN, X., GOU, S., YIN, T., WU, H. & LIU, T. 2017. Overexpression of G protein-coupled receptor GPR87 promotes pancreatic cancer aggressiveness and activates NF-kappaB signaling pathway. *Mol Cancer,* 16**,** 61.

WANG, S., YU, H. & WICKLIFFE, J. K. 2011. Limitation of the MTT and XTT assays for measuring cell viability due to superoxide formation induced by nano-scale TiO2. *Toxicology in Vitro,* 25**,** 2147-2151.

WANG, X. & HAMANN, M. T. 2019. Marine natural products in the discovery and development of potential pancreatic cancer therapeutics. *Adv Cancer Res,* 144**,** 299-314.

WERNITZNIG, D., KIAKOS, K., DEL FAVERO, G., HARRER, N., MACHAT, H., OSSWALD, A., JAKUPEC, M. A., WERNITZNIG, A., SOMMERGRUBER, W. & KEPPLER, B. K. 2019. First-in-class ruthenium anticancer drug (KP1339/IT-139) induces an immunogenic cell death signature in colorectal spheroids in vitro†. *Metallomics,* 11**,** 1044-1048.

XU, D., HU, M. J., WANG, Y. Q. & CUI, Y. L. 2019. Antioxidant Activities of Quercetin and Its Complexes for Medicinal Application. *Molecules,* 24.

YAMASAKI, A., YANAI, K. & ONISHI, H. 2020. Hypoxia and pancreatic ductal adenocarcinoma. *Cancer Letters,* 484**,** 9-15.

YANG, J., XU, R., WANG, C., QIU, J., REN, B. & YOU, L. 2021. Early screening and diagnosis strategies of pancreatic cancer: a comprehensive review. *Cancer Commun (Lond),* 41**,** 1257-1274.

YANG, X. Y., LU, Y. F., XU, J. X., DU, Y. Z. & YU, R. S. 2023. Recent Advances in Well-Designed Therapeutic Nanosystems for the Pancreatic Ductal Adenocarcinoma Treatment Dilemma. *Molecules,* 28.

YUNIS, A. A., ARIMURA, G. K. & RUSSIN, D. J. 1977. Human pancreatic carcinoma (MIA paca-2) in continuous culture: Sensitivity to asparaginase. *International Journal of Cancer,* 19**,** 128-135.

ZANGRANDO, E., BEGUM, M. S., SHEIKH, M. C., MIYATAKE, R., HOSSAIN, M. M., ALAM, M. M., HASNAT, M. A., HALIM, M. A., AHMED, S., RAHMAN, M. N. & GHOSH, A. 2017. Synthesis, characterization, density functional study and antimicrobial evaluation of a series of bischelated complexes with a dithiocarbazate Schiff base ligand. *Arabian Journal of Chemistry,* 10**,** 172-184.

ZHANG, C., XU, C., GAO, X. & YAO, Q. 2022. Platinum-based drugs for cancer therapy and anti-tumour strategies. *Theranostics,* 12**,** 2115-2132.

ZHAO, H., JAFFER, T., EGUCHI, S., WANG, Z., LINKERMANN, A. & MA, D. 2015. Role of necroptosis in the pathogenesis of solid organ injury. *Cell Death Dis,* 6**,** e1975.

ZHUANG, H., WANG, S., CHEN, B., ZHANG, Z., MA, Z., LI, Z., LIU, C., ZHOU, Z., GONG, Y., HUANG, S., HOU, B., CHEN, Y. & ZHANG, C. 2021. Prognostic Stratification Based on HIF-1 Signaling for Evaluating Hypoxic Status and Immune Infiltration in Pancreatic Ductal Adenocarcinomas. *Front Immunol,* 12**,** 790661.

COSSARIZZA, A., CHANG, H. D., RADBRUCH, A., ACS, A., ADAM, D., ADAM-KLAGES, S., AGACE, W. W., AGHAEEPOUR, N., AKDIS, M., ALLEZ, M., ALMEIDA, L. N., ALVISI, G., ANDERSON, G., ANDRÄ, I., ANNUNZIATO, F., ANSELMO, A., BACHER, P., BALDARI, C. T., BARI, S., BARNABA, V., BARROS-MARTINS, J., BATTISTINI, L., BAUER, W., BAUMGART, S., BAUMGARTH, N., BAUMJOHANN, D., BAYING, B., BEBAWY, M., BECHER, B., BEISKER, W., BENES, V., BEYAERT, R., BLANCO, A., BOARDMAN, D. A., BOGDAN, C., BORGER, J. G., BORSELLINO, G., BOULAIS, P. E., BRADFORD, J. A., BRENNER, D., BRINKMAN, R. R., BROOKS, A. E. S., BUSCH, D. H., BÜSCHER, M., BUSHNELL, T. P., CALZETTI, F., CAMERON, G., CAMMARATA, I., CAO, X., CARDELL, S. L., CASOLA, S., CASSATELLA, M. A., CAVANI, A., CELADA, A., CHATENOUD, L., CHATTOPADHYAY, P. K., CHOW, S., CHRISTAKOU, E., ČIČIN-ŠAIN, L., CLERICI, M., COLOMBO, F. S., COOK, L., COOKE, A., COOPER, A. M., CORBETT, A. J., COSMA, A., COSMI, L., COULIE, P. G., CUMANO, A., CVETKOVIC, L., DANG, V. D., DANG-HEINE, C., DAVEY, M. S., DAVIES, D., DE BIASI, S., DEL ZOTTO, G., DELA CRUZ, G. V., DELACHER, M., DELLA BELLA, S., DELLABONA, P., DENIZ, G., DESSING, M., DI SANTO, J. P., DIEFENBACH, A., DIELI, F., DOLF, A., DÖRNER, T., DRESS, R. J., DUDZIAK, D., DUSTIN, M., DUTERTRE, C. A., EBNER, F., ECKLE, S. B. G., EDINGER, M., EEDE, P., EHRHARDT, G. R. A., EICH, M., ENGEL, P., ENGELHARDT, B., ERDEI, A., et al. 2019. Guidelines for the use of flow cytometry and cell sorting in immunological studies (second edition). *Eur J Immunol,* 49**,** 1457-1973.

DEPENBROCK, H., SCHMELCHER, S., PETER, R., KEPPLER, B. K., WEIRICH, G., BLOCK, T., RASTETTER, J. & HANAUSKE, A. R. 1997. Preclinical activity of trans-indazolium [tetrachlorobisindazoleruthenate(III)] (NSC 666158; IndCR; KP 1019) against tumour colony-forming units and haematopoietic progenitor cells. *European Journal of Cancer,* 33**,** 2404-2410.

FANG, Y. T., YANG, W. W., NIU, Y. R. & SUN, Y. K. 2023. Recent advances in targeted therapy for pancreatic adenocarcinoma. *World J Gastrointest Oncol,* 15**,** 571-595.

FERRARO, M. G., PICCOLO, M., MISSO, G., SANTAMARIA, R. & IRACE, C. 2022. Bioactivity and Development of Small Non-Platinum Metal-Based Chemotherapeutics. *Pharmaceutics,* 14.

GUPTA, S., VANDEVORD, J. M., LOFTUS, L. M., TOUPIN, N., AL-AFYOUNI, M. H., ROHRABAUGH, T. N., JR., TURRO, C. & KODANKO, J. J. 2021. Ru(II)-Based Acetylacetonate Complexes Induce Apoptosis Selectively in Cancer Cells. *Inorg Chem,* 60**,** 18964-18974.

KALAIVANI, P., SARANYA, S., POORNIMA, P., PRABHAKARAN, R., DALLEMER, F., VIJAYA PADMA, V. & NATARAJAN, K. 2014. Biological evaluation of new nickel(II) metallates: Synthesis, DNA/protein binding and mitochondrial mediated apoptosis in human lung cancer cells (A549) via ROS hypergeneration and depletion of cellular antioxidant pool. *European Journal of Medicinal Chemistry,* 82**,** 584-599.

KARPIŃSKA, M. & CZAUDERNA, M. 2022. Pancreas-Its Functions, Disorders, and Physiological Impact on the Mammals' Organism. *Front Physiol,* 13**,** 807632.

KAZEMINEJAD, Z., MARZI, M., SHIROUDI, A., KOUHPAYEH, S. A., FARJAM, M. & ZARENEZHAD, E. 2022. Novel 1, 2, 4-Triazoles as Antifungal Agents. *Biomed Res Int,* 2022**,** 4584846.

ROHINI, G., HARIBABU, J., ANEESRAHMAN, K. N., BHUVANESH, N. S. P., RAMAIAH, K., KARVEMBU, R. & SREEKANTH, A. 2018. Half-sandwich Ru(II)(η6-p-cymene) complexes bearing N-dibenzosuberenyl appended thiourea for catalytic transfer hydrogenation and in vitro anticancer activity. *Polyhedron,* 152**,** 147-154.

YOO, J., LEE, J. M., JOO, I., LEE, D. H., YOON, J. H., YU, M. H., JANG, J. Y. & LEE, S. H. 2023. Post-neoadjuvant treatment pancreatic cancer resectability and outcome prediction using CT, (18)F-FDG PET/MRI and CA 19-9. *Cancer Imaging,* 23**,** 49.

Appendices

Appendix A: Ethics Clearance Waiver Certificate

UNIVERSITY OF THE WITWATERSRAND, JOHANNESBURG

HUMAN RESEARCH ETHICS COMMITTEE (MEDICAL)

Office of the Deputy Vice-Chancellor (Research & Post Graduate Affairs)

TO: Ms Y Stofile
School: Clinical Medicine
Department: Department of Surgery
Medical School
University
E-mail: ystofile@wsu.ac.za

CC: Supervisor: Dr P Fru <Pascaline.Fru@wits.ac.za>
and <HREC-Medical.ResearchOffice@wits.ac.za>

FROM: Iain Burns
Human Research Ethics Committee (Medical)
Tel: 011 717 1252

E-mail: Iain.Burns@wits.ac.za

DATE: 02/03/2020

REF: *R14/49*

PROTOCOL NO: W-CBP-200302-01 (This is your ethics application study reference number. Please quote this reference number in all correspondence relating to this study)

PROJECT TITLE: *Pancreatic cancer inhibitory potential of hydrazones ligands and their corresponding metal complexes*

Please find attached the Ethics Waiver Certificate for the above project. I hope it goes well and that an article in a recognized publication comes out of it. This will reflect well on your professional standing and contribute to the Government funding of the University.

Appendix B: Characterization of the metal complexes

Supplementary Information

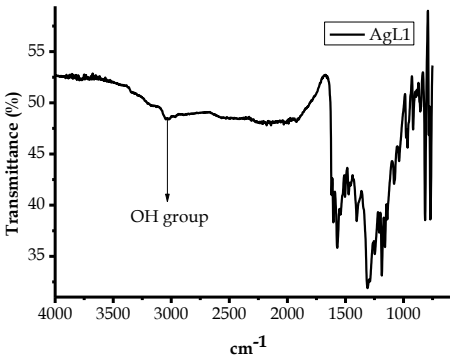
AgL1
OH group
Transmittance (%)
cm-1

(a)

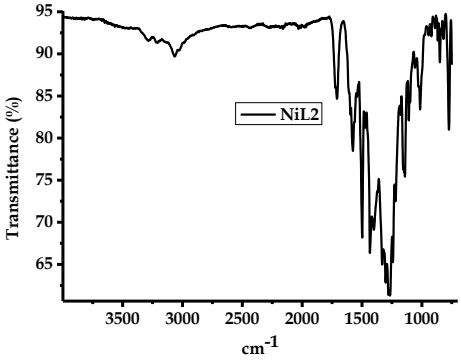
NiL2
Transmittance (%)
cm-1

(b)

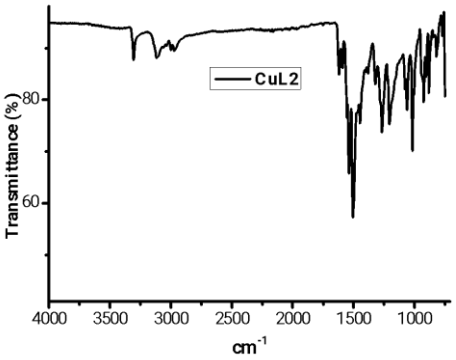
CuL2
Transmittance (%)
cm-1

(c)

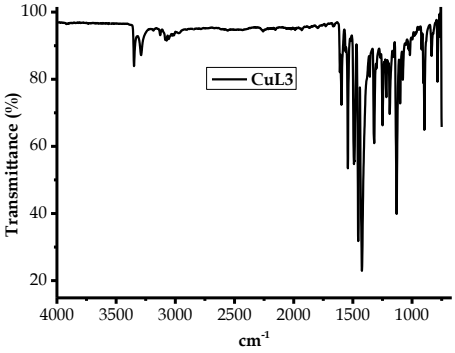
CuL3
Transmittance (%)
cm-1

(d)

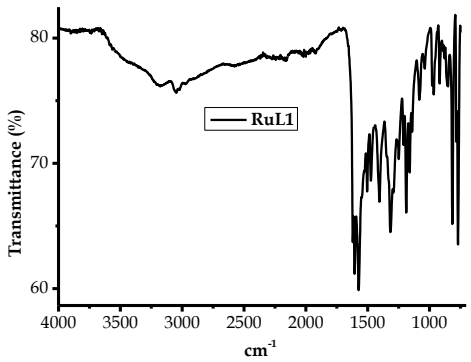
RuL1
Transmittance (%)
cm-1

(e)

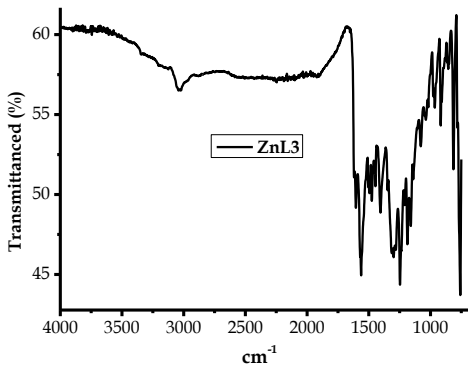
ZnL3
Transmittanced (%)
cm-1

(f)

Figure S1: The FTIR spectra of (a) AgL1, (b) NiL2, (c) CuL2, (d) CuL3, (e) RuL1 and (f) ZnL3

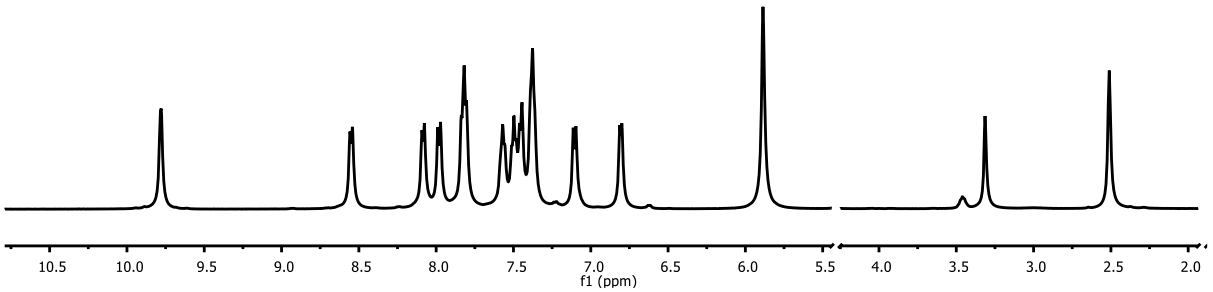

Figure S2: ^{1}H NMR spectral of L1 in DMSO-d_6

L1 (Molecular Weight - 225.30 g/mol)

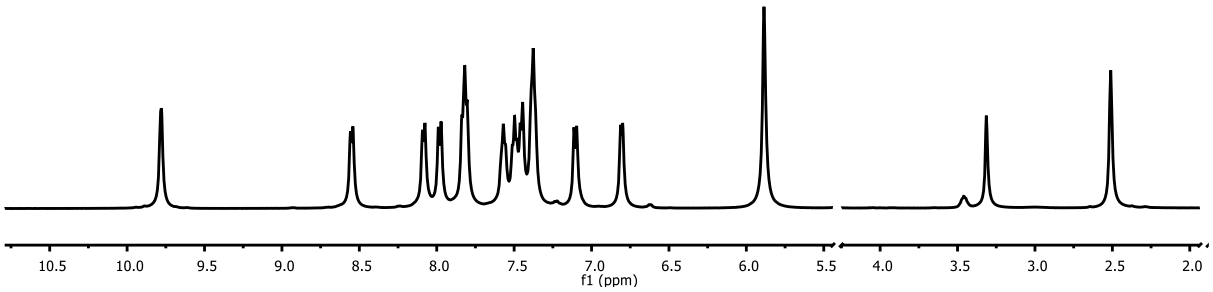

Figure: S2 ^{1}H NMR spectral of **L2** in DMSO-d_6

L2 (MW = 349.41 g/mol)

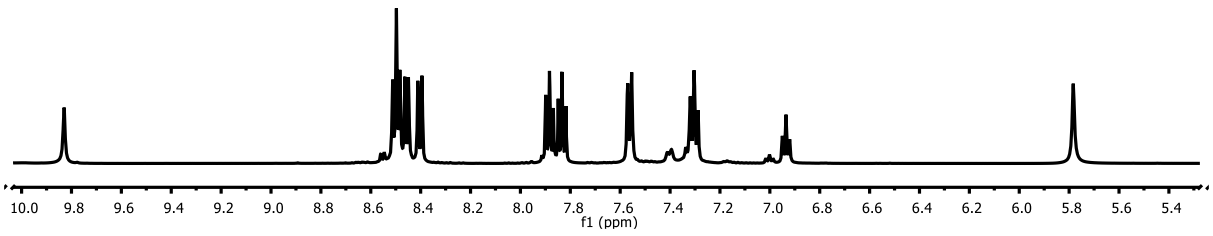

Figure: S3 ^{1}H NMR spectral of **L3** in DMSO-d_6

L3 (MW = 302.37 g/mol)

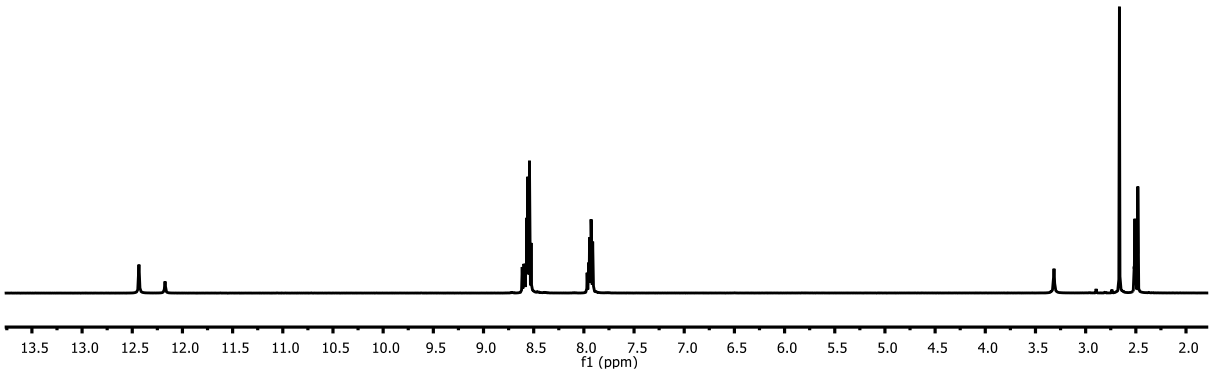

Figure: S3 ^{1}H NMR spectral of **L3** in DMSO-d_6

NiL3 (MW = 732.89 g/mol)

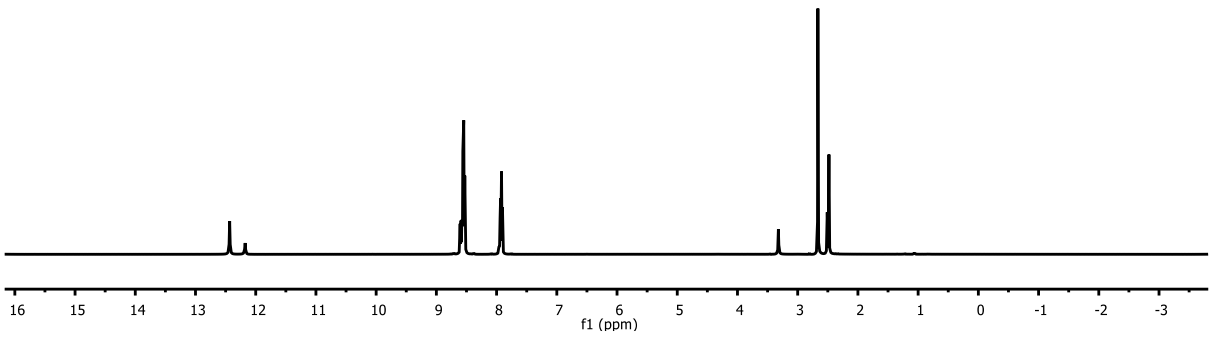

Figure: S4 ^{1}H NMR spectral of **NiL3** in DMSO-d_6

RuL1 (MW = 609.98 g/mol)

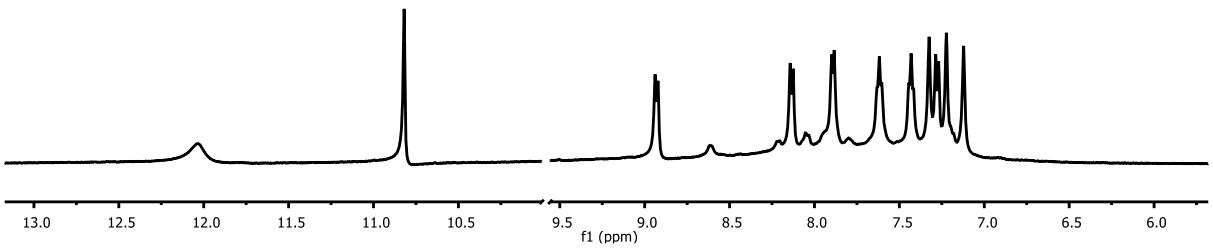

Figure: S5 ^{1}H NMR spectral of **RuL1** in DMSO-d_6

ZnL3 (MW = 670.11 g/mol)

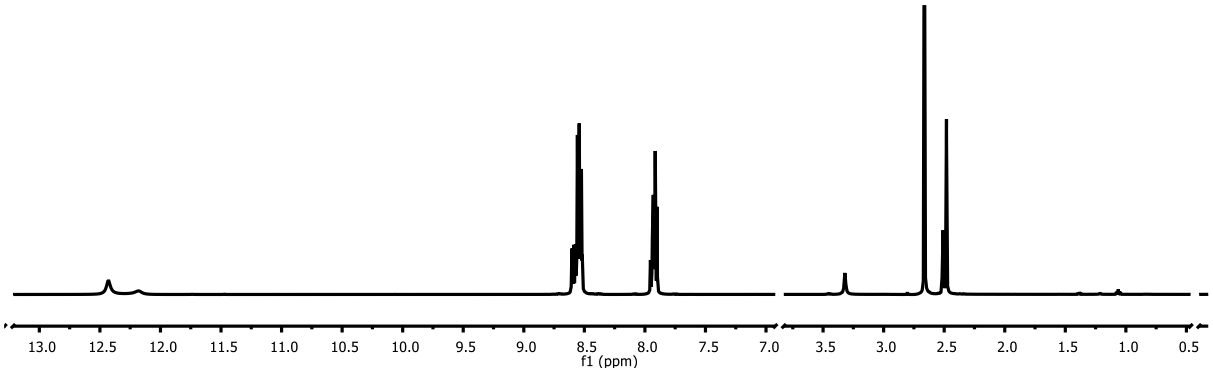

Figure: S6 ^{1}H NMR spectral of **ZnL3** in DMSO-d_6

Appendix C: The comparison of the Cytotoxicity effect of the Ligands

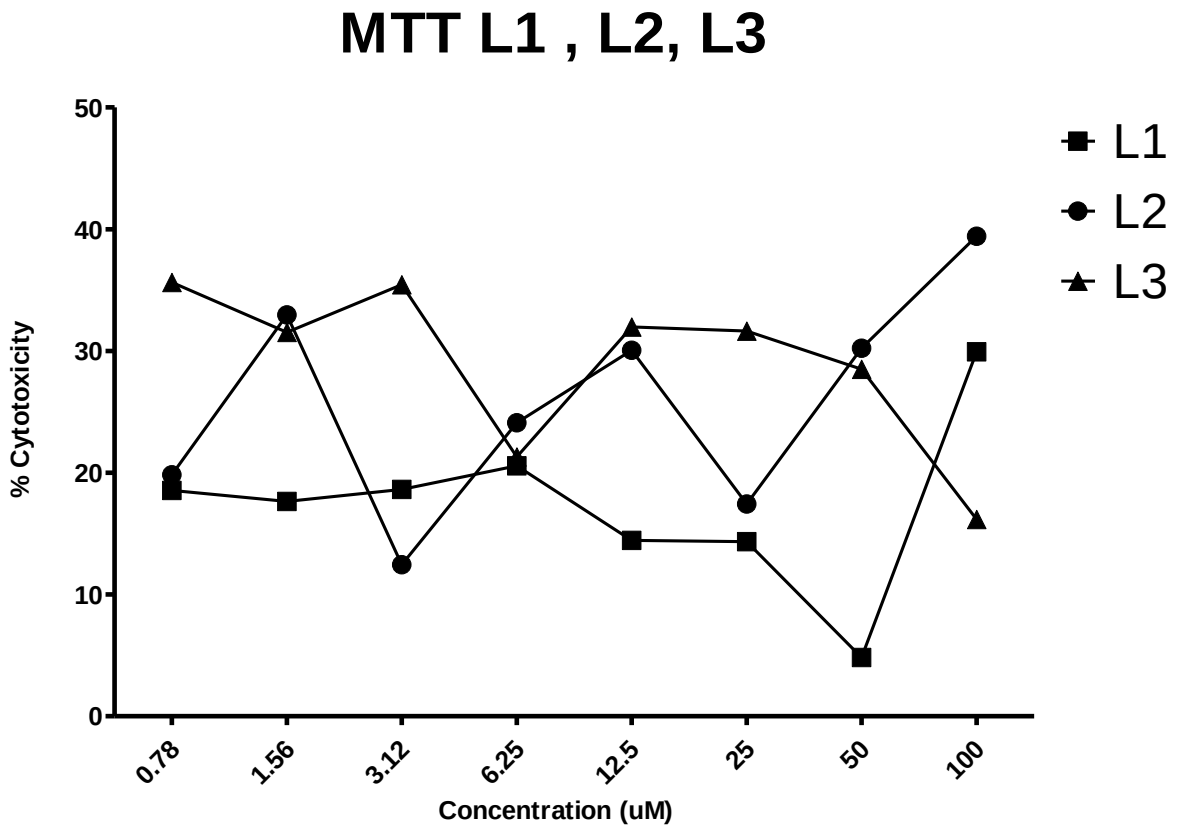

Comparison of all ligands. None exhibited a statistical significance difference.

Appendix D: Cytotoxic effect of metal complexes with the same metal ion

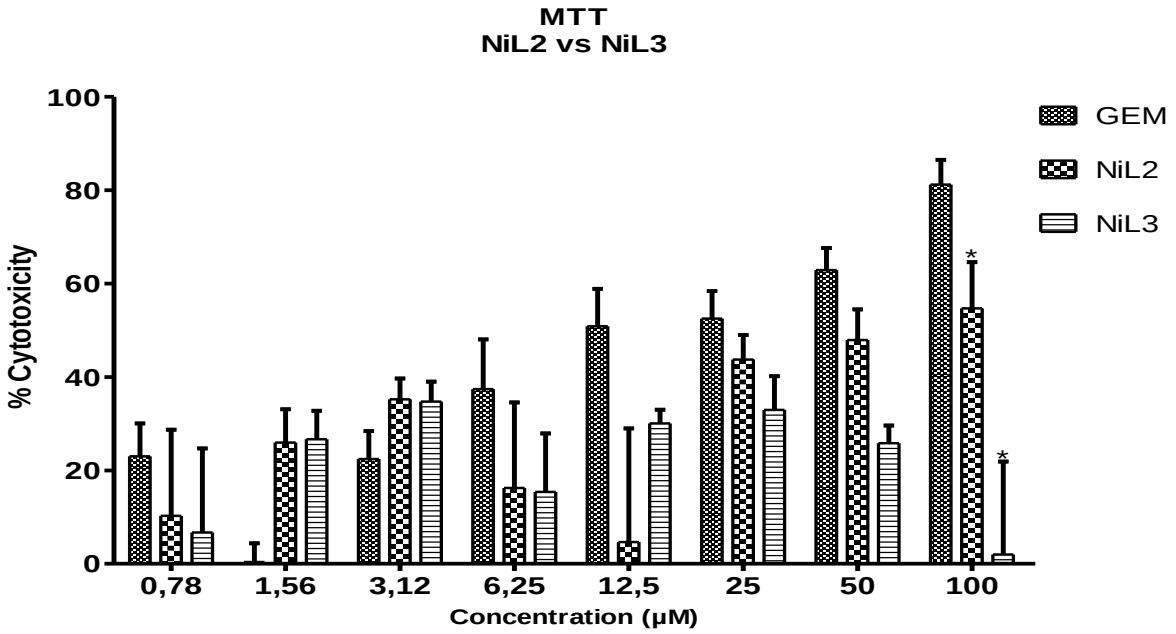

Comparison of the same metal coupled with different ligands. The NiL2 and NiL3 compounds exhibited a statistically significant difference in the cytotoxic effect at a concentration of 100 µM with NiL2 being more cytotoxic than NiL3 (p-value of less than 0.05).

Appendix E: Cytotoxic effect of metal complexes on Vero vells

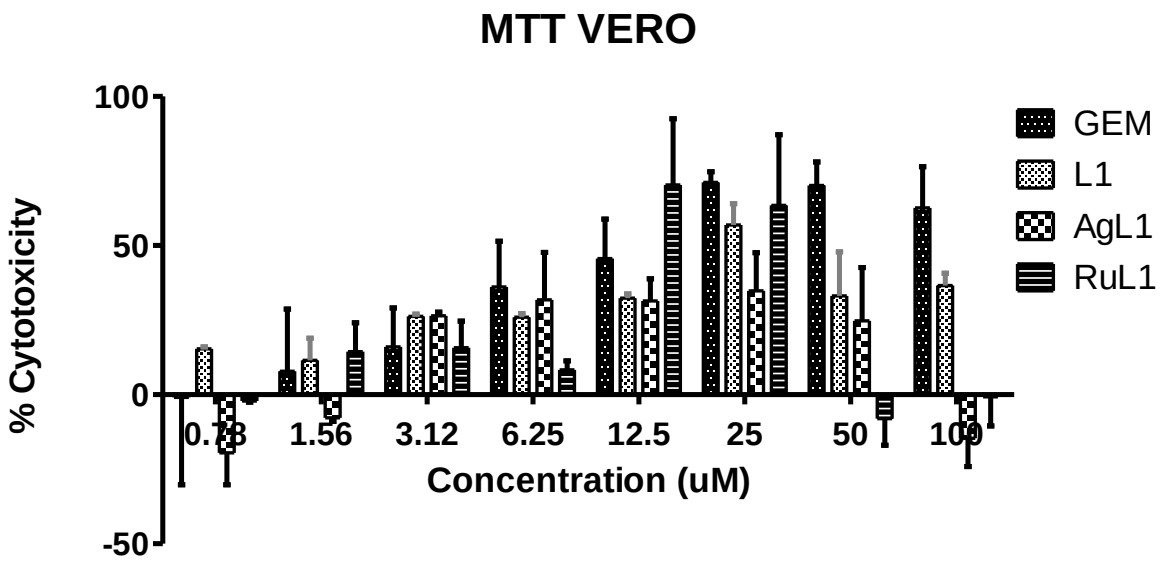
MTT VERO
100
50
0
-50
% Cytotoxicity
0.78
1.56
3.12
6.25
12.5
25
50
100
Concentration (uM)
GEM
L1
AgL1
RuL1

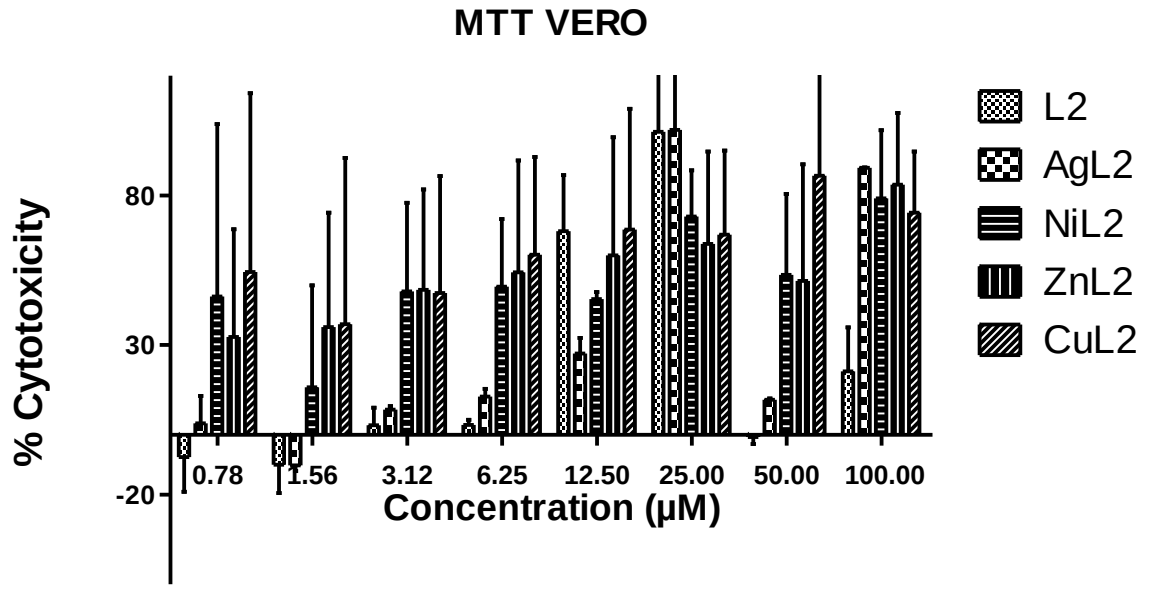
MTT VERO
80
30
-20
% Cytotoxicity
0.78
1.56
3.12
6.25
12.50
25.00
50.00
100.00
Concentration (µM)
L2
AgL2
NiL2
ZnL2
CuL2

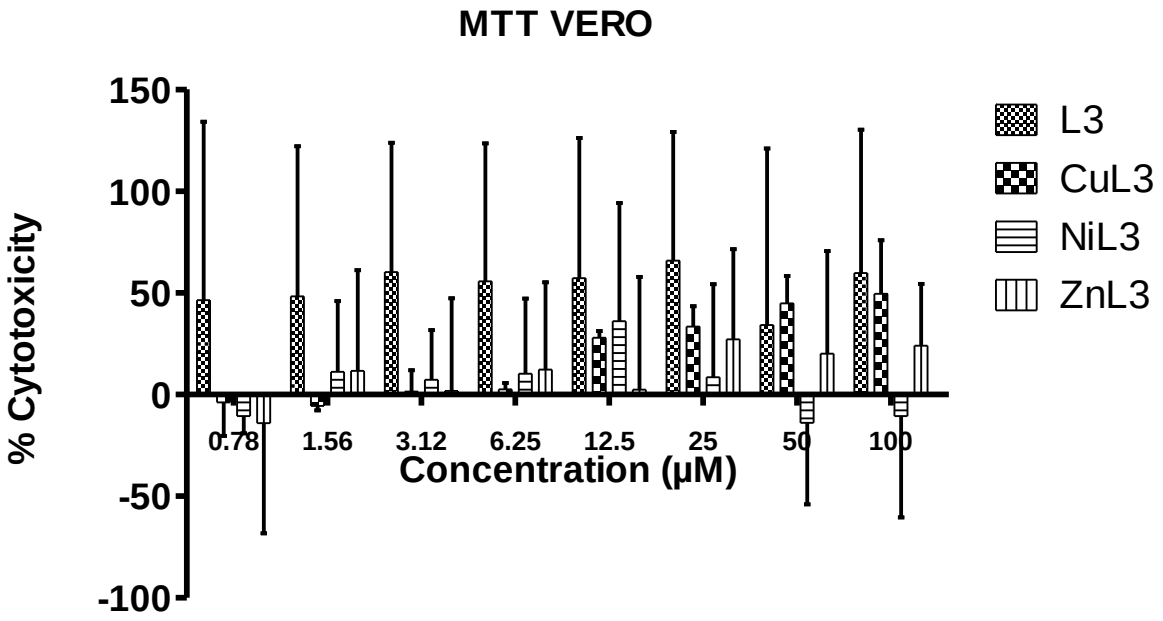
MTT VERO
% Cytotoxicity
150
100
50
0
-50
-100
0.78
1.56
3.12
6.25
12.5
25
50
100
Concentration (µM)
L3
CuL3
NiL3
ZnL3

Appendix F: Cytotoxicity effect of XTT on MIA Paca-2 cells

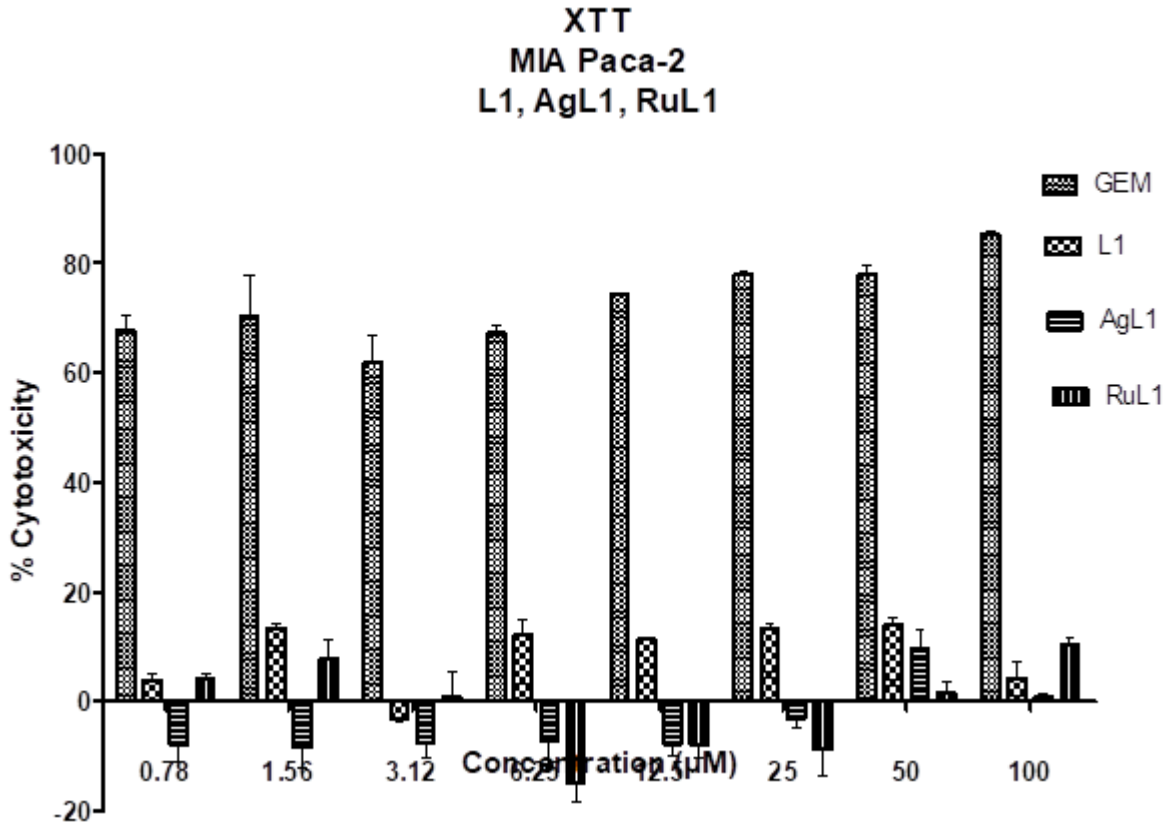

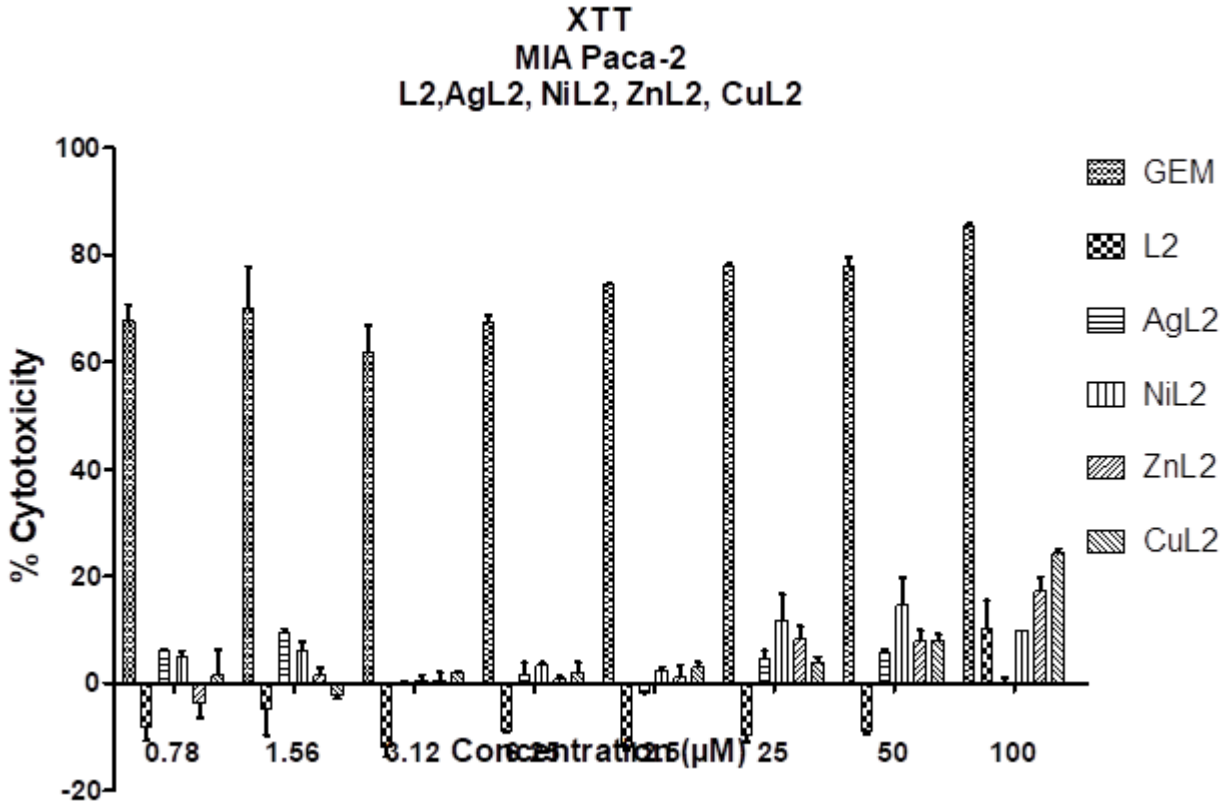
XTT
MIA Paca-2
L2,AgL2, NiL2, ZnL2, CuL2
% Cytotoxicity
100
80
60
40
20
0
-20
0.78
1.56
3.12
25
50
100
GEM
L2
AgL2
NiL2
ZnL2
CuL2

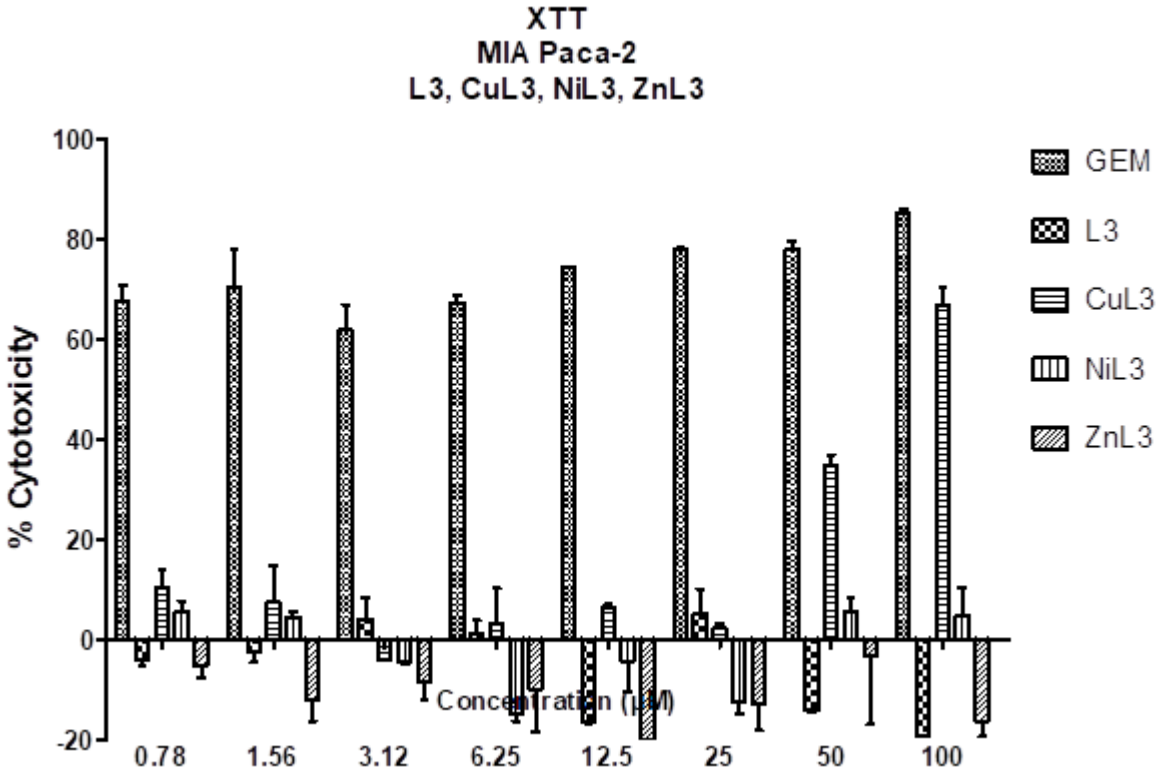
XTT
MIA Paca-2
L3, CuL3, NiL3, ZnL3
% Cytotoxicity
100
80
60
40
20
0
-20
Concentration (µM)
0.78
1.56
3.12
6.25
12.5
25
50
100
GEM
L3
CuL3
NiL3
ZnL3

Appendix G: Cytotoxicity effect of XTT on Vero cells

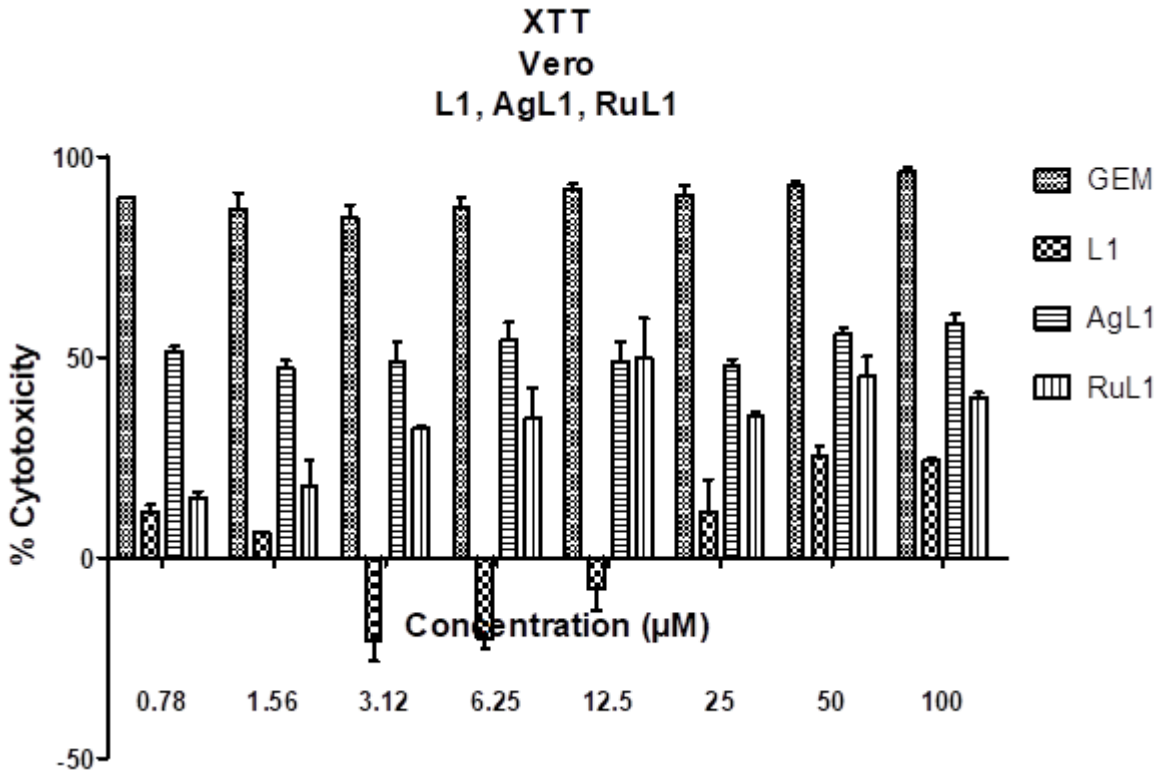

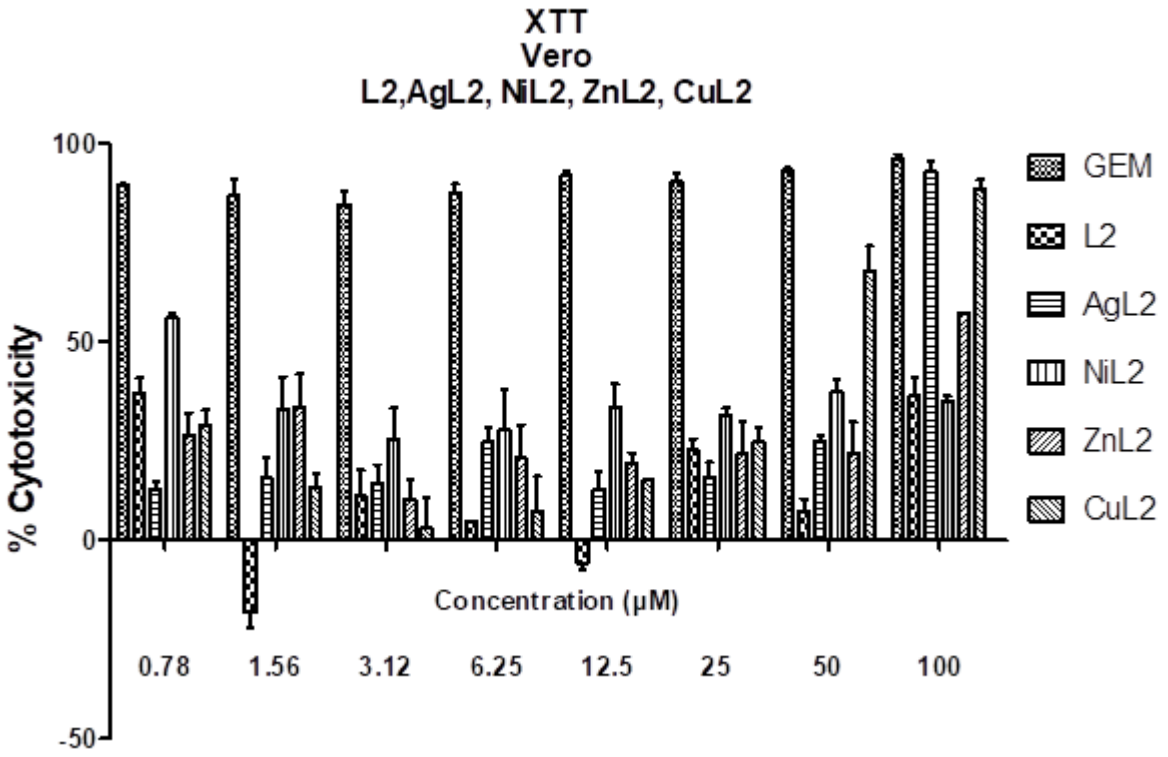
XTT
Vero
L2,AgL2, NiL2, ZnL2, CuL2
% Cytotoxicity
100
50
0
-50
Concentration (µM)
0.78
1.56
3.12
6.25
12.5
25
50
100
GEM
L2
AgL2
NiL2
ZnL2
CuL2

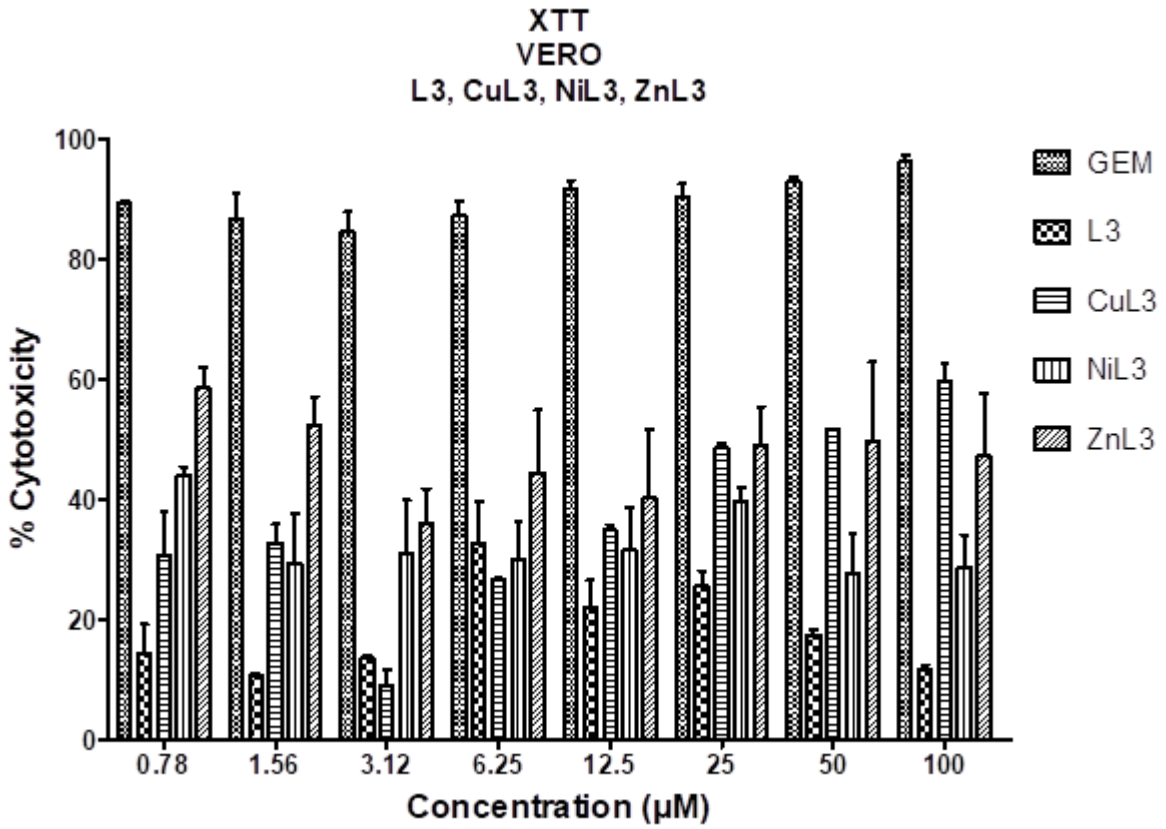
XTT
VERO
L3, CuL3, NiL3, ZnL3
% Cytotoxicity
100
80
60
40
20
0
0.78
1.56
3.12
6.25
12.5
25
50
100
Concentration (µM)
GEM
L3
CuL3
NiL3
ZnL3

Appendix H: Comparison Of the antioxidant activity of the same metal complex coupled to different ligands.

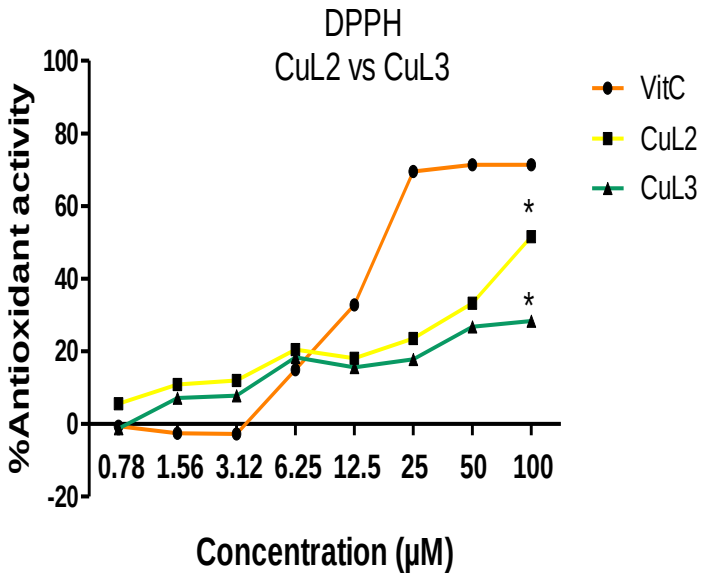

Comparison of the same metal coupled with different ligands. The comparison of CuL2 and CuL3 compounds exhibited a statistically significant effect at the tested concentration of 100 µM with a p-value of less than 0.05.

Appendix I: Plagiarism Report

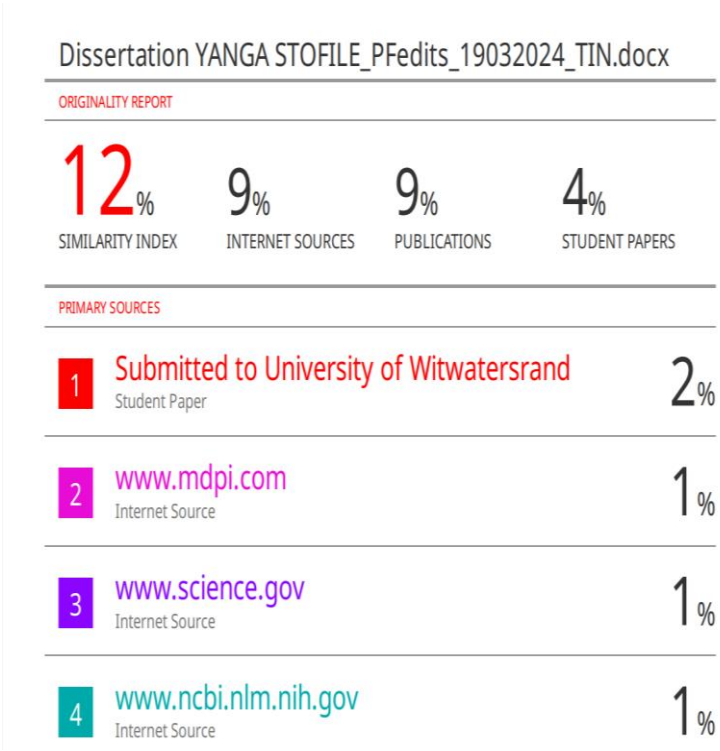

Dissertation YANGA STOFILE_PFedits_19032024_TIN.docx

ORIGINALITY REPORT

12%	9%	9%	4%
SIMILARITY INDEX	INTERNET SOURCES	PUBLICATIONS	STUDENT PAPERS

PRIMARY SOURCES

1	Submitted to University of Witwatersrand Student Paper	2%
2	www.mdpi.com Internet Source	1%
3	www.science.gov Internet Source	1%
4	www.ncbi.nlm.nih.gov Internet Source	1%

Appendix J: Permission to use image by Iqbal et al, 2023.

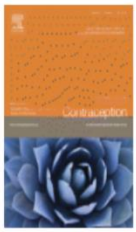

Pancreatic adenocarcinoma in the elderly – recurrence and survival: A physician's challenge

Author: Mashood Iqbal,Uzzam Ahmed Khawaja,Umar Soomro,Syed A.A. Rizvi,Zoya H. Rizvi

Publication: Advances in Cancer Biology - Metastasis

Publisher: Elsevier

Date: July 2023

Appendix I: Permission to use image by Atkinson et al, 2020 (Figure 1.3)

SPRINGER NATURE

Organisation of the human pancreas in health and in diabetes

Author: Mark A. Atkinson et al
Publication: Diabetologia
Publisher: Springer Nature
Date: Sep 7, 2020

Quick Price Estimate